Synthesizing the sit-to-stand movement using fuzzy logic-based control and a simple biomechanical model

by

Robert K. Prinz
B.Eng., University of Victoria, 2005

A Thesis Submitted in Partial Fulfillment of the
Requirements for the Degree of

Master of Applied Science

in the Department of Electrical Engineering

Synthesizing the sit-to-stand movement using fuzzy logic-based control and a simple biomechanical model

by

Robert K. Prinz
BEng, University of Victoria, 2005

Supervisory Committee

Dr. S. Neville, Co-supervisor (Dept. of Elec. and Comp. Eng.)

Dr. N. Livingston, Co-supervisor (CanAssist Dept. of Biology)

Dr. W. Lu, Departmental Member (Dept. of Elec. and Comp. Eng.)

Supervisory Committee

Dr. S. Neville, Co-supervisor (Dept. of Elec. and Comp. Eng.)

Dr. N. Livingston, Co-supervisor (CanAssist Dept. of Biology)

Dr. W. Lu, Departmental Member (Dept. of Elec. and Comp. Eng.)

Abstract

This thesis puts forward a fuzzy logic-based control strategy for artificially reproducing the sit-to-stand movement. The aim of this work is to contribute to the machine intelligence being developed for advanced mobility support devices; and specifically, those which are able to assist the mobility impaired user with the sit-to-stand task. Three fuzzy logic controllers were designed. The first controller seeks to move the model into the "most stable" configuration. The second seeks to move the model toward the goal configuration (i.e., standing). And the third combines the output from the first two controllers to produce a unified control action. Each controller was implemented and tested in software using Mathwork's MATLAB™. The results of the software simulation were compared against motion capture data taken from a single healthy male test subject. The automated controller was shown to produce a movement very similar to the natural sit-to-stand movement.

Table of Contents

List of Tables

List of Figures

Acknowledgements

I would like to thank my co-supervisor Dr. Stephen Neville for his guidance and support over the course of this project, in particular the time and effort put into proof-reading conference papers and this document and making time for regular meetings.

I would also like to express my thanks to my co-supervisor Dr. Nigel Livingston, for encouraging my entrance into graduate school, to explore interdisciplinary research, for his financial support that made this work possible, and the opportunity to be a part of the University of Victoria assistive technology team, CanAssist.

Chapter 1

Introduction

1.1 Mobility Impairment and the Sit-to-Stand Task

Rising from a seated position is an activity carried out by most people numerous times a day. But for those with a mobility impairment, even a seemingly simple task like rising from a chair can pose great difficulty. According to Statistics Canada [4], mobility problems are the disability most often reported by adults aged 15 and over, and it comes as no surprise that the number of mobility impaired persons increases with age. In 2001, it was reported that 695,400 individuals (2.7% of the population) aged 12 or older living in private households required a mobility support device to get around. Within the senior population (individuals aged 65 or older) 12.3% required the use of a mobility support device, confirming, as one might expect, difficulty with mobility increases with age. As the "baby boom" generation ages, Canada is faced with a rapid growth in its elderly population over the next 10+ years. Therefore, it is expected that the number of Canadians experiencing difficulty with mobility will also increase within this time frame.

Sit-to-stand is simply the movement from a sitting to standing position. Also known as chair rise, it's regarded as one of the most mechanically demanding tasks undertaken during daily activities and is generally accepted as a prerequisite for gait [1]. For persons with a physical disability - or more generally, those afflicted with

a mobility impairment - sit-to-stand can pose an especially laborious and problematic task.

1.2 Assisted Sit-to-Stand

Standing frames, or standers, are devices which assist in moving the mobility impaired individual from a seated to standing position. They are typically large, slowly actuated devices which do not attempt to reproduce the natural sit-to-stand movement (i.e., as performed by a healthy individual). Self-righting chairs are also available which slowly lift the seated individual into a standing position. However, with advances in sensor and actuator technologies, a new class of mobility support device has emerged: advanced mobility support devices in the form of motorized quasi robotic suits. Extremely limited in their commercial availability, these powered exoskeletons (as they are sometimes referred) provide active mobility assistance to the wearer by way of small, yet powerful, electric motors [12, 29]. The rigid-body structure supports the individual's posture, much like a traditional orthosis, while motorized joints actively promote proper joint movement. Still in their infancy, these devices have the potential to benefit a much broader section of the disabled community than conventional mobility support devices.

1.3 Intelligent Mobility Support

While standers are simple devices, actuated by direct means - with little or no need for device intelligence - advanced mobility support devices require a control system to interpret sensory data and dictate dictate an appropriate actuator response, (i.e., to govern how and when the system should move or react). As the dynamics of human motion are quite complex, control systems are often developed for specific movement tasks such as sit-to-stand, stair climbing, or walking. In this work, an artificially intelligent control system is developed for assisting the mobility impaired individual with the sit-to-stand movement, and specifically, it is designed to accommodate the

input/output characteristics of an advanced mobility support device, such as a powered exoskeleton. Powered exoskeletons, worn by the mobility impaired individual, use joint encoders and tilt sensors to monitor the orientation and movement of each body segment of interest. Actuators, acting on the joints of the lower limbs, such as the ankle, knee, and hip, contribute mechanical energy to the movement of the wearer. An ability to maintain balance, statically or dynamically, and recover from perturbation are key requirements of a mobility aid. Therefore, the control system must map sensory input to appropriate actuator response. Fuzzy logic was used to determine the nature of this mapping.

1.4 Expert Knowledge and Fuzzy Logic

Fuzzy logic is an organized and mathematical method of handling inherently imprecise (or vague) concepts. It extends conventional Boolean logic to accommodate the notion of partial truth. Originally introduced as a means to model the uncertainty of natural language, its most successful applications have been the development of the low-cost controllers.

For some industrial processes a human operator has been shown to be more efficient than a conventional automatic controller [26]. This tends to be the case when the process being controlled is more complex than we can deal with mathematically. Fuzzy control can be used to model a human operator's actions using a structured set of IF-THEN rules. For example, the human operator may dictate that

IF *temperature* is *hot* THEN *fan speed* should be *high*

Using a collection of these rules, referred to as a rule-base, expert knowledge of a control process is incorporated into the function of the fuzzy control system itself. No explicit mathematical model of the system being controlled, or *plant*, is

required. As a result, it's possible to develop solutions to complex control problems in a relatively short period of time, which usually translates to cost effective solutions. While conventional trajectory generation methods could also be used to synthesize the sit-to-stand movement, a fuzzy control based approach is appealing for a number of reasons, namely:

- Fuzzy logic accommodates the use of natural language, and there exists a great deal of expert knowledge about the sit-to-stand task, some of which is stated in the language of the human expert. Therefore, fuzzy logic allows us to encapsulate certain forms of expert knowledge [of a control process] that other control methodologies can not.

- The rule base directly relates to our understanding of the process being controlled. This makes it easier to understand the operation of the control system and to maintain it.

- It does not rely on an explicit mathematical model of the plant. Generating detailed mathematical models of complex nonlinear systems can be very costly and even impractical. This cost is only compounded if a detailed model must be created for every instance of controller implementation, e.g., if every user of a system needed to be modeled in detail. Therefore, if an acceptable solution can be found without the use of a detailed mathematical model of the plant, a cost benefit is likely to be had. In other circumstances, it may simply make a practical solution feasible.

- It can be a very powerful tool for dealing quickly and efficiently with imprecision and nonlinearity. The dynamics of the biomechanical model commonly used for sit-to-stand analysis are represented by a system of nonlinear equations. Furthermore, because the model is a gross simplification of the human musculoskeletal system, and the true segment masses of an individual cannot be

measured directly, parameters of the biomechanical model are estimated values. Fuzzy control provides a means of dealing with the nonlinearity of the model's dynamics and the inherent imprecision in the model parameters.

- Good control can be achieved in a relatively short development cycle, again promoting a cost effective solution.

Other motivating factors for the use of fuzzy logic control include:

- The argument has been made that the concepts of fuzzy logic control provide a useful and "biologically compatible" way of describing sensorimotor behavior in animals [21, 22].

- A large body of, primarily semantic, knowledge about the sit-to-stand task already exists

For these reasons, fuzzy control was selected as the control methodology applied in this work.

1.5 Thesis Description and Approach

This thesis presents a fuzzy logic-based control strategy for synthesizing (i.e., artificially reproducing) the sit-to-stand movement, and specifically, one which suits the operation of an advanced mobility support device where the ankle, knee, and hip joints are to be controlled. As is commonly done in sit-to-stand analysis, a simple biomechanical model was used to represent the human musculoskeletal system. It consists of three rigid bodies: the shank, thigh, and HAT (i.e., a single rigid body which represents the head, arms, and trunk). The left and right legs are modelled as a single entity since only a single plane of movement (i.e., the sagittal plane) is considered. This is commonly done because the the sit-to-stand movement is generally considered to be symmetrical about this plane (as illustrated in Figure 2.2).

The joints of the biomechanical model were modelled as perfect hinge (i.e., revolute) joints (also commonly done in sit-to-stand simulation and analysis). Joint stiffness and dampening effects were not modelled. Their effect on the solution is believed to be minimal and an absence of dampening effects allows us to observe any under-damped response in the proposed control system. Also, any sensor noise within the system was assumed to be negligible - a reasonable assumption given that only relatively crude measures of joint angle are required for this particular application (i.e., the value of interest is orders of magnitude larger than high frequency noise present on sensor devices such as optical encoders).

The proposed fuzzy control system was implemented in software using Mathwork's MATLAB^{TM} . For comparison purposes, a motion tracking system was used to collect sit-to-stand data from a single healthy male subject (see Appendix C for details). This set of data was then compared to the simulation results. Impulse testing was used to demonstrate the control system's ability to recover from perturbation (i.e., disturbance).

1.6 Terminology

The use of the term *stability* will generally refer to the biomechanical stability of the three-link biomechanical model (i.e., the plant, or system being controlled), and not the stability of the control system as would be expected in the context of (engineering) control theory.

The term *assistive* (as in "assistive device") will refer to any device which aids or augments the capability of the user. This is not to be confused with the *assist-as-needed* control paradigm where the device is used to bridge the gap between the user's current level of capability and the level of capability required to perform the desired task.

Joint torque refers to the moment of force applied to a joint of the biomechanical

model. The output produced by the proposed control system in this work is a set of joint torques wich correspond to moments of force applied to the ankle, knee, and hip joints respectively.

Bilateral symmetry, or *midline symmetry*, refer to the symmetry of the human body with respect to the left and right portions when divided in half by the midline. The sagittal plane divides the human body into left and right portions.

1.7 Goals

The goals of this work may be summarized as:

- Guide a simple biomechanical model through the sit-to-stand movement
- Develop a control strategy which promotes biomechanical stability (even over energy efficiency)
- Produce a cost-effective and clinically viable control strategy
- Devise a control strategy which avoids the need for re-engineering a solution for potential user
- In keeping with commerically available assistive sit-to-stand devices - produce a slow controlled movement

1.8 Success Criteria

Sit-to-stand was defined as the movement from quiet sitting to quiet standing (i.e., the transition from an inactive sitting configuration to an inactive standing one). Therefore, for the movement produced by the automatic controller to be considered a success, the biomechanical model must achieve quiet standing. In terms of the simulation parameters, "quiet standing" is defined as the configuration of the model where: 1) each joint angle falls within 1 degree of its end-target configuration value, and 2) each joint angle velocity is less than 1 degree/s.

1.9 Organization of Thesis

The remainder of the thesis is organized follows:

- **Chapter 2** presents conventional approaches to rigid body mechanism movement planning and control, namely, trajectory generation and following methods normally applied to industrial robots. The use of model-based control techniques is also introduced for the linear and nonlinear control of a system. Finally, the concept of fuzzy logic, as it applies to the design of fuzzy control systems, is introduced. The basic operation of a fuzzy control system is reviewed in detail.

- **Chapter 3** presents a detailed look at the sit-to-stand movement and common strategies employed by different demographics of the mobile community. The biomechanical model used throughout this work is also presented, from its representation to simulation.

- **Chapter 4** presents the design of each fuzzy system associated with the proposed sit-to-stand control strategy. Three main collaborative control systems are developed: i) a stability controller which promotes improved stability of the plant, ii) a goal controller which tends to motion the biomechanical model toward the goal configuration, and iii) a fuzzy system which interpolates the output of the first two controllers in a desirable fashion.

- **Chapter 5** presents the simulation results and analysis for each of the three main fuzzy control systems developed in Chapter 4. A comparison against the motion capture data provided in Appendix C is also made. Simulation results of impulse testing and model parameter variation are also provided.

- **Chapter 6** provides a summary of the results obtained in this thesis, the concluding remarks, and a discussion of possible future work.

Chapter 2

Movement Planning and Control

2.1 Introduction

The neuromusculoskeletal system is responsible for the control of human movement. Motor control signals originate in the central nervous system. Excitatory and inhibitory signals are summed and then input to motor neurons responsible for the contraction of muscle fibres. A single alpha motor neuron and the muscle fibres it innervates form a motor unit. Motor units typically work together to coordinate the contraction of a single muscle. Muscle contractions, in turn, generate moments of force about our joints. The moments present at two or more joints often collaborate to produce a desired motion.

Automated control systems, used to synthesize human movement, also typically plan the movement at a high-level (and often only one movement task at a time), using either a trajectory generation and following scheme or using expert knowledge of the movement process. Overall, their goal is to coordinate the actions of the controllable joints so that the desired motion (i.e., kinematic) effects are produced. In this respect, the control system mimics the role played by the central nervous system in human movement planning and control. An advanced mobility support device parallels the operation of the human neuromusculoskeletal system, using its actuators (i.e., motors) to assist the wearer as required. Sensors provide the necessary

input to the controller so that an appropriate control action (i.e., actuator response) may be computed. Figure 2.1 provides a system overview of the role a control system plays in a typical advanced mobility support device.

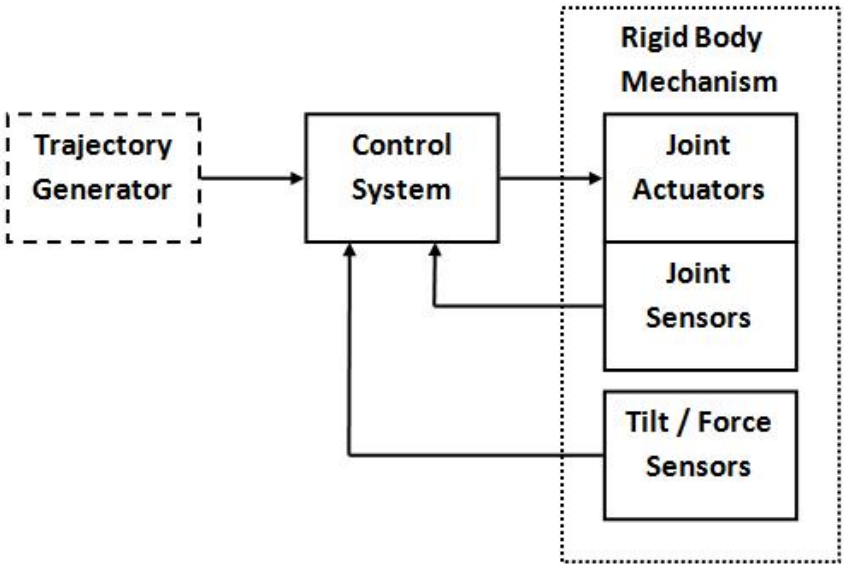

Figure 2.1: Block diagram of a control system's purpose in an advanced mobility support device.

2.2 Control Problem

In this thesis, the control problem involves guiding (i.e., providing appropriate control actions for) a simple biomechanical model through the sit-to-stand movement. A biomechanical model commonly used to analyze and simulate the sit-to-stand movement is shown in Figure 2.2a. The model is a simplified mechanical representation of the human musculoskeletal system. Three joints: the ankle, knee, and hip, articulate a three-link rigid body mechanism, composed of a shank, thigh, and head, arms, trunk (HAT) composite object. Also commonly done in the literature, only movement in the sagittal plane is considered. See Figure 2.2b for a depiction of the sagittal plane. Given this planar restriction, each joint has but one degree of freedom - for a total of three degrees of freedom in the model. Details of the model are discussed in Chapter 3.

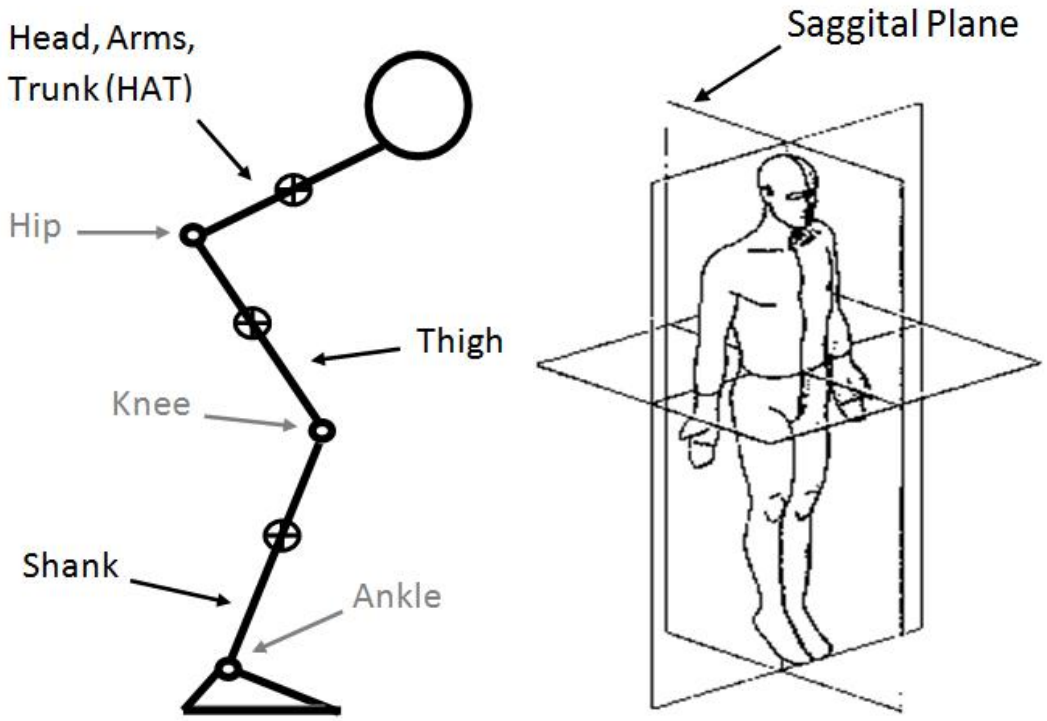

(a) The basic three-link model **(b)** Body planes

Figure 2.2: A simple biomechanical model for sagittal plane study of the sit-to-stand movement.

The availability of a biomechanical model allows us to extend principles and mathematical tools of mechanics to the study and control of human movement. Complete with joint sensors and revolute actuators, the model is essentially a three-link robotic mechanism. Therefore, modelling conventions and mathematical tools normally applied to standard robot manipulators apply equally well to this domain.

Moments of force applied to each joint, are referred to as "joint torques." The solution to the sit-to-stand control problem is therefore a set of joint torques, or control actions,

$$\tau(k) = \begin{bmatrix} \tau_1(k) & \tau_2(k) & \tau_3(k) \end{bmatrix}$$

for $k = 1, 2, \ldots, K$, where K is the number of discrete time steps over the course of the sit-to-stand movement.

2.3 Conventional Movement Planning and Control

Conventional movement planning of a robot manipulator is essentially a two part process: i) the establishment of a trajectory which moves the manipulator from its initial configuration to the desired one, and ii) the design of a control system that causes the robot to follow this trajectory. Here, trajectory refers to the time history of position, velocity, and acceleration for each degree of freedom.

Given that a robot manipulator can be programmed to follow arbitrary paths, polynomials are typically used as a basis for establishing a trajectory. Polynomial functions - and their derivatives - are smooth continuous functions, making them an attractive choice.

In the simplest case cubic splines are used to describe a path from one point in space to another. They can be combined in a piecewise manner to create more complex movement sequences. The use of higher-order polynomials may be desirable as it allows for a greater degree of freedom in the movement but also allows us to specify the desired acceleration at the beginning and end of path segments. Constraints are then placed on the motion in order to arrive at a unique solution. The trajectory may be optimized for energy efficiency, joint torque, or to minimize jerk (i.e., the derivative of acceleration). Constrained optimization techniques have been used to generate movement trajectories for simple biomechanical models in walking [3] as well as the sit-to-stand movement [2, 23].

Since the joints of most robotic systems are purely revolute (i.e., rotational), inverse kinematics is used to transform the desired Cartesian trajectory into a set of corresponding joint angles denoted θ_d.

2.3.1 Trajectory Following

Once a desired trajectory has been established (see Figure 2.3), a control system must then be designed to follow the model. Figure 2.4 provides a block diagram of a trajectory follower.

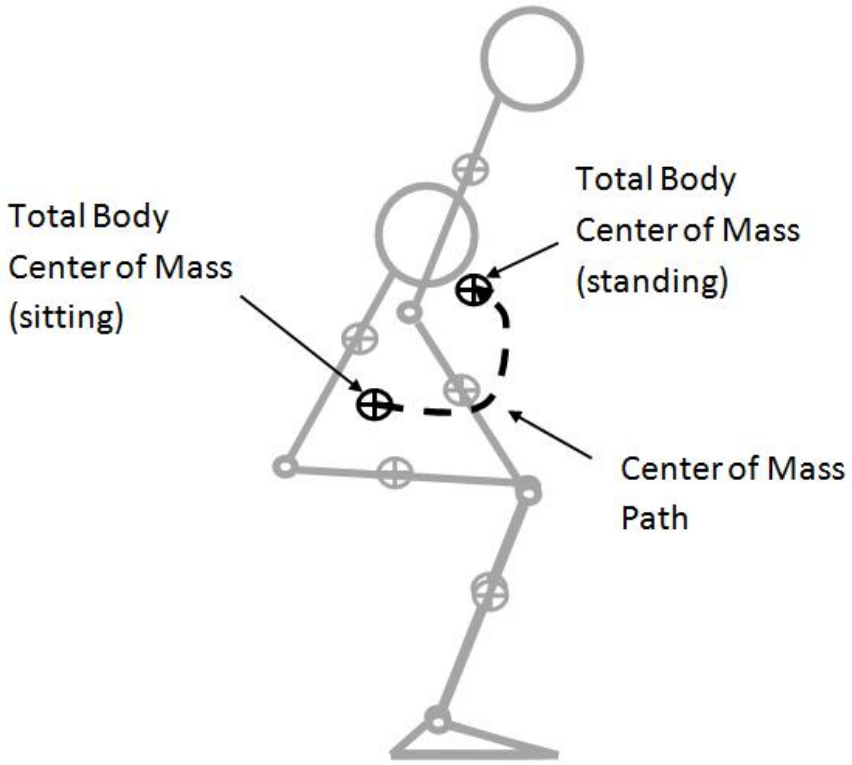

Figure 2.3: Example of a desired Cartesian trajectory.

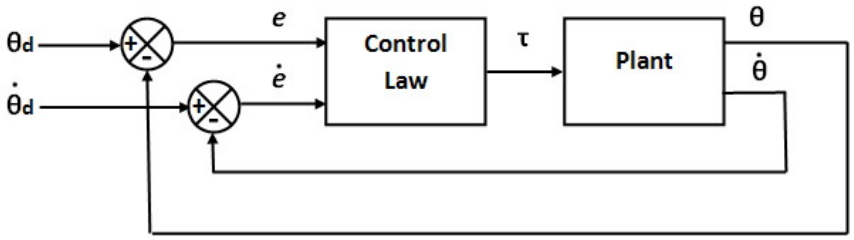

Figure 2.4: Block diagram of a trajectory follower.

Generally, joint sensors are used to feedback position and velocity information from each joint to achieve closed-loop control. The difference between the desired

position and velocity, denoted θ_d and $\dot{\theta}_d$ respectively, and the actual position and velocity, θ and $\dot{\theta}$, is referred to as the servo error. The servo error is calculated as

$$e = \theta_d - \theta \tag{2.1a}$$

$$\dot{e} = \dot{\theta}_d - \dot{\theta} \tag{2.1b}$$

where e and $\dot{e}$ are the errors in position and angular velocity respectively.

The servo error represents how far from the desired trajectory the plant has strayed. Control actions dictated by a closed-loop controller attempt to correct for this error.

2.3.2 Error-Driven Control

Error-driven control schemes rely solely on the servo error for computing their output. One of the most common error-driven control schemes is proportional-integral-derivative (PID) control. The servo error is used by the PID control law to dictate an appropriate control action. The PID control law is written as

$$u = K_p \cdot e + K_i \cdot \int e \cdot dt + K_d \cdot \dot{e} \tag{2.2}$$

where u is the control action output by the controller, K_p the proportional gain, K_i the integral gain, K_d the derivative gain, and e the servo error.

The gains K_p, K_i, and K_d must be adjusted, or "tuned," to achieve the desired controller performance. Typically, average gains are selected which provide (near) critical dampening of disturbances in the most active regions of the system being controlled. However, gains are also generally kept high to quickly suppress unanticipated joint errors - such as those which result from coupling effects, (i.e., the error which develops at one joint due to the actuation of another). Most modern-day industrial robots use simple error-driven control schemes where each joint is controlled

independently with a localized controller. Proportional-derivative control is the most common control scheme applied to the movement control of robot manipulators.

Beyond wide sweeping application in industrial automation and robotics, PID-based error driven control has also been applied to the control of biomechanical models directly [9].

2.3.3 Including a Model

Instead of relying solely on error-driven control, it is sometimes possible to include a model-based term in the control law. Perhaps one of the simplest examples of a model-based controller is the inclusion of a gravity model term in the PID control law

$$u = K_p \cdot e + K_i \cdot \int e \cdot dt + K_d \cdot \dot{e} + \hat{G} \tag{2.3}$$

where $\hat{G}$ is a model-based estimate of gravitational loading effects.

If the model-based portion of the control law is accurate, the use of a model-based term will likely result in improved controller performance. The servo error then serves to correct for unmodelled system dynamics.

2.3.4 Nonlinear Model-Based Control

Systems of rigid bodies, such as the three-link model employed in this work, are governed by nonlinear dynamics whose dynamic equation is commonly written in the form

$$\tau = M(\theta) \cdot \ddot{\theta} + V(\theta, \dot{\theta}) + G(\theta) \tag{2.4}$$

where τ is the set of joint torques (or moments of force) applied to each joint, $M(\theta)$ is the n x n inertia matrix, $\ddot{\theta}$ is an n x 1 vector of joint angular accelerations, $V(\theta, \dot{\theta})$ is an n x 1 vector of centrifugal and Coriolis terms, and $G(\theta)$ is an n x 1 vector of gravity terms.

Given an explicit mathematical model of the plant, the control architecture of the

trajectory follower depicted in Figure 2.4 could be modified to include a (nonlinear) model-based portion in its control law. If a desired acceleration profile, denoted $\ddot{\theta}_d$, were also available, the control architecture could take the form depicted in Figure 2.5. The model-based portion of the control law is included in the feed-forward, or open-loop path, of the controller. It essentially provides a "best guess" at an appropriate control action, denoted τ'. Feedback is used to correct for unmodelled system dynamics, in effect, "fine tuning" the open-loop estimate.

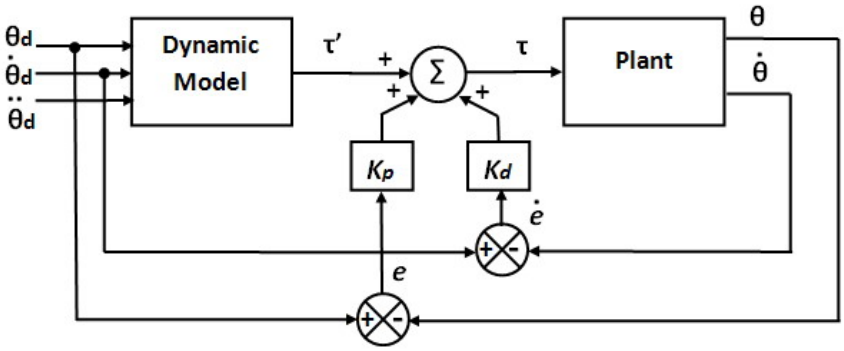

Figure 2.5: Block diagram of a model-based trajectory follower.

The control law for this control system now includes a (nonlinear) model-based portion as well as the servo portion

$$\tau = \tau' + K_p \cdot e + K_d \cdot \dot{e} \tag{2.5}$$

If a highly accurate model of the system is available, it's possible to control the movement of a powered mobility assist device, almost entirely, using the forces acting on the device itself [13, 39]. Other model-based mobility assistance include [17].

2.3.5 Linear Model-Based Control

A linear model may be used to approximate the nonlinear dynamics of a system in regions of operation where the nonlinearities are not severe. Linearization is conducted at specific operating points - usually at points of equilibrium or in regions where the

plant dynamics are slowly varying. The linear approximation is only valid within the neighborhood of its associated operating point. Using the sit-to-stand movement as an example, quiet sitting and quiet standing are both natural points of equilibrium where linearization techniques would be viable.

Using a linear model approximation not only reduces the complexity of the control problem, but it makes available a number of control engineering tools which exist for dealing with linear systems. For example, only linear systems may be represented in the convenient state-space vector-matrix form

$$\dot{x}(t) = A(t) \cdot x(t) + B(t) \cdot u(t) \tag{2.6a}$$

$$y(t) = C(t) \cdot x(t) + D(t) \cdot u(t) \tag{2.6b}$$

where x is an n x 1 vector of state variables, $\dot{x}$ is the time derivative of x, y is the q x 1 output vector, u is the p x 1 input vector, A is the n x n state matrix, B is the n x p input matrix, C is the q x n output matrix, and D is the q x p feedforward matrix. Also, methods for the stability analysis and optimization of linear systems are particularly useful.

Once the system has been linearized, a simple controller may be designed for each linear approximation. The result is a family of linear controllers each of which provides satisfactory control in its respective region of operation. Switching between linear controllers (as the plant moves out of the neighborhood of one operating point and into the bounds of another), results in a piecewise linear solution to the nonlinear control problem.

For example, this control strategy might be used in the automated flight control system of an aircraft. A series of linear controllers, each optimized for different flight conditions such as altitude or the mass of the aircraft (since its mass will lessen over time as a result of fuel consumption), is designed. One controller is

selected over another based on its relevance to the current operating condition of the aircraft. Interpolating between controllers often results in improved control system performance. This is most apparent when there is only a handful of controllers to choose from and large "gaps" between operating points make controller selection ambiguous.

Linear control for synthesizing the sit-to-stand movement was conducted in [16]. An explicit movement trajectory was not generated; instead, linear control systems were designed to meet specific movement objectives. A simple Gaussian function was used to interpolate between the controllers. One controller was weighted more heavily in regions of operation near quiet sitting while the other was weighted move heavily in the neighborhood of quiet standing. Using a simple mathematical function to interpolate between two linear controllers will not likely result in the production of a natural sit-to-stand movement; however, the concept is a notable one.

2.3.6 Summary of Model-Based Control

Linear model-based control is not typically used with robot manipulators given their tendency to constantly move between widely separated regions of their workspace. And while model-based control strategies can offer improved performance over solely error-driven control schemes, this is only the case if a reasonably accurate model of the plant is attainable. Since model-based parameters are included in the control law, inaccuracies in these parameters propagate through the controller and will likely have unwanted direct effects on controller performance. A lack of system parameter information may nullify the benefits of using a model-based approach. In fact, if the model is a poor approximation of the true system dynamics, inferior control may result as compared to simpler error-driven control techniques such as PID control. For this reason, many present-day industrial robot manufacturers have opted to use simple control schemes which contain no model-based element whatsoever, or possibly only very simple model-based elements such as gravity compensation.

2.3.7 Summary of Conventional Movement Planning and Control

Certainly conventional trajectory generation and following schemes could be used with the rigid-body biomechanical model depicted in Figure 2.2a, but their practicality regarding the movement planning and control of advanced mobility support devices for a diverse range of users is questionable.

Movement trajectories must be planned in their entirety prior to executing the movement. Trajectory generation is a precise mathematical operation; therefore, an accurate model of the system being controlled is often required to support it. Due to the anatomical variation between clients, a certain degree of remodelling and redesign can be expected when using these methods.

Assuming a polynomial based trajectory scheme is used; selecting too low an order polynomial will not allow for a natural movement. Higher order polynomials, on the other hand, require schemes, such as optimization, to arrive at a unique solution. While optimization is possible, a complete mathematical model of the client plus mobility support apparatus must be available in order for the results to be meaningful.

The potential remodelling and redesign between clients puts the efficacy of conventional movement planning and control approaches into question for this problem domain. Furthermore, little expert knowledge of the task itself is incorporated into the movement planning process. For example, objective functions, used to optimize human movement trajectories, often rely on a single quantity, such as joint torque to compute the necessary control actions. Little to no expert knowledge of the sit-to-stand movement is incorporated into such a movement planning process. However, the human expert may be aware of when it is best to trade off energy efficiency for stability over the course of the movement.

Therefore, movement planning and control schemes which rely less heavily on detailed mathematical models, and more heavily on expert knowledge of the control

process, may lead to more practical, cost effective, control solutions for the advanced mobility support device.

2.4 Human-in-the-Loop Control

Until now, only fully automated movement control systems that do no rely on user input have been considered. The trajectory generation process and other model-based approaches have so far relied on prescribed movement objectives. But in the design of an active mobility assist device, there may be cases where the user is able to provide valuable input to the movement control process.

Because high-level motor control signals ultimately result in muscle activity patterns, one means of discerning user intention is to sample their gross motor activity. Small biosensors are placed on the surface of the skin, located above the muscle groups of interest. Once sampled (using surface electromyography, or SEMG), muscle activity patterns are forwarded to the control system on board the mobility assist device. The control system is used to map muscle input patterns to appropriate joint actions [7, 14, 25].

The HAL (Hybrid Assistive Limb) quasi robotic exoskeleton [6, 11] in particular uses a hybrid control approach where a fully automated movement control solution is computed in addition to user directed (or human-in-the-loop) movement control processes. The human-in-the-loop control scheme effectively amplifies the wearer's strength by mapping their muscle activity patterns to joint motors on the exoskeleton.

2.5 Fuzzy Logic Control

2.5.1 Leveraging Expert Knowledge

Biosignal control leverages the user's innate movement planning and control capabilities and incorporates them into the control strategy of the power assist device. This control scheme is best suited to individuals who possess good muscle coordination

and wish to augment their physical strength. While likely not an appropriate solution for the typical mobility impaired person, drawing on human experience to direct the actions of the mobility support device has proven to be an effective control strategy which does not require a mathematical model.

But, because a large body of knowledge about the sit-to-stand operation already exists, if this information could be incorporated into the control system itself, there would be little need to rely on input from the user. Therefore, not only could individuals with poor muscle coordination make use of such a system, but preconceived notions of proper movement would eliminate the need for generating arbitrary polynomial-based trajectories. Thus, good control could also potentially be achieved, again without the use of a detailed math model, while offering support to a wider section of the mobility impaired community. The end-goal would be a system that can be easily adapted or "tuned" to the needs of the user without a significant amount of biomechanical remodelling or control system redesign. Ultimately, this would translate into a viable and cost effective solution for the control of advanced mobility support devices.

2.5.2 Introduction to Fuzzy Logic-Based Control

Fuzzy control is the most successful application of fuzzy logic. While fuzzy logic is an organized method of handling inherently imprecise concepts, fuzzy control is a formal methodology for representing and implementing heuristic knowledge of a control process [19].

Fuzzy logic is a multi-valued logic system which extends conventional set theory to accommodate the notion of partial set membership. Classical set theory allows an element to hold one of two membership states in any given set: membership, or non-membership. The membership function $\mu_A(x)$ for the set A and element x can take on one of two values: $\{0, 1\}$, with 0 indicating non-membership and 1 indicating membership. However, fuzzy logic allows elements to hold partial set membership.

The fuzzy membership function can take on any value in the range $[0, 1]$. The degree of membership reflects the certainty that an element x belongs to a set A.

Fuzzy logic was originally introduced as a means to model the uncertainty of natural language. It allows the human expert to express their understanding of a control process in the form of a structured linguistic description.

2.5.3 Linguistic Variables and Values

We denote the system input variables as u_i existing on the domain U_i, where $i = 1, 2, \ldots, n$ and the system output variables as y_i existing on Y_i where $i = 1, 2, \ldots, m$. The variables u_i and y_i are ordinary or "crisp" (i.e., non-fuzzy) variables. In the literature, the domains U_i and Y_i are known as *universes of discourse* [38]. u_i and y_i are ordinary variables that take on "crisp" (i.e., non-fuzzy) real numbered values. Linguistic variables, denoted $\tilde{u}_i$ and $\tilde{y}_i$, are used to describe characteristics of u_i and y_i respectively. They are assigned linguistic values rather than real numbers. For example, the linguistic value "warm" may be assigned to the linguistic variable *temperature*. Let $\tilde{A}^i_j$ represent the j^{th} linguistic value of the linguistic variable $\tilde{u}_i$. The set of linguistic values, $\tilde{A}_i$, associated with $\tilde{u}_i$ is written as

$$\tilde{A}_i = \left\{ \tilde{A}^i_j : j = 1, 2, \ldots, N_i \right\}$$

2.5.4 Membership Functions

Membership functions are mathematical functions which describe the certainty that an element, taken from a universe of discourse, is characterized by a particular linguistic value. Let U_i denote a universe of discourse and $\tilde{A}^i_j \in \tilde{A}_i$ denote a particular linguistic value for the linguistic variable $\tilde{u}_i$. The membership function $\mu(u_i)$, associated with the linguistic value $\tilde{A}^i_j$, specifies the certainty that the crisp input $u_i \in U_i$ may be characterized as $\tilde{A}^i_j$. Certainties are stated as numeric values existing on the

range [0,1]. Therefore, the membership function $\mu()$ maps the universe of discourse U_i to [0,1].

Take, for example, the height of all men in a given population. Using membership functions, we may quantify the certainty we have in characterizing a particular height as either "short" and/or "tall." Figure 2.6 illustrates this point.

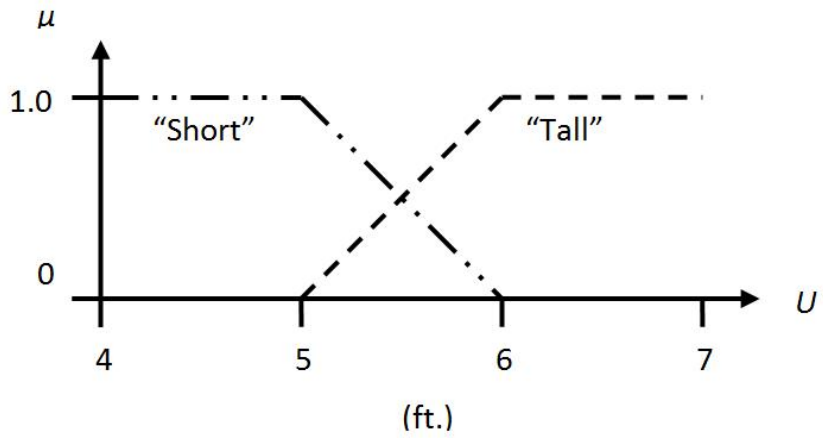

Figure 2.6: Membership functions for the linguistic variables "short" and "tall".

In this example, we are entirely certain that a height of 6 ft. or greater should be characterized as "tall," while heights below 5 ft. should be characterized as "short." Heights falling within this range are characterized as "short" and "tall" to varying degrees of certainty. From Figure 2.6 it can be seen that membership functions can be represented graphically as a two-dimensional graph with the domain U on the horizontal axis and the membership μ on the vertical axis.

Types of Membership Functions

Two commonly employed types of membership functions are: i) triangular, and ii) Gaussian. A triangular membership function has the form

$$\mu(x) = \begin{cases} 0 & x < \gamma - \sigma, \\ 1 - \frac{|x-\gamma|}{\sigma} & \gamma - \sigma \leq x \leq \gamma + \sigma, \\ 0 & x > \gamma + \sigma \end{cases}$$

where the parameter γ specifies the center of the triangular function, and the parameter σ specifies its width, while a Gaussian membership function is of the form

$$\mu(x) = exp\left[-\left(\frac{x-\gamma}{\sigma}\right)\right]$$

where the parameter γ specifies the center of the Gaussian function, and the parameter σ specifies its width.

Triangular membership functions are particularly common; especially in systems with limited computational power. This is because mathematical operations involving triangles are simple, and can therefore be evaluated quickly. Gaussian membership functions are continuous, differentiable functions which provide smooth transitions between neighboring functions on the same universe of discourse. Calculation of the exponential term, however, puts greater computational load on the processor used to implement the fuzzy system during the rule firing and defuzzification processes (where "rule firing" and "defuzzification" are explained in Section 2.5.8). In a Takagi-Sugeno system however, the defuzzification process is greatly simplified (through the use of fuzzy singletons), and therefore, the use of Gaussian membership functions does not load the processor any more than would triangular membership functions. The exponential term of the Gaussian would have to be computed during the rule firing process however, in order to determine the relevance of each rule to the controller input.

Triangular membership functions are normally defined such that they overlap one another, similar to the functions presented in Figure 2.6. This ensures that a linear blending of membership values takes place in regions of the universe of discourse where neighboring membership functions overlap.

In this work, only triangular types of membership functions were used. This was done for design simplicity in defining the membership functions themselves (linear

definitions are straightforward), and for computational simplicity during rule firing. Also, the possibility of implementing adaptive control is left available to the control engineer in using triangular membership functions, which is attractive. Gaussian membership functions specify some finite non-zero membership over the entire universe of discourse. This may be undesirable in fuzzy systems utilizing adaptive control techniques because of its effects on the adaptation algorithm [8, 32], (i.e., the algorithm may modify fuzzy sets, where "fuzzy sets" are explained in Section 2.5.5), which are far from the current operating region.

2.5.5 Fuzzy Sets

Fuzzy sets are simply the pairing of elements, taken from a universe of discourse, with their respective membership function values. The fuzzy set, denoted A_j^i, associated with the linguistic value $\tilde{A}_j^i$, for the input variable $u_i \in U_i$ is defined as

$$A_j^i = \left\{ (u_i, \mu_{A_j^i}(u_i)) | u_i \in U_i \right\}$$

where the membership function $\mu_{A_j^i}(u_i)$ describes the certainty in which the element u_i has membership in fuzzy set A_j^i.

2.5.6 Fuzzy Rule Base

Fuzzy control relies on control directives, or rules, in the form

IF premise THEN consequent.

For example, the human expert may dictate:

IF *temperature* is "hot" THEN *fan speed* is "high"

The linguistic input variable *temperature* is assigned the linguistic value "hot," while

the linguistic output variable *fan speed* is assigned a linguistic value "high." The collective set of rules associated with a fuzzy system is referred to as a rule base. The rule base allows the fuzzy system to emulate the human decision making process.

Fuzzy systems perform a static nonlinear mapping between their inputs and outputs. The nature of the mapping is, in large part, dictated by the rule base.

Rule Base Characteristics

Properties of a rule base include *completeness* and *consistency*.

1. **Completeness**

   For a rule-base to be complete, a conclusion must be reached (i.e., an output specified) for every possible input to the controller. Generally, completeness is assured if a consequent is specified for every premise in the rule base.

2. **Consistency**

   For a rule-base to be consistent, no two rules which share the same premise may state conflicting consequents.

2.5.7 Types of Fuzzy Inference Systems

Standard, or Mamdani type, fuzzy systems use linguistic variables in both the premise and consequent of their rules. The Takagi-Sugeno type however, uses linguistic variables only in the premise of its rules; its consequent is a linear (or affine) function [28]. Consequents of this type do not have an associated membership function. The function specified in the consequent of the i^{th} rule is evaluated to produce a single numeric result b_i. The consequents, therefore, exist only as fuzzy singletons, located at b_i on the output space Y. Rules for a multiple-input single-output (MISO) Takagi-Sugeno type fuzzy inference system are written in the form

IF u_1 is $\tilde{A}_j^1$ and u_2 is $\tilde{A}_k^2$ and $\ldots$ and u_n is $\tilde{A}_l^n$ THEN $b_i = f_i(\cdot)$

where b_i is the consequent of the i^{th} rule and $f_i(\cdot)$ represents an linear or affine function. Often $f_i(\cdot)$ is a function of the input variables such that

$$f_i(u_1, u_2, \ldots, u_n) = C_1 \cdot u_1 + C_2 \cdot u_2, + \ldots + C_n \cdot u_n + K$$

where C_1, C_2, ..., C_n, and K are constants.

The Takagi-Sugeno fuzzy system is typically more efficient in its operation than the standard, Mamdani type. This is mostly a result of resolving fuzzy singletons, quickly and efficiently, on the output space rather than dealing with fuzzy sets and membership functions. The ability to specify linear functions in the consequents of the rules is also generally appealing to the control engineer. For example, functions which represent linear control systems may be specified as the consequents of the rules in a Takagi-Sugeno fuzzy system. For these reasons, Takagi-Sugeno fuzzy systems were used exclusively throughout this work.

2.5.8 Fuzzy Control System Architecture and Operation

Four main components make up the fuzzy control architecture: i) fuzzification interface ii) inference mechanism, iii) rule-base, and iv) defuzzification interface (see Figure 2.7).

Fuzzification

The process of fuzzification "transforms" the input u_i into its equivalent fuzzy set A_j^i. Quite often the simplest form of fuzzification, "singleton fuzzification", is used for this purpose. Singleton fuzzification creates a fuzzy set by simply assigning a membership of 1.0 to elements on the universe of discourse U_i where $U_i = u_i$ and 0

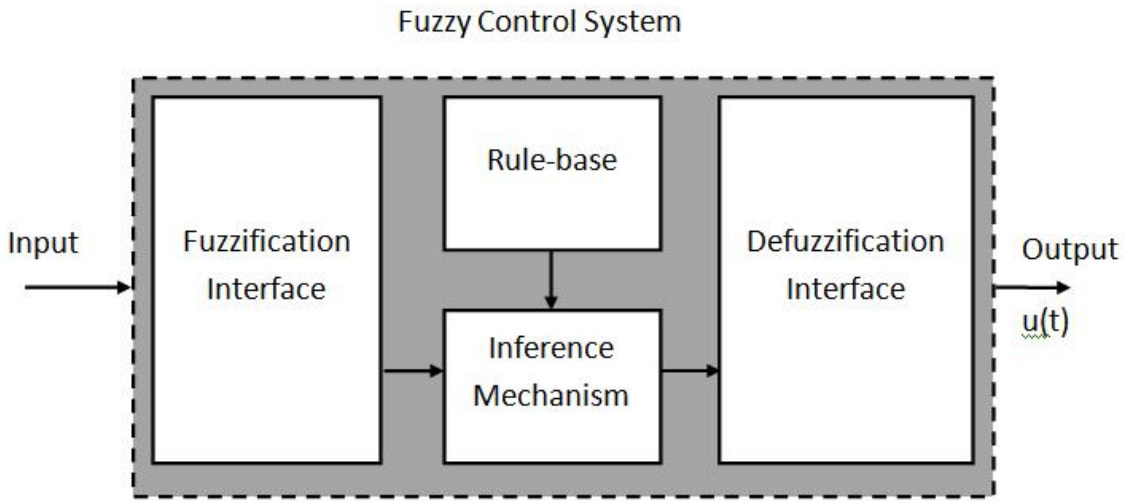

Figure 2.7: Fuzzy control system architecture.

to all others. Its membership function may be stated as

$$\mu_{fuz}(x) = \begin{cases} 1, & x = u_i \\ 0, & \text{otherwise} \end{cases}$$

Singleton fuzzification may be represented as a discrete impulse function (see Figure 2.8.

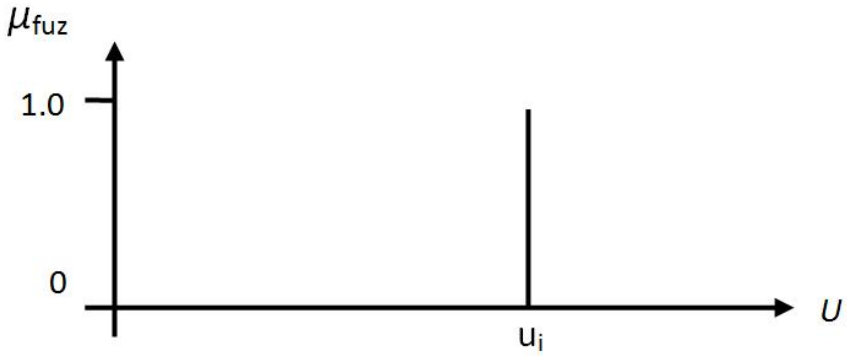

Figure 2.8: Example of a fuzzy singleton.

Inference Mechanism and Rule Firing

The fuzzy sets associated with the input variables, (i.e., $A_j^1, A_k^2, ..., A_l^n$), are used to quantify the elements in the premise of the rules in the rule-base. For a Takagi-Sugeno fuzzy system this takes the form

$$\text{IF } A_j^1 \text{ and } A_k^2 \text{ and } , \ldots , \text{ and } A_l^n \text{ THEN } b_i = f_i()$$

where b_i is the consequent of the i^{th} rule and $f_i()$ represents an affine function.

In this work, the method used to perform the "and" operation in the premise of each rule is the product method where the certainties associated with each term are simply multiplied together. Since singleton fuzzification was used, the relevance of a rule to a given set of input values u_1, u_2, ..., u_n is determined by

$$\mu_i(u_1, u_2, \ldots, u_n) = \mu_{A_j^1}(u_1) \cdot \mu_{A_k^2}(u_2) \cdot \ldots \cdot \mu_{A_l^n}(u_n) \tag{2.7}$$

where $\mu_i(u_1, u2, \ldots, u(n))$, represents the relevance of the i^{th} rule in the rule-base. The consequent of each rule is scaled by the certainty held by its premise to form the implication

$$b_i \cdot \mu_i(u_1, u2, \ldots, u(n)) \tag{2.8}$$

This reflects how certain we are that the i^{th} rule applies to a given set of inputs, and therefore, the degree to which the rule should be fired. All rules in the rule-base are fired to some degree during the inference step.

Defuzzification

Defuzzification is used to transform the implications $b_i \cdot \mu_i(u_1, u2, \ldots, u(n))$ for $i = 1, 2, \ldots, R$ where R is the number of rules in the rule-base, which result from firing all rules in the rule-base, into a crisp output. For the Takagi-Sugeno inference system,

defuzzification may be obtained using

$$y = \frac{\sum_{i=1}^{R} b_i \cdot \mu_i}{\sum_{i=1}^{R} \mu_i} \tag{2.9}$$

where y is the crisp output of the controller. This method of defuzzification is referred to as the "weighted average" method and is used for all Takagi-Sugeno systems developed in this work.

2.5.9 Fuzzy Systems as Nonlinear Interpolators

When multiple rules are fired, a Mamdani fuzzy system, in effect, performs a nonlinear interpolation between the linguistic values implied by the consequents of the rules. A Takagi-Sugeno fuzzy system, then, performs a nonlinear interpolation between the linear functions defined in its consequents. This attribute of Takagi-Sugeno fuzzy systems has proven to be particularly useful for interpolating between sets of linear controllers.

2.5.10 Fuzzy Systems as Universal Approximators

Many fuzzy systems are known to satisfy the universal approximation property [31, 37], meaning, they are able to approximate any real continuous function on a closed and bounded set to an arbitrary degree of precision. This property serves as an existence theorem; that if an optimal solution to the control problem exists, there exists a fuzzy system which can approximate this solution to any desired degree of accuracy.

2.5.11 Controller Tuning

The fuzzy logic controller must often be refined or "tuned" to achieve the desired controller performance. Tunable parameters of the fuzzy control system include: i) the number of input variables, ii) the number of linguistic values which may be used

to describe them, iii) the size, shape, and position of the membership functions, iv) and the nature of the rules in the rule base.

2.6 Chapter Summary

While conventional approaches to movement planning and control could be applied to quasi robotic systems, such as advanced mobility support devices, their need for a complete, and often accurate, mathematical model (of the system being controlled) may very well render them cost ineffective and clinically infeasible. A system, which leverages the body of knowledge about the sit-to-stand movement, and does not require a great deal of remodelling or system redesign between clients, offers a potentially cost effective and clinically viable solution. For this reason fuzzy logic-based control was explored in this work.

Chapter 3

Biomechanical Modelling and the Sit-to-Stand Task

3.1 Introduction

In this chapter, a detailed discussion of the sit-to-stand movement is presented along with the biomechanical model used throughout this work. This in-depth examination of the sit-to-stand movement allows its key characteristics and phases of operation to be identified which inform the construction of the knowledge base required for its artificial reproduction. Also, simulating the movement provides insight into the motor torque requirements of the physical actuators needed to assist an individual with the movement and helps identify the most effective control strategies.

3.2 Biomechanical Model

As is commonly done in sit-to-stand analysis, only movement in the sagittal plane is considered (see Figure 2.2b). The sagittal plane is the imaginary plane that divides the body into left and right halves (assuming midline, or *bilateral*, symmetry), and it is within this plane that the vast majority of the sit-to-stand movement takes place. Under the assumption of bilateral symmetry, only movement in the sagittal plane must be considered. The human musculoskeletal system is represented as a serial

linkage of three rigid body segments [1, 27] - the shank, thigh, and head-arms-trunk (HAT) (see Figure 2.2a). Given that the movement is symmetrical about the sagittal plane, the left and right legs are often modelled as a single entity with twice the mass. As is also commonly done in sit-to-stand analysis, the foot is only shown for reference, but was not included as part of the dynamic model (since it plays no role in the dynamics of the movement). Revolute, or "hinge" joints are used to articulate the model at the ankle, knee, and hip. Each joint has a single degree of freedom (DOF) whose axis of rotation is perpendicular to the sagittal plane. The model, therefore, has a total of three degrees of freedom. A revolute actuator, or *torque motor*, is connected to each joint so that moments of force may be generated about the axis of rotation (see Figure 3.10).

3.2.1 Frames of Reference and the World Coordinate System

Frames of reference are attached to the base of each rigid-body segment, or *member*. They are coordinate systems which allow us to describe and manipulate the orientation of a segment. In this work, reference frames are denoted by a set of curly braces containing the frame's number, e.g., {1} would indicate frame one. The X-Axis of each reference frame is aligned along the length of the member, while the Z-Axis coincides with the axis of rotation (perpendicular to the sagittal plane). The positive Z-Axis is defined as coming out of the page. The Y-Axis is orthogonally projected from the X-Z plane using right-hand-rule (RHR) convention (see Figure 3.1).

Frame {0}, located at the ankle, serves as a world coordinate system (WCS) reference for the biomechanical model. The ankle is located at its origin, $\begin{bmatrix} 0 & 0 \end{bmatrix}$. The WCS provides an absolute (or "global") sense of position and orientation. X_0 is projected along the horizontal, while Y_0 is projected along the vertical, and Z_0 is the imaginary rotational axis orthogonal to the sagittal plane (coming out of the page). Frame {1} is attached to the base of the shank at the ankle with its X-Axis, X_1,

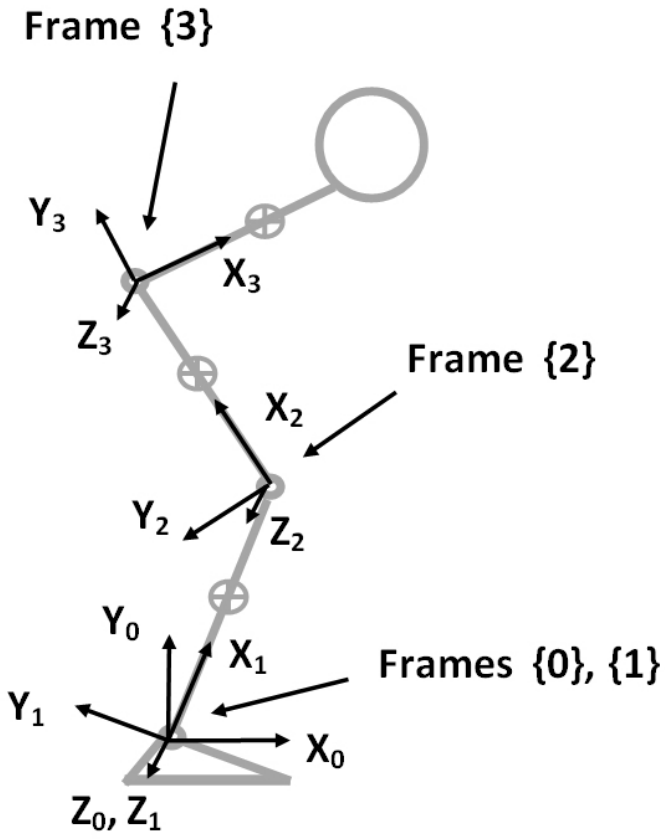

Figure 3.1: Biomechanical model with frames of reference.

projected along the length of the shank. Similarly, frame {2} is attached to the base of the thigh at the knee, and frame {3} is attached to the HAT at the hip.

3.2.2 Anatomical Parameters

Anatomical parameters of the model, including link length, segment mass, moment of inertia, etc., were determined using methods adopted from Winter [35]. Details of the anthropometric property calculations of the biomechanical model are included in Appendix A, while a summary of the anthropometric data provided by Winter is included in Table 3.1.

The mass of the i^{th} rigid body segment was represented as a point mass located at the center of mass location $l_{CoM(i)}$ (see Figure 3.2).

The mass of the i^{th} rigid body segment, l_i, was calculated as a percentage of the total-body mass (tbm) using the Segment Mass Ratio provided in Table 3.1, e.g., for

	Shank	Thigh	HAT
Segment Mass Ratio (Segment Mass/ Total Body Mass)	0.0465	0.100	0.678
Segment Length Ratio (Segment Length/ Total Body Height)	0.246	0.245	0.288
Center of Mass Ratio (Center of Mass/ Segment Length)	0.567	0.567	0.626
Radius of Gyration Ratio (Radius of Gyration/ Segment Length)	0.302	0.323	0.496

Table 3.1: Anthropometric Data for the Biomechanical Model.

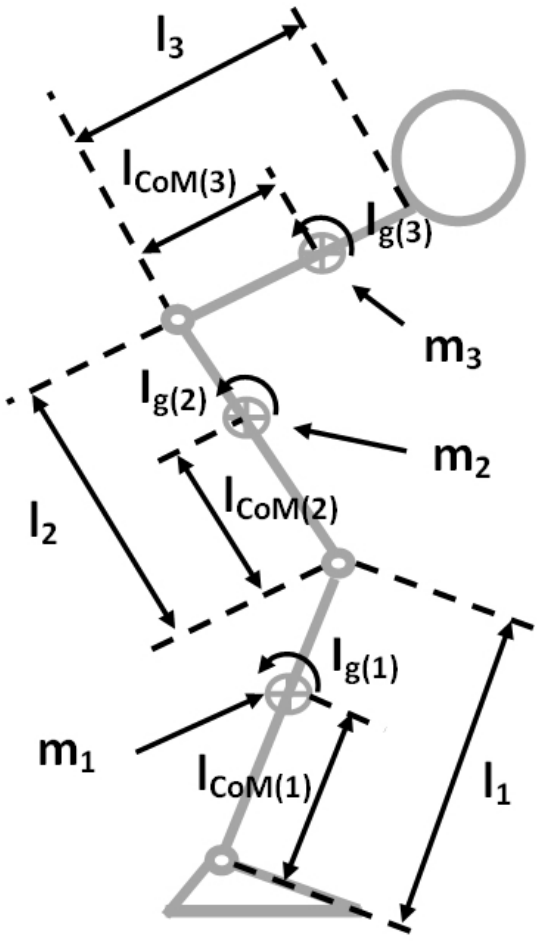

Figure 3.2: Biomechanical model with anthropometric measures.

the shank

$$m_1 = 2 \cdot 0.0465 \cdot tbm$$

where the 2 times multiplication factor is used because the left and right legs were modelled as a single entity with twice the mass.

The length of the i^{th} rigid body segment, l_i, was calculated as a percentage of the total-body height (tbh) using the Segment Length Ratio provided in Table 3.1, e.g., for the shank

$$l_1 = 0.246 \cdot tbh$$

The distance of the center of mass for the i^{th} rigid body segment from its base, $l_{CoM(i)}$, was calculated as a percentage of the segment length l_i using the the Center of Mass Ratio provided in Table 3.1, e.g., for the shank

$$l_{CoM(1)} = 0.567 \cdot l_1$$

The radius of gyration for the i^{th} rigid body member, k_i, was calculated as a percentage of the body segment's length l_i using the Radius of Gyration Ratio provided in Table 3.1, e.g., for the shank

$$k_i = 0.302 \cdot l_1$$

The moment of inertia, about the rotation axis, Z_i, for the i^{th} rigid body member, denoted $I_{g(i)}$, was calculated using the mass m_i and radius of gyration k_i

$$I_{g(i)} = m_i \cdot k_i^2$$

e.g., for the shank

$$I_{g(1)} = m_1 \cdot k_1^2 = m_1 \cdot (0.302 \cdot l_1)^2$$

3.2.3 Rigid Body Center of Mass

The location of the center of mass for the shank $\begin{bmatrix} x_{CoM(1)} & y_{CoM(1)} \end{bmatrix}^T$, thigh $\begin{bmatrix} x_{CoM(2)} & y_{CoM(2)} \end{bmatrix}^T$, and HAT $\begin{bmatrix} x_{CoM(3)} & y_{CoM(3)} \end{bmatrix}^T$ were computed as

$$\begin{bmatrix} x_{CoM(1)} \\ y_{CoM(1)} \end{bmatrix} = {}^0_1R \cdot \begin{bmatrix} l_{CoM(1)} \\ 0 \end{bmatrix} \tag{3.1a}$$

$$\begin{bmatrix} x_{CoM(2)} \\ y_{CoM(2)} \end{bmatrix} = {}^0_2R \cdot \begin{bmatrix} l_{CoM(2)} \\ 0 \end{bmatrix} + {}^0_2P \tag{3.1b}$$

$$\begin{bmatrix} x_{CoM(3)} \\ y_{CoM(3)} \end{bmatrix} = {}^0_3R \cdot \begin{bmatrix} l_{CoM(3)} \\ 0 \end{bmatrix} + {}^0_3P \tag{3.1c}$$

where ${}^0_iR$ is the 2 x 2 rotation matrix representing the rotation of frame $\{i\}$ with respect to frame $\{0\}$ by an angle θ in the form

$$\begin{bmatrix} cos(\theta) & -sin(\theta) \\ sin(\theta) & cos(\theta) \end{bmatrix}$$

and ${}^0_iP$ is a 2 x 1 vector which represents the translation of frame $\{i\}$ with respect to frame $\{0\}$.

3.2.4 Total Body (Whole Body) Center of Mass

The location of the center of mass (CoM) for a system of n rigid bodies, $\begin{bmatrix} x_{CoM} & y_{CoM} \end{bmatrix}$, is found using the weighted sum

$$x_{CoM} = \frac{\sum_{i=1}^{n} m_i \cdot x_{CoM(i)}}{\sum_{i=1}^{n} m_i} \tag{3.2a}$$

$$y_{CoM} = \frac{\sum_{i=1}^{n} m_i \cdot y_{CoM(i)}}{\sum_{i=1}^{n} m_i} \tag{3.2b}$$

where $\begin{bmatrix} x_{CoM(i)} & y_{CoM(i)} \end{bmatrix}$ is the location of the center of mass of the i^{th} rigid body segment (Equation 3.1) and m_i its mass.

Therefore, for the model depicted in Figure 3.1, the total body (or whole body) center of mass is calculated as

$$x_{CoM} = \frac{m_1 \cdot x_{CoM(1)} + m_2 \cdot x_{CoM(2)} + m_3 \cdot x_{CoM(3)}}{m_1 + m_2 + m_3} \tag{3.3a}$$

$$y_{CoM} = \frac{m_1 \cdot y_{CoM_(1)} + m_2 \cdot y_{CoM_(2)} + m_3 \cdot y_{CoM_(3)}}{m_1 + m_2 + m_3} \tag{3.3b}$$

where the locations of the centers of mass of the rigid body segments, denoted $\begin{bmatrix} x_{CoM(i)} & y_{CoM(i)} \end{bmatrix}$ for $i = 1, 2, 3$ are given in Equation 3.1, and the segment masses m_1, m_2, and m_3, are given in Appendix A.

3.2.5 Model Parameter Estimates

Because the mass and the location of the center of mass of a limb segment cannot be easily measured, it would be unrealistic to assume perfect knowledge of these model parameters; therefore, estimates for these parameters were used instead. Because the HAT's mass, denoted m_3, is by far the most influential mass within the rigid body

system, it was varied by a tolerance α

$$\hat{m}_3 = m_3 \pm m_3 \cdot \alpha \tag{3.4}$$

where α is a tolerance $\in \{-0.25, 0, 0.25\}$. These values were used because it was assumed that the human expert is able to estimate mass parameter m_3 within 25% of its true value; therefore, the worst case estimates occured at $\pm 25\%$ of the true value.

Furthermore, it was assumed, for simulation purposes, that the center of mass of each rigid body segment was located at its midpoint

$$\hat{l}_{CoM(i)} = \frac{l_i}{2} \tag{3.5}$$

where $\hat{l}_{CoM_{(i)}}$ is the estimated location of the center of mass for the i^{th} rigid body member and l_i is its length. As seen in Table 3.1, the true locations of the center of mass for each rigid-body segment lie along the member at $0.567 \cdot l_1$, $0.567 \cdot l_2$, and $0.626 \cdot l_3$, for the shank, thigh, and HAT respectively. The midpoint is a reasonably accurate approximation of these values and, of equal importance, can be easily identified through measurement.

Substituting these estimates for the model parameters in Equation 3.2

$$\hat{x}_{CoM} = \frac{m_1 \cdot \hat{x}_{CoM(1)} + m_2 \cdot \hat{x}_{CoM(2)} + m_3 \cdot \hat{x}_{CoM(3)}}{m_1 + m_2 + \hat{m}_3} \tag{3.6a}$$

$$\hat{y}_{CoM} = \frac{m_1 \cdot \hat{y}_{CoM(1)} + m_2 \cdot \hat{y}_{CoM(2)} + m_3 \cdot \hat{y}_{CoM(3)}}{m_1 + m_2 + \hat{m}_3} \tag{3.6b}$$

3.2.6 Base of Support and Model Stability

A base of support (BoS) is the area bounded by all points of contact between the biomechanical model and the supporting surfaces [33], (i.e., the ground and/or chair's

surface in the case of sit-to-stand). Since our model exists in the 2-dimensional sagittal plane, its base of support while standing is defined as the linear region extending from the heel of the foot to the toe. While the foot was not included as part of the biomechanical model, its dimensions were used in establishing the base of support. Dimensions for the foot are shown in Figure 3.3, and dimensions a and b were computed as given in Equation 3.7.

$$a = 0.34 \cdot l_{foot} \tag{3.7a}$$

$$b = 0.66 \cdot l_{foot} \tag{3.7b}$$

where the values 0.34 and 0.66 are proportions representing the distance from the ankle to the heel and ankle to the toe respectively, recorded for the test subject used to collect the motion capture data in Appendix C, and the length of the foot, l_{foot} is found as

$$l_{foot} = 0.152 \cdot tbh \tag{3.8}$$

where the value 0.152 is the ratio of the length of the foot segment to the total body height (tbh) provided by Winter.

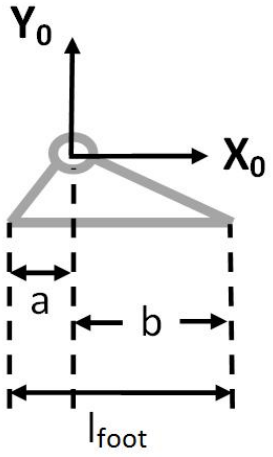

Figure 3.3: Dimensions of the foot. Values for dimensions a and b are given in Equation 3.7

While seated, both the seat and the floor provide support to the model in the form of ground reaction forces. The base of support, in the seated configuration, is defined as the linear region extending from the hip (at the edge of the chair's surface) to the toe of the foot. Figure 3.4 depicts the base of support for the biomechanical model in the seated and standing configurations. The biomechanical model is considered

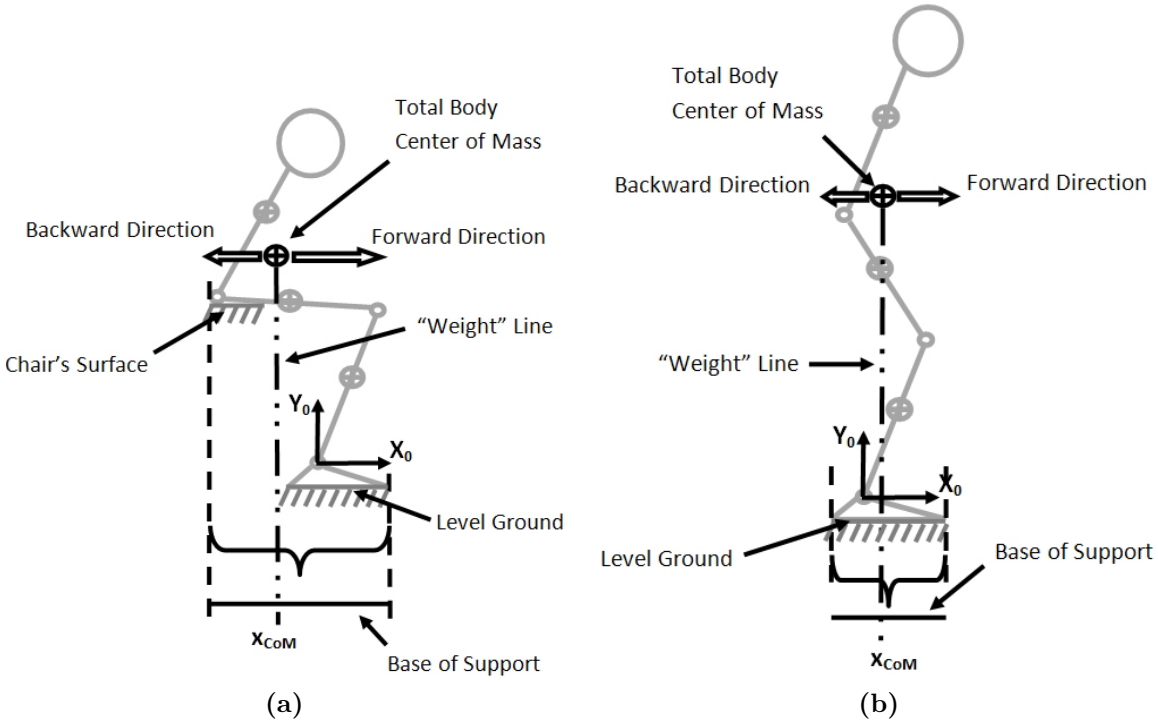

Figure 3.4: Biomechanical model with base of support while (a) seated, and (b) standing.

to be (biomechanically) *stable* so long as the imaginary vertical line drawn through its total-body center of mass, often referred to as the "gravity" or "weight" line, remains within the base of support. Also, in a biomechanical analysis of the model, the larger the distance between the "gravity" line and the edge of the base of support, the more stable the model. Also, biomechanical stability of the model is directional. The vector from the weight line to the edge of the base of support at the heel of the foot describes the biomechanical stability of the model in the backward direction. Similarly, the vector created from the weight line to the toe of the foot describes the

biomechanical stability of the model in the forward direction. For example, given a configuration near standing (see Figure 3.4, configuration (b)), the biomechanical model is slightly more stable in the forward direction than the backward one. This is because the distance from the "gravity" line to the edge of the base of support at the toe of the foot is greater than its distance to the base of support boundary at the heel of the foot. And wile seated (see Figure 3.4, configuration (a)), the model is considered to be more stable in the forward direction than the backward one. Again, the distance from the "gravity" line to the to the edge of the base of support at the toe of the foot is greater than its distance to the base of support boundary at the heel of the foot.

The "gravity" line meets the axis X_0 at $\begin{bmatrix} x_{CoM} & 0 \end{bmatrix}$ - the location of the total body center of mass projected onto the X_0 axis. Therefore, x_{CoM} provides a useful measure of stability.

3.2.7 Inverted Pendulum Representation

The ankle can be thought of as a fixed pivot point about which the entire body rotates. A vector of length R_{CoM} and angle θ_{CoM} is created between the ankle and the total-body center of mass located at $\begin{bmatrix} x_{CoM} & y_{CoM} \end{bmatrix}$. The vector $\begin{bmatrix} R_{CoM} & \theta_{CoM} \end{bmatrix}$ is found as,

$$R_{CoM} = \sqrt{\hat{x}_{CoM}{}^2 + \hat{y}_{CoM}{}^2} \tag{3.9a}$$

$$\theta_{CoM} = arctan\left(\frac{\hat{y}_{CoM}}{\hat{x}_{CoM}}\right) \tag{3.9b}$$

where $\begin{bmatrix} x_{CoM} & y_{CoM} \end{bmatrix}$ is found using Equation 3.6.

The vector $\begin{bmatrix} R_{CoM} & \theta_{CoM} \end{bmatrix}$ is simply the polar coordinate representation of the total-body center of mass location in absolute space. This representation of the model is not unlike that of an inverted pendulum (see Figure 3.5), where the total-body mass

$m = m_1 + m_2 + \hat{m}_3$ is concentrated at the end of a massless rod of length R_{CoM} and an angle θ_{CoM} from the horizontal (i.e., X_0).

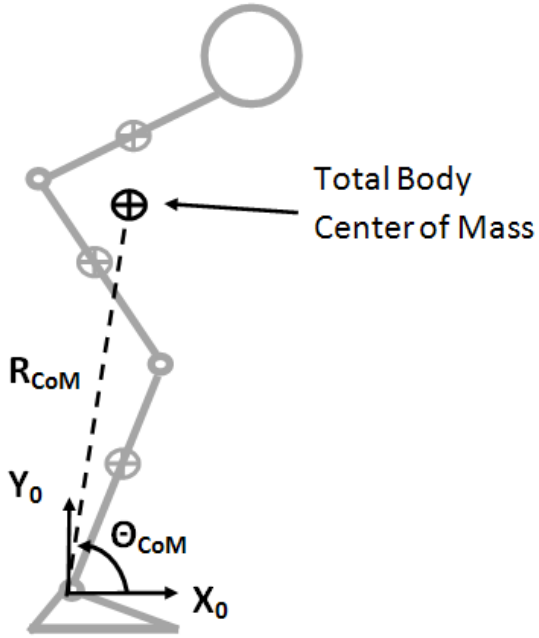

Figure 3.5: Inverted pendulum representation of a biomechanical model.

The inverted pendulum representation of a biomechanical model has been used to generate bipedal walking patterns in robots using the linear inverted pendulum mode [10] and gravity-compensated inverted pendulum mode [18]. This representation played an integral part in the control of the sit-stand model in this work. For example, the inclination of the total-body center of mass, represented by θ_{CoM}, was calculated for the end-goal configuration (namely, standing), to serve as a reference value $\theta_{CoM(Ref)}$. The error in total-body center of mass inclination - between any given configuration of the model and the end-goal configuration - is then given by

$$\theta_{CoM(Err)}(t) = \theta_{CoM(Ref)} - \theta_{CoM}(t) \tag{3.10}$$

Note that, in this work, a dependency on time is generally assumed for all positional, velocity, and acceleration values. Notation, stating an explicit dependence on time, is

suppressed for brevity. This is done quite typically in robotics, and is the convention adopted here. Therefore, the equation above will be generally written as

$$\theta_{CoM(Err)} = \theta_{CoM(Ref)} - \theta_{CoM} \tag{3.11}$$

3.2.8 The Thigh-HAT Composite Object

Rather than consider the entire system of rigid bodies of the biomechanical model, the thigh and HAT rigid body segments may be viewed as a double inverted pendulum whose pivot is located at the knee joint (see Figure 3.6).

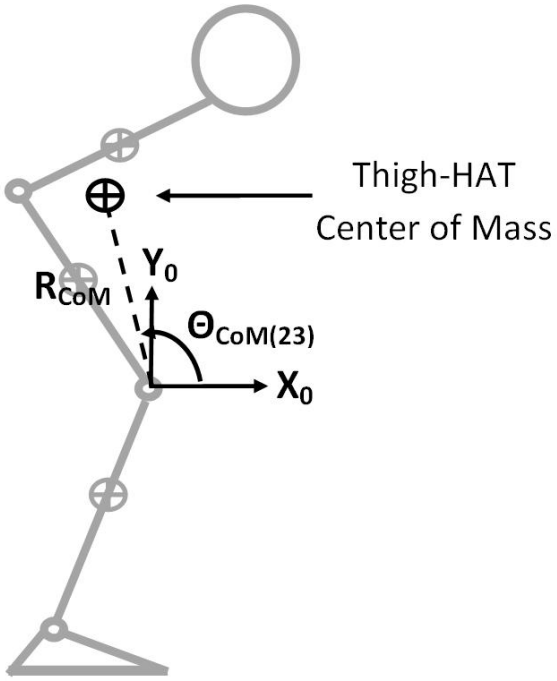

Figure 3.6: The thigh-HAT composite object.

This subset of rigid bodies is referred to as the thigh-HAT composite object. The center of mass for this system of rigid bodies, $\begin{bmatrix} x_{CoM(23)} & y_{CoM(23)} \end{bmatrix}$, is calculated

as

$$x_{CoM(23)} = \frac{m_2 \cdot x_{CoM(2)} + m_3 \cdot x_{CoM(3)}}{m_2 + m_3} \tag{3.12a}$$

$$y_{CoM(23)} = \frac{m_2 \cdot y_{CoM(2)} + m_3 \cdot y_{CoM(3)}}{m_2 + m_3} \tag{3.12b}$$

where m_2 and m_3 are the segment masses for the thigh and HAT rigid body segments respectively, and $\begin{bmatrix} x_{CoM(i)} & y_{CoM(i)} \end{bmatrix}$ for $i = 2, 3$, their respective locations of center of mass. Substituting the estimate for mass m_3 and the estimated locations of center of mass for both rigid body members, the estimated center of mass for the thigh-HAT composite object $\begin{bmatrix} \hat{x}_{CoM(23)} & \hat{y}_{CoM(23)} \end{bmatrix}$ is computed as

$$\hat{x}_{CoM(23)} = \frac{m_2 \cdot \hat{x}_{CoM(2)} + m_3 \cdot \hat{x}_{CoM(3)}}{m_2 + \hat{m}_3} \tag{3.13a}$$

$$\hat{y}_{CoM(23)} = \frac{m_2 \cdot \hat{y}_{CoM(2)} + m_3 \cdot \hat{y}_{CoM(3)}}{m_2 + \hat{m}_3} \tag{3.13b}$$

The polar coordinate transform of $\begin{bmatrix} \hat{x}_{CoM(23)} & \hat{y}_{CoM(23)} \end{bmatrix}$ gives

$$R_{CoM(23)} = \sqrt{\hat{x}_{CoM(23)}{}^2 + \hat{y}_{CoM(23)}{}^2} \tag{3.14a}$$

$$\theta_{CoM(23)} = arctan\left(\frac{\hat{y}_{CoM(23)}}{\hat{x}_{CoM(23)}}\right) \tag{3.14b}$$

where $\theta_{CoM(23)}$ represents the angle between the horizontal and a vector of length $R_{CoM(23)}$ projected from the knee to the thigh-HAT center of mass. The vector $\begin{bmatrix} R_{CoM(23)} & \theta_{CoM(23)} \end{bmatrix}$ can be thought of as an inverted pendulum representation of the thigh-HAT composite object (see Figure 3.6).

3.2.9 Joint Angles

Joint angles, denoted θ, are relative measures of angular displacement between two adjoining rigid bodies. The frames of reference attached to these bodies are used to

calculate the joint angle. Specifically, θ_i is calculated as the rotation of axis X_i with respect to X_{i-1}. For example, θ_1 represents the rotation of axis X_1 with respect to axis X_0, or more generally, because a 2-dimensional space was used, it represents the rotation of $\{1\}$ with respect to $\{0\}$. The sign of the joint angle is determined using right-hand rule convention, (i.e., counter-clockwise rotations are positive-going). The set of joint angles

$$\boldsymbol{\theta} = \begin{bmatrix} \theta_1 & \theta_2 & \theta_3 \end{bmatrix}^T \tag{3.15}$$

describes the configuration of the three-link biomechanical model at any given instant (see Figure 3.7).

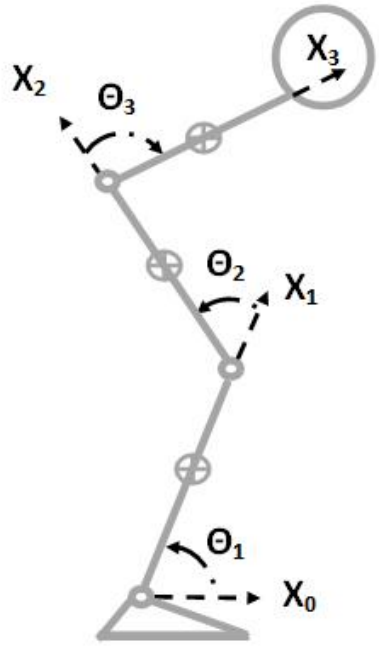

Figure 3.7: Joint angle definitions for a three-link biomechanical model.

Joint angle velocity, denoted $\dot{\boldsymbol{\theta}}$, is simply the time derivative of the joint angles

$$\begin{aligned} \dot{\theta} &= \begin{bmatrix} \dot{\theta}_1 & \dot{\theta}_2 & \dot{\theta}_3 \end{bmatrix}^T \\ &= \begin{bmatrix} \frac{d\theta_1(t)}{dt} & \frac{d\theta_2(t)}{dt} & \frac{d\theta_3(t)}{dt} \end{bmatrix}^T \end{aligned}$$

	Full Flexion	Full Extension
θ_1	$\frac{\pi}{4}$	$\frac{\pi}{2}$
θ_2	$\frac{\pi}{2}$	0
θ_3	$\frac{-3\pi}{4}$	0

Table 3.2: Joint Range of Motion

For simulation purposes $\dot{\theta}_i$ was calculated as

$$\dot{\theta}_i(k\Delta t) = \frac{\theta_i(k\Delta t) - \theta_i((k-1)\Delta t)}{\Delta t}$$

and Δt is the sampling period.

3.2.10 Joint Range of Motion

The range of motion (ROM) of a joint is the range of its angular displacement from maximum extension to maximum flexion. As a point of terminology, flexion of the ankle joint is referred to as dorsiflexion while extension of the ankle is referred to as plantarflexion. Ranges of motion (ROMs) for the three-link model depicted in Figure 3.7 are defined in Table 3.2.

Figure 3.8 provides an illustration of the biomechanical model with all joint angles at maximum flexion.

3.2.11 Limb-segment Angles

Limb-segment angles describe the orientation of a rigid-body with respect to absolute space, (i.e., the world coordinate system), and specifically the axis X_0. Limb-segment angles for the three-link model depicted in Figure 2.2a can be found by summing the joint angles along the kinematic chain from the base to the limb segment of interest. The limb-segment angle for the shank is simply θ_1. For the thigh, angles θ_1 and θ_2 are combined to form the limb-segment angle θ_{12}

$$\theta_{12} = \theta_1 + \theta_2$$

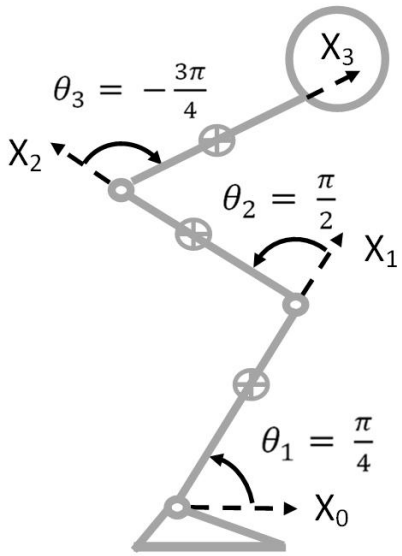

Figure 3.8: Biomechanical model with each joint at maximum flexion.

and similarly for the HAT, θ_{123} is calculated as

$$\theta_{123} = \theta_1 + \theta_2 + \theta_3$$

Therefore, the set of limb-segment angles may be defined as

$$\theta_{\mathbf{Limb}} = \begin{bmatrix} \theta_1 & \theta_{12} & \theta_{123} \end{bmatrix}^T$$

where θ_1, θ_{12}, and θ_{123} represent the limb-segment angles of the shank, thigh, and HAT respectively. Figure 3.9 illustrates the definitions for the limb segment angles.

3.2.12 Dynamic Equation of the Biomechanical Model

The dynamics of the three-link rigid-body model depicted in Figure 2.2a are described by a set of nonlinear differential equations, usually written compactly in the (linear) form

$$\boldsymbol{\tau} = \mathbf{M}(\boldsymbol{\theta}) \cdot \ddot{\boldsymbol{\theta}} + \mathbf{V}(\boldsymbol{\theta}, \dot{\boldsymbol{\theta}}) + \mathbf{G}(\boldsymbol{\theta}) \tag{3.17}$$

where $\boldsymbol{\tau}$ is the set of joint torques (or moments of force) applied to each joint, $\mathbf{M}(\boldsymbol{\theta})$

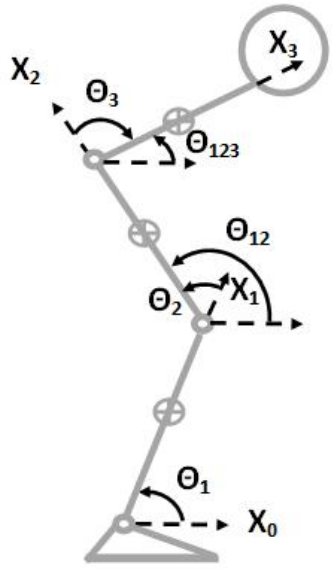

Figure 3.9: Limb segment angles for a three-link biomechanical model.

is the 3 x 3 inertia matrix, $\ddot{\boldsymbol{\theta}}$ is a 3 x 1 vector of joint angular accelerations, $\mathbf{V}(\boldsymbol{\theta}, \dot{\boldsymbol{\theta}})$ is a 3 x 1 vector which includes the centrifugal and Coriolis terms, and $\mathbf{G}(\boldsymbol{\theta})$ is a 3 x 1 vector of gravity terms. Since the model's dynamics are nonlinear in nature, matrix $\mathbf{M}$, and vectors $\mathbf{V}$, and $\mathbf{G}$, contain nonlinear elements.

The Lagrangian dynamic formulation, commonly applied to mechanical manipulators with rigid links, was used to derive Equation 3.17. It relies on an expression for the kinetic and potential energies of the rigid body system. The kinetic energy of the i^{th} rigid body segment, denoted T_i, is given by

$$T_i = \frac{1}{2} \cdot m_i \cdot v_{G(i)}^2 + \frac{1}{2} \cdot I_{G(i)} \cdot \dot{\theta}_i^2 \tag{3.18}$$

where m_i is the mass of the i^{th} rigid body segment, $v_{G(i)}$ is the segments's translational velocity (with respect to its center of gravity), $I_{G(i)}$ is the moment of inertia of the body (about its center of gravity), and $\dot{\theta}_i$ is the angular velocity of the body (about its center of gravity), and the potential energy is given by

$$V_i = m_i \cdot g \cdot y_{CoM(i)} \tag{3.19}$$

where m_i is the mass of the i^{th} rigid body segment, g is the acceleration due to gravity ($9.81 m/s^2$), and $y_{CoM(i)}$ is the y-component of the body's center of mass location. The kinetic energies of each rigid body are summed to form T, the total kinetic energy of the system, as

$$T = T_1 + T_2 + T_3 \tag{3.20}$$

where T_1, T_2, and T_3, represent the kinetic energies of the shank, thigh, and HAT respectively. Similarly, the potential energies of each rigid body segment are summed to form the total potential energy of the system V, as

$$V = V_1 + V_2 + V_3 \tag{3.21}$$

The Lagrangian dynamic formulation is then found using Equation 3.22

$$\boldsymbol{\tau} = \frac{d}{dt}\left(\frac{\partial T}{\partial \dot{\boldsymbol{\theta}}}\right) - \frac{\partial T}{\partial \boldsymbol{\theta}} + \frac{\partial V}{\partial \boldsymbol{\theta}} \tag{3.22}$$

where $\boldsymbol{\tau}$ is the 3 x 1 vector of actuator torques, T is the total kinetic energy of the system given by Equation 3.20, V is the total potential energy of the system given by Equation 3.21, $\boldsymbol{\theta}$ is the set of joint angles given in Equation 3.15 and $\dot{\boldsymbol{\theta}}$ is the set of joint angular velocities given in Equation 3.16. Details of the Lagrangian formulation are included in Appendix B. Like terms are gathered to form the dynamic equation of 3.17.

It can be seen from Equation 3.17 that the inertial and gravitational parameters depend solely on the model's configuration, while the Coriolis and centrifugal terms additionally depend on the joint angle velocities represented by $\dot{\boldsymbol{\theta}}$. The dynamic equation relates the joint torques applied to the system, represented here by $\boldsymbol{\tau}$, to the joint angular accelerations $\ddot{\boldsymbol{\theta}}$ for a given system state defined by $\boldsymbol{\theta}$ and $\dot{\boldsymbol{\theta}}$. Solving

for the angular acceleration of the joints gives

$$\ddot{\boldsymbol{\theta}} = \mathbf{M}^{-1}(\boldsymbol{\theta}) \cdot (\boldsymbol{\tau} - \mathbf{V}(\boldsymbol{\theta}, \dot{\boldsymbol{\theta}}) - \mathbf{G}(\boldsymbol{\theta})) \tag{3.23}$$

The net torque experienced by the joints is given by

$$\boldsymbol{\tau}_{net} = \mathbf{M}(\boldsymbol{\theta}) \cdot \ddot{\boldsymbol{\theta}}$$

or equivalently

$$\boldsymbol{\tau}_{net} = \boldsymbol{\tau} - \mathbf{V}(\boldsymbol{\theta}, \dot{\boldsymbol{\theta}}) - \mathbf{G}(\boldsymbol{\theta})$$

For every moment of force, or joint torque, applied to a rigid body member, there is an equal and opposite moment of force also acting about the joint. Figure 3.10 depicts the joint moments of force acting on the model.

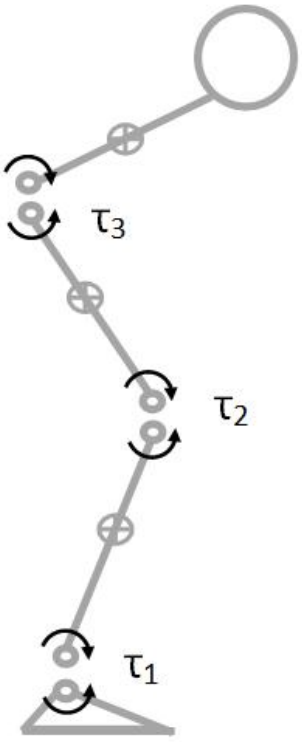

Figure 3.10: Free body diagram with joint torques.

3.2.13 Calculation of Work

The work done by a joint actuator is calculated as the moment of force it applies to a joint, denoted as τ, multiplied by the angular displacement of the joint, denoted $d\theta$, from time t_1 to t_2, such that

$$W = \int_{\theta(t_1)}^{\theta(t_2)} \tau(t) \cdot d\theta \tag{3.24}$$

where $\theta(t_1)$ represents the angular position of the joint at time t_1 and $\theta(t_2)$ is the position at time t_2.

If the torque applied by a joint actuator, τ is constant over an angular displacement $\Delta\theta = \theta(t_2) - \theta(t_1)$, the expression for work done by a joint actuator may be written as

$$W = \tau_{1-2} \cdot \Delta\theta \tag{3.25}$$

where τ_{1-2} signifies the value of τ on the interval $t = [t_1, t_2]$.

Since discrete time steps were used to simulate the sit-to-stand movement in this work (discussed further in Sections 3.3.5 and 3.3.6), moments of force applied to a joint, by a joint actuator, were constant for the duration of each time step. Therefore, the work done by a joint actuator, or set of joint actuators, who apply a moment of force (i.e., motor torque) of $\boldsymbol{\tau}$ over the course of the entire sit-to-stand movement, is given by

$$W = \sum_{k=1}^{n-1} \tau(k \cdot \Delta t) \cdot (\theta((k+1) \cdot \Delta t) - \theta(k \cdot \Delta t)) \tag{3.26}$$

were W is the work done by the joint actuator(s) in Joules (J), and Δt is the simulation time step.

3.3 Sit-to-Stand

Sit-to-stand, also known as chair rise, is the activity in which an individual rises from a seated position to a standing one. The movement may be viewed as a transition from one statically stable position (quiet sitting) to another (quiet standing).

3.3.1 Sit-to-Stand Movement Strategies

Riley et al. [24] identified two common sit-to-stand movement strategies utilized by the general population: 1) the momentum-transfer strategy, and 2) the stabilization strategy (see Figure 3.11).

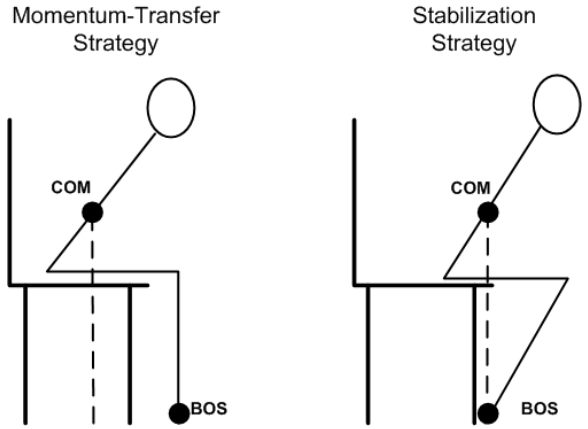

Figure 3.11: Key concepts behind commonly employed sit-to-stand strategies.

Momentum-transfer involves developing a forward momentum of the HAT which is quickly transferred to the whole of the body during "hip-lock". The individual lifts off from the chair and a predominately horizontal momentum transitions into a vertical one.

In the stabilization strategy, the individual shifts their center of mass forward along on the chair's surface while also retracting their feet toward the chair's base. By doing so, the individual brings their center of mass into close proximity of their base of support (i.e., their feet). The individual lifts themselves in a controlled (i.e., balanced) manner from the chair's surface.

Younger, healthier individuals tend to use the momentum-transfer strategy while older, or mobility impaired individuals tend to favor the stabilization strategy. Momentum-transfer is considered the more efficient of the two methods.

3.3.2 Phases of the Sit-to-Stand Cycle

The sit-to-stand movement is divided it into several key phases: i) initiation, ii) seat unloading, iii) vertical ascension, and, iv) balance recovery and stabilization. Early studies identified only two or three distinct phases for the movement cycle, while Kralj et al. [15] enriched these to the four phases above, which are illustrated in Figure 3.12.

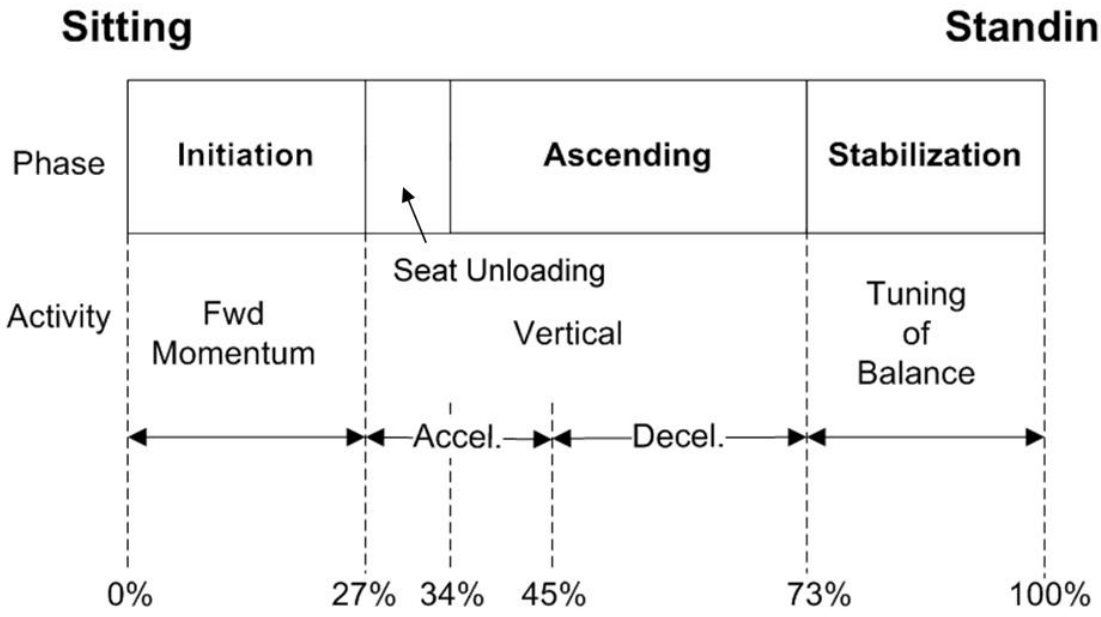

Figure 3.12: Phases of the sit-to-stand movement.

Phase 1: Initiation

Event Boundaries: quiet sitting to hip-lock

Initiation is a progression from quiet sitting to hip-lock. At the onset of the initiation phase the individual is seated and unmoving. The hip flexors are used to generate a forward momentum of the HAT. As the degree of forward lean

increases, moments of force about the hip (from the gravitational loading of the HAT) are mitigated by an opposing hip extensor torque. Initiation ends with a locking of the hip joint (referred to as "hip-lock") to encourage momentum transfer (i.e., from the HAT to the whole of the body).

Phase 2: Seat Unloading

Event Boundaries: hip-lock to lift-off / seat-off

Seat unloading begins at hip-lock where the HAT is quickly decelerated using the hip extensors. This is done to encourage momentum transfer from the HAT to the whole of the body. Moments of force about the ankle and knee support a continued movement forward while also introducing an upward movement component resulting in "lift-off" or "seat-off."

Phase 3: Vertical Ascension

Event Boundaries: seat-off to balance recovery

Forward lean gives rise to vertical displacement as the joints are extended toward the standing configuration. During vertical ascension, the total body center of mass tends to be slightly forward the value achieved in quiet standing. This prompts a small amount of balance recovery during stabilization.

Phase 4: Recovery and Stabilization

Event Boundaries: balance recovery to quiet standing

The center of mass of the body is shifted backward into its final (quiet standing) location directly over the base of support. A plantarflexor torque at the ankle contributes to balance recovery and stabilization. A stable (quiet) standing configuration is achieved.

3.3.3 Simulation Initial and Final Conditions

It is assumed that the initial (seated upright) and final (standing) configurations of the model, represented by $\boldsymbol{\theta}_0$ and $\boldsymbol{\theta}_f$ respectively, are known. The desired, or

standing, configuration will be defined, in this work, as

$$\boldsymbol{\theta}_f = \begin{bmatrix} 85 & 10 & -10 \end{bmatrix}^T \text{deg} \tag{3.27}$$

where $\boldsymbol{\theta}_f$ represents an offset of 5 deg from the vertical at every joint of the biomechanical model. These values have been arbitrarily selected, but yield a realistic standing configuration which favorably places the total body center of mass within the base of support (i.e., slightly forward of the ankle, near the midpoint of the base of support).

The initial time, t_0, marks the onset of the sit-to-stand movement, while the final time, t_f, marks the movement's end. Estimates for the location of the total-body center of mass in each of these configurations, denoted $\begin{bmatrix} x^0_{CoM} & y^0_{CoM} \end{bmatrix}$ and $\begin{bmatrix} x^f_{CoM} & y^f_{CoM} \end{bmatrix}$ respectively, can be found using Equation 3.3, where

$$x^f_{CoM} = x_{CoM}(t)|_{t=t_0} \tag{3.28a}$$

$$y^f_{CoM} = y_{CoM}(t)|_{t=t_0} \tag{3.28b}$$

and

$$x^f_{CoM} = x_{CoM}(t)|_{t=t_f} \tag{3.29a}$$

$$y^f_{CoM} = y_{CoM}(t)|_{t=t_f} \tag{3.29b}$$

Using the value for $\boldsymbol{\theta}_f$ given in Equation 3.27, the estimated location of the total body center of mass in the standing configuration, given by $\begin{bmatrix} \hat{x}^f_{CoM} & \hat{y}^f_{CoM} \end{bmatrix}$, may be found using Equations 3.3 and 3.1, where Equation 3.1 gives

$$\begin{bmatrix} \hat{x}^f_{CoM(1)} \\ \hat{y}^f_{CoM(1)} \end{bmatrix} = {}^0_1R \cdot \begin{bmatrix} \hat{l}_{CoM(1)} \\ 0 \end{bmatrix}$$

$$= \begin{bmatrix} cos(85) & -sin(85) \\ sin(85) & cos(85) \end{bmatrix} \cdot \begin{bmatrix} \frac{0.246 \cdot 1.89}{2} \\ 0 \end{bmatrix} \tag{3.30a}$$

$$\begin{bmatrix} \hat{x}^f_{CoM(2)} \\ \hat{y}^f_{CoM(2)} \end{bmatrix} = {}^0_2R \cdot \begin{bmatrix} \hat{l}_{CoM(2)} \\ 0 \end{bmatrix}$$

$$= \begin{bmatrix} cos(85+10) & -sin(85+10) \\ sin(85+10) & cos(85+10) \end{bmatrix} \cdot \begin{bmatrix} \frac{0.245 \cdot 1.89}{2} \\ 0 \end{bmatrix} \tag{3.30b}$$

$$\begin{bmatrix} \hat{x}^f_{CoM(3)} \\ \hat{y}^f_{CoM(3)} \end{bmatrix} = {}^0_3R \cdot \begin{bmatrix} \hat{l}_{CoM(3)} \\ 0 \end{bmatrix}$$

$$= \begin{bmatrix} cos(85+10+(-10)) & -sin(85+10+(-10)) \\ sin(85+10+(-10)) & cos(85+10+(-10)) \end{bmatrix} \cdot \begin{bmatrix} \frac{0.288 \cdot 1.89}{2} \\ 0 \end{bmatrix} \tag{3.30c}$$

and the estimated locations of center of mass for each rigid body member, $\hat{l}_{CoM(i)}$, are found using Equation 3.5 and the values included in Table 3.1 with a total body height (tbh) of 1.89 m (corresponding to a height of 6'2"). 1.89 m was selected as the total body height because it represents the height of the test subject used to collect

the motion capture data provided in Appendix C. Similarly, a total body mass (tbm) of 86.4 kg was used. With the values

$$\begin{aligned} m_1 &= 0.0465 \cdot 86.4 \\ &= 4.02kg \\ m_2 &= 0.100 \cdot 86.4 \\ &= 8.64kg \\ \hat{m}_3 &= 0.678 \cdot 86.4 \\ &= 58.6kg \end{aligned}$$

(where $\hat{m}_3$ is found using $\alpha = 0$ in Equation 3.4) Equation 3.3 gives

$$\hat{x}_{CoM} = \frac{4.02 \cdot \hat{x}_{CoM(1)} + 8.64 \cdot \hat{x}_{CoM(2)} + 58.6 \cdot \hat{x}_{CoM(3)}}{4.02 + 8.64 + 58.6} \tag{3.32a}$$

$$\hat{y}_{CoM} = \frac{4.02 \cdot \hat{y}_{CoM(1)} + 8.64 \cdot \hat{y}_{CoM(2)} + 58.6 \cdot \hat{y}_{CoM(3)}}{4.02 + 8.64 + 58.6} \tag{3.32b}$$

Substituting Equation 3.30 into Equation 3.32 gives a final total body center of mass location of

$$\begin{bmatrix} \hat{x}^f_{CoM} \\ \hat{y}^f_{CoM} \end{bmatrix} = \begin{bmatrix} 0.0228 \\ 1.00 \end{bmatrix} \tag{3.33}$$

The inverted pendulum representation of the total-body center of mass may then be calculated for each configuration using Equation 3.9. For the initially seated configuration:

$$R_{CoM(0)} = \sqrt{\hat{x}_{CoM(0)}{}^2 + \hat{y}_{CoM(0)}{}^2} \tag{3.34a}$$

$$\theta_{CoM(0)} = arctan\left(\frac{\hat{y}_{CoM(0)}}{\hat{x}_{CoM(0)}}\right) \tag{3.34b}$$

and the final standing configuration:

$$R_{CoM(f)} = \sqrt{{\hat{x}^f_{CoM}}^2 + {\hat{y}^f_{CoM}}^2} \tag{3.35a}$$

$$\theta^f_{CoM} = arctan\left(\frac{\hat{y}^f_{CoM}}{\hat{x}^f_{CoM}}\right) \tag{3.35b}$$

Substituting values for $\begin{bmatrix} \hat{x}^f_{CoM} & \hat{y}^f_{CoM} \end{bmatrix}$ given in Equation 3.33 into Equation 3.35 gives the final inclination of the total body center of mass θ^f_{CoM} as

$$\begin{aligned} \theta^f_{CoM} &= arctan\left(\frac{1.00}{0.0228}\right) \\ &= 88.7 \end{aligned}$$

Since the biomechanical begins at rest, the initial velocity vector is all zeros

$$\dot{\boldsymbol{\theta}}_0 = \begin{bmatrix} 0 & 0 & 0 \end{bmatrix}^T$$

3.3.4 Modelling the Effects of a Chair

For the purpose of sit-to-stand analysis and simulation, chairs are often modeled as spring-damper systems [2]. While no explicit model of a chair was used in this work, the effects of a chair on the seated individual were simulated in the following manner. If it was determined that the set of joint torques τ were not sufficient to lift the biomechanical model from the chair's surface, the angular acceleration of the ankle and knee joints were set to zero. The seated configuration was therefore maintained while also allowing the hip joint to function normally (i.e., $\ddot{\theta}_3$ was found using Equation 3.23). If, instead, the joint torques were sufficient to lift the model from the chair's surface, no intervening action was taken and the angular acceleration of each joint was determined using Equation 3.23. This scheme allows us to simulate

the effects of a chair without the use of an explicit chair model. It may be summarized as

$$\ddot{\boldsymbol{\theta}} = \begin{cases} \begin{bmatrix} 0 & 0 & \ddot{\theta}_3 \end{bmatrix}^T, & \boldsymbol{\tau} < \boldsymbol{\tau}' \\ \mathbf{M}^{-1}(\boldsymbol{\theta}) \cdot (\boldsymbol{\tau} - \mathbf{V}(\boldsymbol{\theta}, \dot{\boldsymbol{\theta}}) - \mathbf{G}(\boldsymbol{\theta})), & \text{otherwise} \end{cases}$$

where $\boldsymbol{\tau}'$ is the set of joint torques sufficient to lift the model from the chair's surface and

$$\ddot{\theta}_3 = M_{31}^{-1} \cdot (\tau_1 - V_1 - G_1) + M_{32}^{-1} \cdot (\tau_2 - V_2 - G_2) + M_{33}^{-1} \cdot (\tau_3 - V_3 - G_3)$$

3.3.5 Forward Simulation

Euler integration was used to conduct the forward time simulation of the model. The joint angles and angular velocities were updated using

$$\boldsymbol{\theta}(k+1) = \boldsymbol{\theta}(k) + \dot{\boldsymbol{\theta}}(k) \cdot \Delta t + \frac{1}{2} \cdot \ddot{\boldsymbol{\theta}}(k) \cdot (\Delta t)^2 \tag{3.37a}$$

$$\dot{\boldsymbol{\theta}}(k+1) = \dot{\boldsymbol{\theta}}(k) + \ddot{\boldsymbol{\theta}} \cdot \Delta t \tag{3.37b}$$

where Δt is the simulation time step.

3.3.6 Simulation Time Step

The time step Δt is the time between successive iterations of the simulation. The time step should be sufficiently small to yield accurate results, but not be so small that the simulation takes an unreasonable amount of time to execute. Also, a time step must be selected which is appropriate for the movement task of interest, namely, in this work, the sit-to-stand movement.

Frequency components observed in the kinematics of human movement tend to be quite low in frequency. For example in normal walking, kinematic analysis of the foot showed that the vast majority of signal energy resided in frequency components below 6 Hz, and for other parts of the body, below 3 Hz [36]. A kinematic analysis

of the sit-to-stand movement (whose results are given in Appendix C) showed the majority of signal energy resides in even lower frequencies (< 2 Hz). A 10^{th} order Butterworth filter, with a corner frequency f_c of 2 Hz, removed only noise on the kinematic signals without dampening the signals of interest themselves.

Furthermore, inertia of the human body tends to dampen external influences applied to it, as does the gearing ratio of joint actuators typically used in advanced mobility support devices (worn by the mobility impaired individual). While a slow and controlled movement is typically desirable when assisting persons with movement tasks (and especially those with mobility impairments), the system being developed in this work must also be able to respond to sudden and undesired external influences (perturbations).

A sampling rate (or *servo update rate*) of 35 Hz, which corresponds to a sampling period of 0.0286 s, is thought to be sufficiently fast for responding to external perturbations applied to the biomechanical system, while more than sufficient for the reproduction of the sit-to-stand movement itself. The sampling period of 0.0286 s, doubling as the simulation time step, is thought to be sufficiently small for achieving near-realistic simulation results, while not so small that the simulation takes an unreasonable time to execute.

Chapter 4

Control System Design

4.1 Introduction

In this chapter the control strategy employed for synthesizing the sit-to-stand movement is presented. Fuzzy control was selected as the sole control methodology for multiple reasons, but most importantly because:

1. **Leveraging expert knowledge**. As discussed in Chapter 3, the sit-to-stand movement is well studied and a large body of knowledge about the task already exists, but primarily as semantic knowledge. Given this wealth of semantic knowledge and the complexity of human movement, fuzzy control becomes an attractive control methodology, as it accommodates the use of expert knowledge of a control process rather than relying on detailed mathematical models of the plant to be controlled. Math models of the biomechanical system would vary considerably from individual to individual, and certainly for persons with a mobility impairment.

2. **Cost effectiveness**. Allows for a solution that is easily tunable to the individual; whereas, classical control would require a detailed model to be produced for each individual.

It should also be noted that energy efficient movement is possible using a fuzzy control-based solution. While fuzzy systems do not normally accommodate the use of optimization techniques, human movement is, in general, considered to be energy efficient in nature [30]. Therefore, by simply mimicking the natural sit-to-stand movement; and avoiding unnecessary antagonist co-contractions (i.e., moments of force acting on the same joint which oppose one another) of the over-actuated system (i.e., the biomechanical model with both feet on the ground), a reasonably energy efficient solution will likely result. While energy efficiency is a secondary concern to the production of stable movements, portable systems, i.e., those relying on battery power, must be conservative in their energy use.

4.2 Control System Overview

The "plant," or system under control is the three-link biomechanical model introduced in Chapter 3 whose dynamic equation is given by Equation 3.17. The control action delivered to the plant, denoted $\boldsymbol{\tau}$, is formed by combining a gravity compensation action $\hat{\mathbf{G}}$ with a motion control directive $\boldsymbol{\tau}'$. Three fuzzy systems were used to form the motion control directive $\boldsymbol{\tau}'$:

1. **Stability controller**. A control system which oriented the model toward the most stable configuration.

2. **Goal controller**. A control system which oriented the model toward the goal (i.e., standing) configuration.

3. **A fuzzy-based interpolator**. A fuzzy system was used to assess the stability of the biomechanical model, and produce the weighting factor, μ_{stab}. μ_{stab} was used to combine the outputs of the first two controllers in a way that emphasized stability of the biomechanical model while also advancing it toward the goal configuration.

The control architecture of the sit-to-stand controller is shown in Figure 4.1.

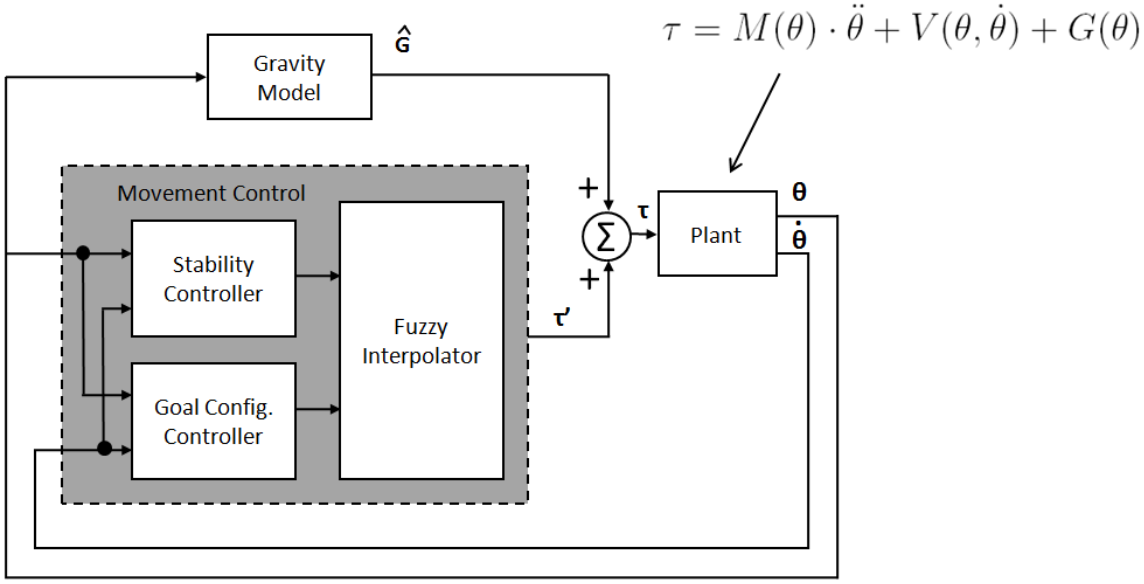

Figure 4.1: High-level control system architecture.

While a complete mathematical model of the plant was not incorporated into the control strategy, model-based estimates were used to establish: i) a basic gravity model of the plant (explained in Section 4.3), and ii) the locations of the centers of mass of the rigid-body segments (as explained in Section 3.5).

4.3 Gravity Compensation

A simple gravity model of the plant was used to estimate the gravitational loading effects on the ankle, knee, and hip joints. A 3 x 1 vector of gravity terms, denoted as $\mathbf{G}(\boldsymbol{\theta})$ (included in Equation 3.17), served as the gravity model. The terms $G_1(\boldsymbol{\theta})$, $G_2(\boldsymbol{\theta})$, and $G_3(\boldsymbol{\theta})$ (derived in Appendix B) represent the joint torques required to counteract the effects of gravity at the ankle, knee, and hip respectively. Estimates for the anatomical parameters of the biomechanical model are used to calculate the

gravity compensation estimates $\hat{G}_1(\boldsymbol{\theta})$, ..., $\hat{G}_3(\boldsymbol{\theta})$

$$\begin{aligned}\hat{G}_1(\boldsymbol{\theta}) = &- \hat{m}_1 \cdot g \cdot \hat{l}_{CoM(1)} \cdot s_1 - \hat{m}_2 \cdot g \cdot (l_1 \cdot s_1 + \hat{l}_{CoM(2)} \cdot s_{12}) \\ &- \hat{m}_3 \cdot g(l_1 \cdot s_1 + l_2 \cdot s_{12} + \hat{l}_{CoM(3)} \cdot s_{123}) \end{aligned} \tag{4.1a}$$

$$\hat{G}_2(\boldsymbol{\theta}) = - \hat{m}_2 \cdot g \cdot \hat{l}_{CoM(2)} \cdot s_{12} - \hat{m}_3 \cdot g \cdot (l_2 \cdot s_{12} + \hat{l}_{CoM(3)} \cdot s_{123}) \tag{4.1b}$$

$$\hat{G}_3(\boldsymbol{\theta}) = - \hat{m}_3 \cdot g \cdot \hat{l}_{CoM(3)} \cdot s_{123} \tag{4.1c}$$

where $\hat{m}_1$, ..., $\hat{m}_3$ are the estimated limb segment masses, $\hat{l}_{CoM(1)}$, ..., $\hat{l}_{CoM(3)}$ are the estimated locations of center of mass for each segment, l_1, ..., l_3 are the limb segment lengths, g denotes the acceleration due to gravity (i.e., 9.81 m/s^2), and s_1, s_{12}, and s_{123} are defined as

$$s_1 = sin(\theta_1) \tag{4.2a}$$

$$s_{12} = sin(\theta_1 + \theta_2) \tag{4.2b}$$

$$s_{123} = sin(\theta_1 + \theta_2 + \theta_3) \tag{4.2c}$$

following the common robotics convention.

The gravity compensation action may then be stated as

$$\hat{\mathbf{G}}(\boldsymbol{\theta}) = \begin{bmatrix} \hat{G}_1(\boldsymbol{\theta}) & \hat{G}_2(\boldsymbol{\theta}) & \hat{G}_3(\boldsymbol{\theta}) \end{bmatrix}^T \tag{4.3}$$

Gravity compensation forms the basis of the control action applied to the plant. It serves as a "best guess" at the moments of force needed to hold the model in a static configuration. Static calibration is used to identify these joint torques for various configurations of the biomechanical model. The model is placed into various configurations and the joint torques required to hold the model in place are identified for each configuration. Interpolation may be used for estimating the set of joint torques

which maintain a static pose for configurations not used in the static calibration process. Because this process is trivial, the true model gravity characteristics (derived in Appendix B) were used in place of $\hat{G}(\boldsymbol{\theta})$ allowing this work to focus entirely on motion control of the plant. Therefore, for simulation purposes

$$\hat{\mathbf{G}}(\boldsymbol{\theta}) = G(\boldsymbol{\theta})$$

$\hat{\mathbf{G}}$ is summed with the movement control action, $\boldsymbol{\tau}'$, to form the final control action $\boldsymbol{\tau}$ as shown in Figure 4.1.

4.4 Fuzzy Control System Implementation

All fuzzy systems used in this work are of the Takagi-Sugeno type. As previously discussed in Section 2.5.7, the consequent of every rule in a Takagi-Sugeno fuzzy system must be a linear or affine function. In this work, numeric constants - each associated with a particular control action - and typically defined on the range $[-1, 1]$, were used to specify the consequent of each rule in the rule-base. Therefore, a coding scheme was developed for each fuzzy system used in this work, where numeric values corresponded to specific control actions. Symbolic names were used to store the numeric values associated with each control action. For example, the value 1 was normally associated with applying a large positive torque to a joint. If we let the symbolic name POSLG represent the value 1, the rule

IF $\theta_{CoM(Err)}$ IS "fwd" AND $\dot{\theta}_1$ IS "zero" THEN $b = 1$

may be stated as

IF $\theta_{CoM(Err)}$ IS "fwd" AND $\dot{\theta}_1$ IS "zero" THEN $b =$ POSLG

making rules in the rule-base slightly more intuitive than using numeric values directly.

Also discussed in Chapter 2, the *product method* was used to perform the "and" operation in the premise of the rules (given by equation 2.7), while defuzzification was accomplished using the weighted average method (as described by Equation 2.9 in Section 2.5.8).

4.5 Stability Controller

The stability controller seeks to direct the biomechanical model toward the most stable configuration at all times. Using the definition of base of support and model stability discussed in Section 3.2.6, as well as expert knowledge of the sit-to-stand task, "maximally" stable configurations of the model were determined for both the seated and not seated conditions. Desired, or reference, values were established for each maximally stable configuration of the biomechanical model.

4.5.1 Reference Values

While seated, the HAT is brought into a forward lean position, shifting the total-body center of mass forward with it. This has the effect of improving model stability in the backward direction (when compared to sitting upright) and reducing it in the forward direction; a desirable effect in anticipation of lifting off from the chair's surface. Reducing model stability in the forward direction allows for generating quicker forward movement, not unlike how a sprinter positions their total-body center of mass as far forward (within their base of support) as possible at the start of a race. Forward lean of the HAT also reduces the moment of inertia (resistance to angular motion) of the body about the ankle and knee joints; another desirable effect in anticipation of seat-off. The desired degree of forward lean, as measured by the limb segment angle θ_{123}, (i.e., the angle which describes the absolute orientation of the

HAT), was specified as

$$\theta_{123(Ref)} = 60 \text{ deg}$$

a typical value observed at hip-lock in the momentum-transfer strategy [15], (i.e., it is at this angle that the hip becomes locked in anticipation of seat-off).

The error between the current limb segment angle θ_{123} and the reference value $\theta_{123(Ref)}$ is given by

$$\theta_{123(Err)}(t) = \theta_{123(Ref)} - \theta_{123}(t) \tag{4.4}$$

When not seated, the biomechanical model, as a whole, was moved toward a configuration in which the total body center of mass, θ_{CoM}, was positioned at the midpoint of the base of support, slightly forward of the ankle(as illustrated in Figure 3.4 b)). The reference value associated with this configuration, denoted as $\theta_{CoM(Ref)}$, was calculated as

$$\theta_{CoM(Ref)} = arccos\left(\frac{x_d}{R_{CoM}}\right) \tag{4.5}$$

where x_d is the midpoint of the base of support defined for the "not seated" condition, and R_{CoM} is the distance from the ankle to the total body center of mass.

The error between the desired value of θ_{CoM}, denoted $\theta_{CoM(Ref)}$, and its current value is given by Equation 3.11.

4.5.2 Controller Architecture

The stability controller produces a control action $\boldsymbol{\tau}_{stab}$ (Nm), where

$$\boldsymbol{\tau}_{stab} = \begin{bmatrix} \tau_{stab(1)} & \tau_{stab(2)} & \tau_{stab(3)} \end{bmatrix}^T$$

and $\tau_{stab(1)}$, $\tau_{stab(2)}$, and $\tau_{stab(3)}$ represent the moments of force applied to the ankle, knee, and hip joint respectively. A separate fuzzy control process is used to generate each of the joint torques $\tau_{stab(1)}$, $\tau_{stab(2)}$, and $\tau_{stab(3)}$. In this respect, the stability con-

troller is a conglomeration of three fuzzy control processes. The control architecture for the stability controller is depicted in Figure 4.2.

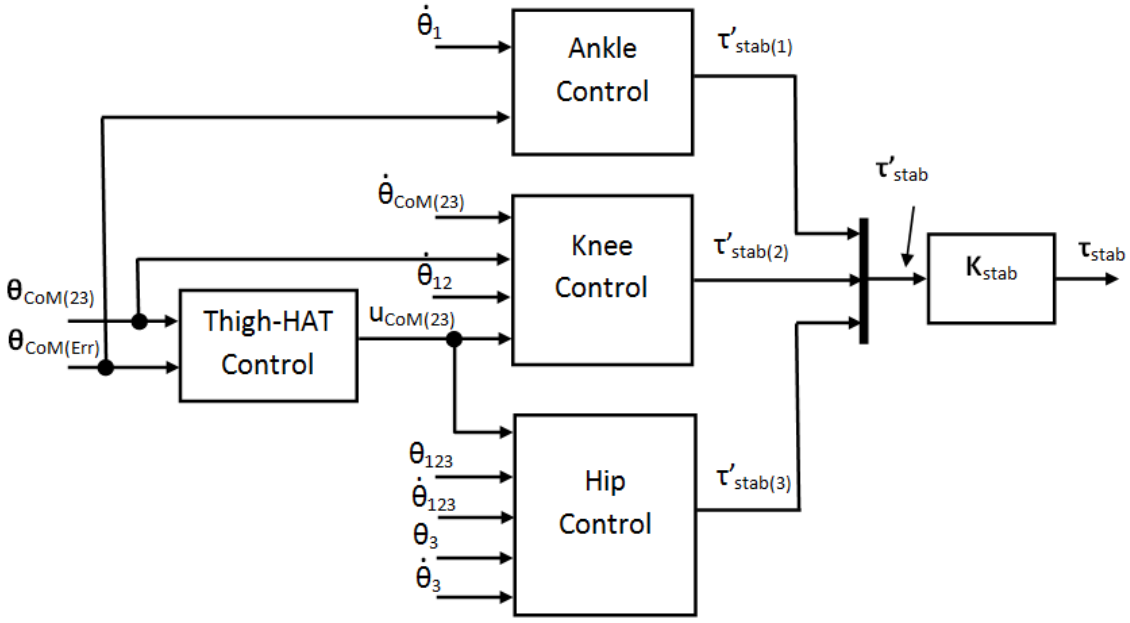

Figure 4.2: Control architecture of the stability controller.

A control preprocess, based upon the control of the thigh-HAT composite object, is used to generate the control directive $u_{CoM(23)}$, as shown in Figure 4.2. This signal is forwarded to the knee and hip joint controllers to help form the motion control action of these joints. The knee joint controller also requires the absolute angular velocity of the thigh, $\dot{\theta}_{12}$, in order to dictate a motion control action. Motion control of the hip is accomplished using $u_{CoM(23)}$ along with the absolute orientation of the HAT θ_{123} and its associated absolute velocity $\dot{\theta}_{123}$. The orientation and angular velocity of the thigh-HAT composite object, denoted $\theta_{CoM(23)}$ and $\dot{\theta}_{CoM(23)}$ respectively, are used to form a control action which maintains the current position of the knee. θ_3 and the joint velocity $\dot{\theta}_3$ are used for a similar purpose in the hip controller. Input to the ankle controller includes the error in the orientation of the total-body center of mass, given by $\theta_{CoM(Err)}$ (given in Equation 3.11), along with the angular velocity of the ankle joint, represented by $\dot{\theta}_1$.

All three joint controllers implement a control architecture similar in style to proportional-derivative (PD) control, (i.e., joint angles and their rates of change serve as primary inputs to each control system). The output of each controller, $\tau'_{stab(1)}$, $\tau'_{stab(2)}$, and $\tau'_{stab(3)}$ respectively, all of which are in the interval $[-1, 1]$, is scaled to form an appropriate control action in Newton-meters (Nm). In the next few sections, the design of each controller is discussed in detail.

4.5.3 Ankle Joint Control

Ankle joint control is based on $\theta_{CoM(Err)}$, (i.e., the error in the degree of forward lean of the whole body inverted pendulum model, as illustrated in Figure 3.5), and the angular velocity of the ankle itself, which is given by $\dot{\theta}_1$. A fuzzy controller is used to map these inputs to an appropriate control action $\tau'_{stab(1)}$.

Controller Architecture

The control architecture of the ankle control system is shown in Figure 4.3.

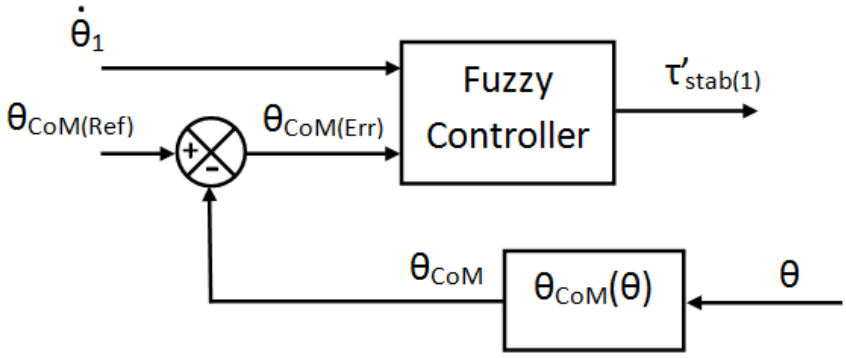

Figure 4.3: Control architecture of the ankle joint controller.

Membership Functions

The membership functions associated with the input variables, $\theta_{CoM(Err)}$ and $\dot{\theta}_1$, are shown in Figure 4.4. As discussed in Section 2.5.4 of Chapter 2, triangular membership functions were used throughout this work. $\theta_{CoM(Err)}$ was defined over the universe of discourse $U_1 = [-5, 5]$ deg (or $[-0.0873, 0.0873]$ rad) while $\dot{\theta}_1$ existed

on the universe of discourse $U_2 = [-15, 15]$ deg/s (or $[-0.2618, 0.2618]$ rad/s). The extents of each universe of discourse are ranges typically used in the control of inverted pendulum systems [26] (recalling that $\theta_{CoM(Err)}$ is associated with the inverted pendulum representation of the biomechanical model as discussed in Section 3.2.7). The error in angular position, given here by $\theta_{CoM(Err)}$, is normally restricted to a tight tolerance (approximately ± 5 deg), while the angular rate, $\dot{\theta}_1$, must be selected appropriately for the application. The value 25 deg/s was originally selected, but through simulated experiments, 15 deg/s (or 0.2618 rad/s) was found to be a more appropriate value for this application.

Values of the input variables which fall outside of the universe of discourse, for any fuzzy system used in this work, were mapped to a membership of 1.0 in the nearest fuzzy set. Membership in the left and rightmost membership functions may then be expressed as

$$\mu_{A_j^i}(x) = \begin{cases} 1 & x < \gamma_1, \\ 1 - \frac{|x-\gamma_1|}{\sigma_1} & \gamma_1 \leq x \leq \gamma_1 + \sigma_1, \\ 0 & x > \gamma_1 + \sigma_1 \end{cases} \tag{4.6a}$$

$$\mu_{A_l^i}(x) = \begin{cases} 0 & x < \gamma_2 - \sigma_2, \\ 1 - \frac{|x-\gamma_2|}{\sigma_2} & \gamma_2 - \sigma_2 \leq x \leq \gamma_2, \\ 1 & x > \gamma_2 \end{cases} \tag{4.6b}$$

where $\mu_{A_j^i}$ is the leftmost membership function for the i^{th} input variable existing on a universe of discourse U_i, $\mu_{A_l^i}$ is the rightmost membership function existing on the same universe of discourse, parameters γ_1 and γ_2 specify the center of each membership function respectively, and parameters σ_1 and σ_2 specify their widths.

Membership functions - and specifically, membership functions centers - are typi-

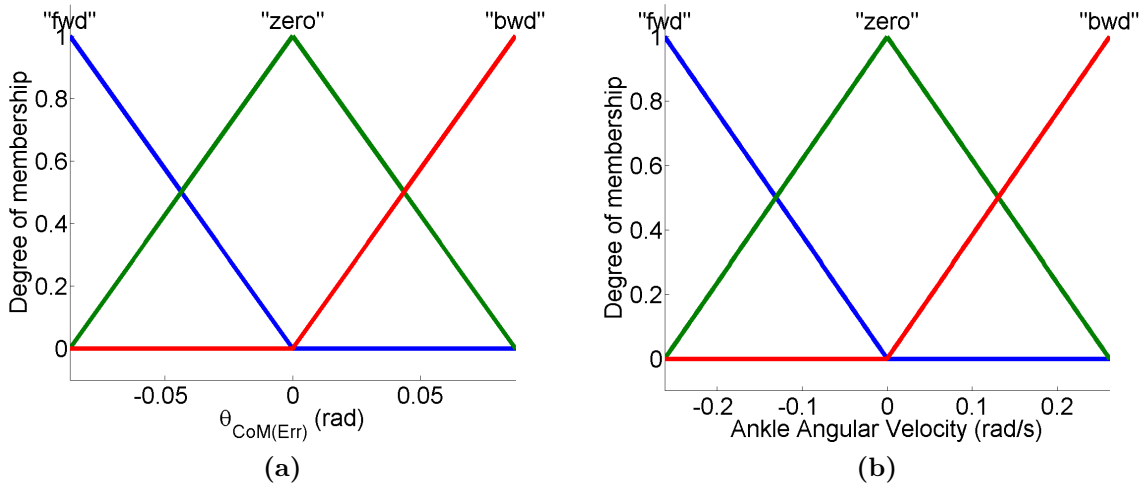

Figure 4.4: Membership functions for the input variables of the ankle joint controller.

Action	**Symbolic Name**	**Value**
Apply large positive torque	POSLG	1
Apply positive torque	POS	0.5
Apply zero torque	ZERO	0
Apply negative torque	NEG	-0.5
Apply large negative torque	NEGLG	-1

Table 4.1: Control actions and the numeric values/symbolic names used to represent them for the output variable $\tau'_{stab(1)}$.

cally distributed evenly over their universe of discourse; however, during the controller tuning process, shifting the membership function centers is one option available to the control engineer. In this work, numeric constants, denoted $K_i : i = 1, 2, \ldots, M$, where M is the number of unique control actions, were used to specify the consequents of the rules, rather than use linguistic values with an associated membership function (as discussed in Sections 2.5.7 and 4.4). Similar to evenly distributing membership function centers across a universe of discourse, fuzzy singletons, located at K_i for $i = 1, 2, \ldots, M$, were spread evenly across the output space (i.e., universe of discourse) Y_i. Using the ankle joint controller as an example, the output space $[-1, 1]$ is divided evenly amongst the control actions defined for the controller, as summarized in table 4.1.

$\tau'_{stab(1)}$		$\theta_{CoM(Err)}$		
		"fwd"	"zero"	"bwd"
$\dot{\theta}_1$	"fwd"	POSLG	POS	ZERO
	"zero"	POS	ZERO	NEG
	"bwd"	ZERO	NEG	NEGLG

Table 4.2: Ankle Joint FAM Table.

FAM Table

A fuzzy associative memory (FAM) table succinctly summarizes the rules employed by a fuzzy system. Linguistic values associated with input variables are listed along the row and column headings. Cells of the table contain each rule's consequent. Using the definitions in Table 4.1, the FAM table for the control of the ankle joint is completed as shown in Table 4.2. Hence, from Table 4.2 the first of the nine rules can be seen to be stated as

IF $\theta_{CoM(Err)}$ IS "fwd" AND $\dot{\theta}_1$ IS "zero" THEN b_1 = POSLG

where b_1 is the consequent of rule #1 and POSLG = 1.

All rules are fired to some degree during the inference step (as discussed in Section 2.5.8). The implication of each rule, (i.e., the consequent of the rule multiplied by the rules relevance), is given by Equation 2.8, restated here as

$$b_i \cdot \mu_i(u_1, u2, \ldots, u(n))$$

where b_i is the consequent of the i^{th} rule and $\mu_i(u_1, u2, \ldots, u(n))$ (given by Equation 2.7) is the certainty that the i^{th} rule is relevant to the controller input.

Figure 4.5 illustrates an example of how the fuzzy rules of the ankle joint controller are evaluated to produce the final output $\tau'_{stab(1)}$. Let $\theta_{CoM(Err)} = -0.04365$ rad (-2.5 deg) and $\dot{\theta}_1 = 0.1309$ rad (7.5 deg/s), and Y_i denote the universe of discourse associ-

ated with the output variable $\tau'_{stab(1)}$. Note that these values exist halfway between 0 and the extents of the respective universes of discourse of the input variables. Each row of graphical elements represents a rule in the rule-base (numbered 1 through 9). The first two columns of this figure represent the membership functions defined for the input variables, $\theta_{CoM(Err)}$ and $\dot{\theta}_1$ (as shown in Figure 4.4), respectively. The third column shows fuzzy singletons, existing on the output space Y_i, whose amplitudes are equal to $\mu_i(u_1, u2)$, (i.e., the rule's relevance to the input values). The range of each graphical element in Figure 4.5 is $[0, 1]$.

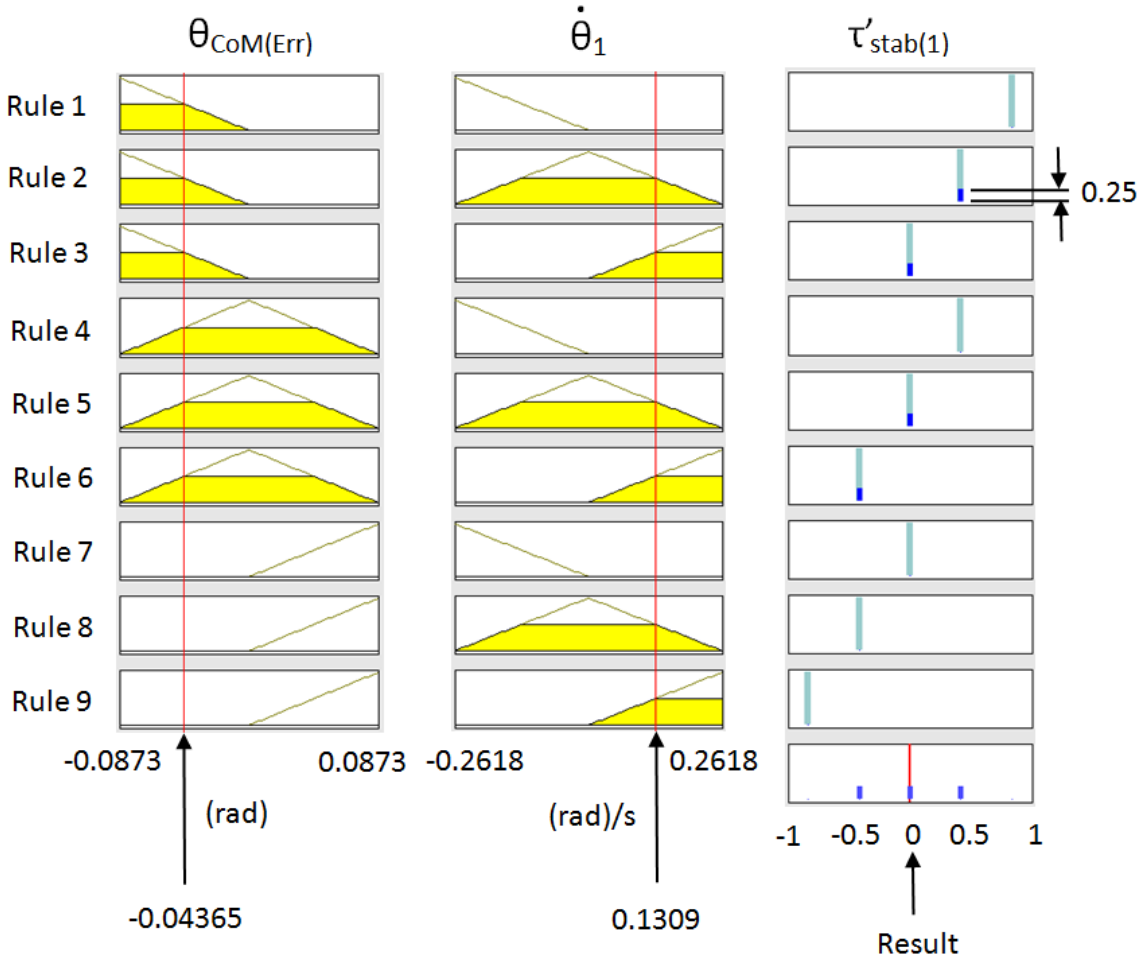

Figure 4.5: An example of how the inputs to the ankle joint controller are evaluated to produce the output $\tau'_{stab(1)}$.

In looking at the first row of graphical elements, which correspond to rule #1, the

input $\theta_{CoM(Err)} = -0.04365$ rad is characterized by the linguistic value "fwd" with a certainty of 0.5, and the input $\dot{\theta}_1 = 0.1309$ rad is characterized by the linguistic value "fwd" with a certainty of 0. The certainty, then, that rule #1 is relevant to the input of the controller, is given by Equation 2.7, as

$$\begin{aligned}\mu_1(u_1, u2) &= 0.5 \cdot 0 \\ &= 0\end{aligned}$$

Rule #1 is therefore fired to a degree of 0, because it holds a relevance of 0 with respect to the controller input. The rule's implication, $b_1 \cdot \mu_1(u_1, u2)$, is calculated as

$$\begin{aligned}b_1 \cdot \mu_1(u_1, u2) &= 1 \cdot 0 \\ &= 0\end{aligned}$$

In order to form a single crisp output value, the weighted average method is used to combine the implications of each rule, as

$$\begin{aligned}y = \frac{\sum_{i=1}^{9} b_i \cdot \mu_i}{\sum_{i=1}^{9} \mu_i} &= 1 \cdot 0 + 0.5 \cdot 0.25 + 0 \cdot 0.25 + 0.5 \cdot 0 + 0 \cdot 0.25 + (-0.5) \cdot 0.25 \\ &\quad + 0 \cdot 0 + (-0.5) \cdot 0 + (-1) \cdot 0 \\ &= 0\end{aligned}$$

The output of the controller then, for this example, is $\tau'_{stab(1)} = 0$ Nm.

4.5.4 Thigh-HAT Composite Control

Control of both the knee and hip joints rely on the absolute inclination of the total body center of mass vector, given by θ_{CoM} (as defined in Equation 3.9), and the inclination of the thigh-HAT composite center of mass vector, represented by $\theta_{CoM(23)}$

(given by Equation 3.14). A fuzzy controller is used to interpret these inputs and output the control action $u_{CoM(23)} \in [-1, 1]$. The thigh-HAT composite controller dictates how the orientation of thigh-HAT composite object is to be adjusted - by way of knee and hip joint actuation - to promote improved stability in the biomechanical model. Three control actions are defined:

1. **Forward** (FWD). Rotate the thigh-HAT composite in the clockwise direction.
2. **Backward** (BWD). Rotate the thigh-HAT composite in the counterclockwise direction.
3. **Hold** (HOLD). Maintain the current orientation of the thigh-HAT composite object.

Control Architecture

The control architecture of the thigh-HAT composite controller is shown in Figure 4.6.

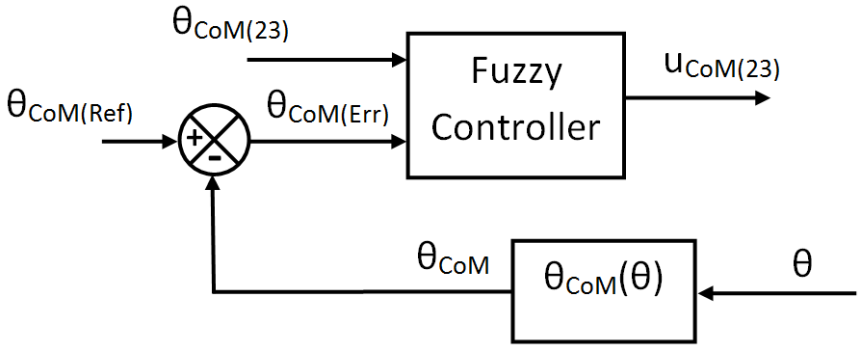

Figure 4.6: Control architecture of the thigh-HAT composite controller.

Membership Functions

Membership functions associated with the input variables are shown in Figure 4.7. Membership function definitions for θ_{CoM} are the same as they were in the ankle joint controller (discussed in Section 4.5.3). Membership function definitions for

Action	Symbolic Name	Value
Rotate thigh-HAT backward	BWD	1
Hold in place	HOLD	0
Rotate thigh-HAT forward	FWD	-1

Table 4.3: Control actions and the numeric values/symbolic names used to represent them for the thigh-HAT composite controller.

$\theta_{CoM(23)}$ were based on the maximum and minimum values achieved by $\theta_{CoM(23)}$. The center of the membership function associated with the linguistic value "bwd" was set to the value of $\theta_{CoM(23)}$ achieved when the biomechanical model was in a seated configuration, namely 1.0974 rad. The center of the membership function associated with the linguistic value "fwd" was set to the value of $\theta_{CoM(23)}$ achieved when the biomechanical model was in a standing, slightly forward leaning configuration, namely -0.3671 rad.

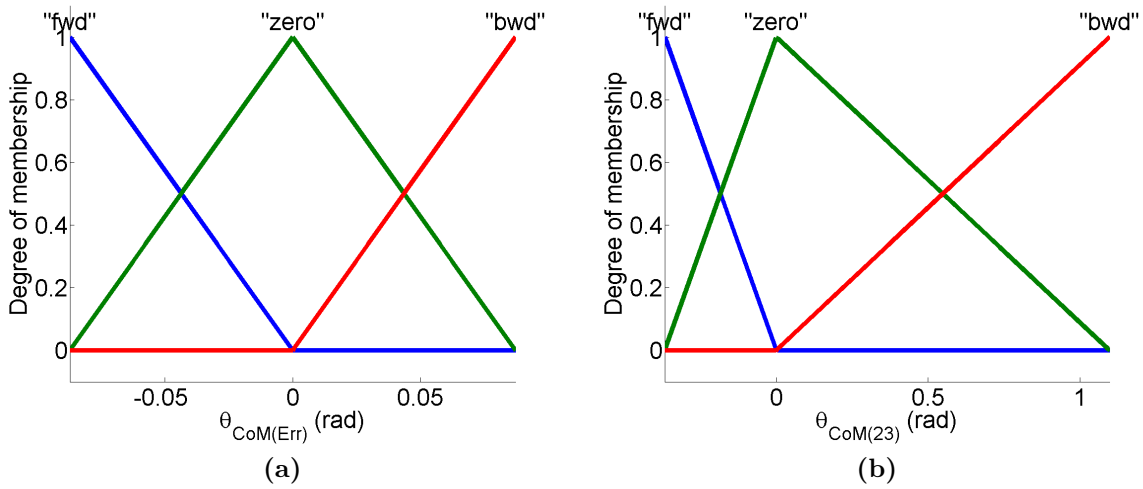

Figure 4.7: Membership functions for the input variables of the thigh-HAT composite controller.

Control actions for the output variable $u_{CoM(23)}$, and the symbolic names and numeric values associated with each, are given in Table 4.3

$u_{CoM(23)}$		$\theta_{CoM(Err)}$		
		"fwd"	"zero"	"bwd"
$\theta_{CoM(23)}$	"fwd"	BWD	HOLD	HOLD
	"zero"	BWD	HOLD	FWD
	"bwd"	HOLD	HOLD	FWD

Table 4.4: Thigh-HAT Composite Object FAM Table.

Controller Guiding Principles

The following principles were used to create the rule-base for the thigh-HAT composite controller:

- If the inclination of the total-body center of mass (θ_{CoM}) has already reached its destination, do not adjust the orientation of the thigh-HAT composite, (i.e., $\theta_{CoM(23)}$) becomes a don't care).
- If the orientation of the thigh-HAT composite is already in favor of correcting for the error in θ_{CoM}, adjust it no further.
- Otherwise, actuate the knee and hip joints so that the orientation of the thigh-HAT composite object tends to correct for the error associated with θ_{CoM}, (i.e., $\theta_{CoM(Err))}$.

FAM Table

Using the guiding principles above and the definitions provided in Table 4.3, the FAM table for the control of the thigh-HAT composite object is completed as shown in Table 4.4.

4.5.5 Hold of Thigh-HAT Composite Object

Two fuzzy controllers, one existing within the control architecture of the knee joint controller, and the other the hip joint controller, were used to implement the "hold" action dictated by the thigh-HAT composite control system (as discussed in Section

4.5.4). The control actions dictated by these "hold" joint controllers worked to maintain the positions of the knee and hip joints respectively. Discussed further in their respective sections (Sections 4.5.6 and 4.5.8), a "hold" action is incorporated into the control law of both the knee and hip joint controllers. This action is weighted more or less heavily depending the weighting factor, $w_{Hold} \in [0, 1]$, which is calculated as

$$w_{Hold} = 1 - \left| u_{CoM(23)} \right| \tag{4.10}$$

where $u_{CoM(23)}$ is the thigh-HAT composite control action.

Internal reference values, (i.e., internal to the knee and hip joint controllers, denoted $\theta_{2(Ref)}$ and $\theta_{3(Ref)}$), are maintained for the knee and hip joints respectively. Any deviation from these values is suppressed by the respective "hold" joint controllers. The deviation, or error, associated with each joint is calculated as

$$\theta_{2(Err)} = \theta_{2(Ref)} - \theta_{CoM(23)} \tag{4.11a}$$

$$\theta_{3(Err)} = \theta_{3(Ref)} - \theta_3 \tag{4.11b}$$

where $\theta_{2(Err)}$ and $\theta_{3(Err)}$ are the joint position errors associated with holding the knee and hip joints in place respectively, $\theta_{2(Ref)}$ and $\theta_{3(Ref)}$ are the orientation of the thigh-HAT composite object and the hip joint angle, respectively, corresponding to the last known stable configuration of the biomechanical model, $\theta_{CoM(23)}$ represents the inclination of the thigh-HAT composite center of mass, and θ_3 is the hip joint angle.

Controller Architecture

A template for the control architecture of the hold joint controllers is shown in Figure 4.8. The controller inputs $\theta_{CoM(23)}$ and $\dot{\theta}_{CoM(23)}$ for the knee hold joint controller, and θ_3 and $\dot{\theta}_3$ for the hip hold joint controller, are interpreted to produce the out-

put $u_{2(Hold)}$ and $u_{3(Hold)} \in [-1, 1]$ respectively, where $u_{2(Hold)}$ and $u_{3(Hold)}$ represent degrees of joint actuation. θ_x is used to represent $\theta_2/\theta_{CoM(23)}$ in the knee hold joint controller and θ_3 in the hip hold joint controller.

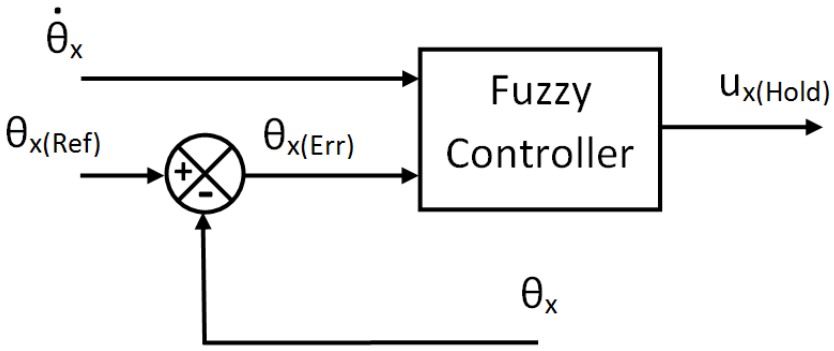

Figure 4.8: Control architecture of the hold joint controller.

Membership Functions

Figure 4.9 shows the membership functions associated with the input variables of the hold joint controllers. Joint position errors, $\theta_{2(Err)}$ and $\theta_{3(Err)}$, and their respective angular rates, $\dot{\theta}_{CoM(23)}$ and $\dot{\theta}_3$, were defined on universes of discourse normally used in the positional control of inverted pendulums (but applies equally well for the purpose of maintaining a desired joint angle). Joint position errors were defined on the input space $U_1 = [-5, 5]$ deg (or $[-0.0873, 0.0873]$ rad) while the angular rates were defined over the domain $U_2 = [-25, 25]$ deg/s (or $[-0.4363, 0.4363]$ rad/s).

Control actions associated with the output variables $u_{x(Hold)}$ where $x = \{2, 3\}$, and the symbolic names and numeric values associated with each, are given in Table 4.5

FAM Table

Using the definitions provided in Table 4.5, the FAM table for the control of the hold joint controllers is completed as shown in Table 4.6.

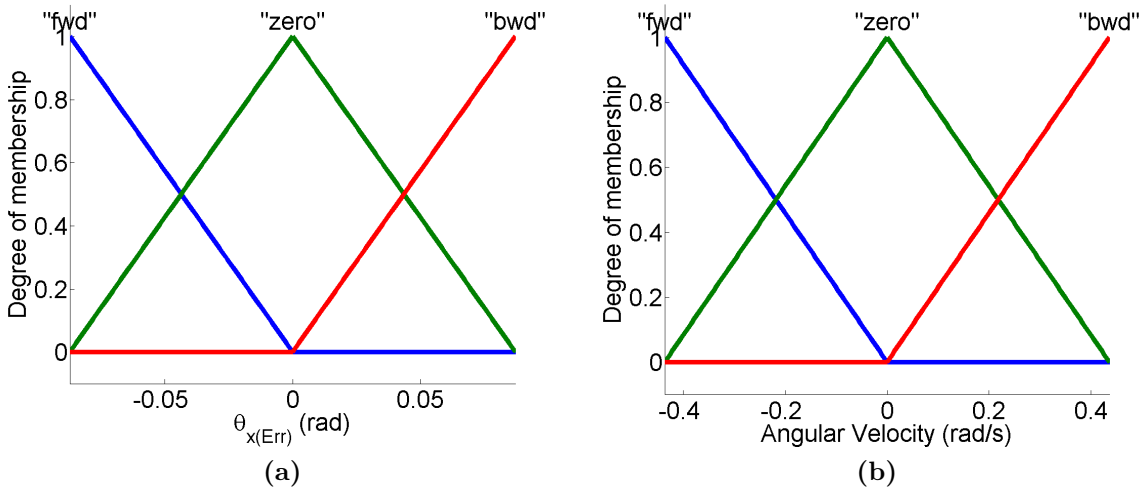

Figure 4.9: Membership functions for the input variables of the hold joint controllers.

Action	**Symbolic Name**	**Value**
Apply large positive torque	POSLG	1
Apply positive torque	POS	0.5
Apply zero torque	ZERO	0
Apply negative torque	NEG	-0.5
Apply large negative torque	NEGLG	-1

Table 4.5: Control actions and the numeric values/symbolic names used to represent them for the thigh-HAT composite controller.

4.5.6 Knee Joint Control

The control law governing the actuation of the knee joint is two part: i) a control action which tends to hold the thigh-HAT composite object in place, denoted as $u_{2(Hold)}$, and ii) a control action which tends to rotate the thigh-HAT composite object clockwise/counterclockwise, denoted $u_{2(Rot)} \in [-1, 1]$. Each of these control actions is

$u_{x(Hold)}$		$\theta_{x(Err)}$		
		"fwd"	"zero"	"bwd"
$\dot{\theta}_x$	"fwd"	POSLG	POS	ZERO
	"zero"	POS	ZERO	NEG
	"bwd"	ZERO	NEG	NEGLG

Table 4.6: Hold Joint Controller FAM Table.

generated by a separate fuzzy controller: i) the knee hold joint controller (discussed in Section 4.5.5) which produces the control action $u_{2(Hold)}$, and ii) the knee joint rotational controller (discussed in Section 4.5.7) which produces the control action $u_{2(Rot)}$. A weighting factor $w_{(Hold)}$ (given by Equation 4.10) is applied to the hold control action portion of the control law. This value is dictated by the thigh-HAT composite controller, as discussed in Section 4.5.5. The control law for the knee joint controller may be written as

$$\tau'_{stab(2)} = w_{(Hold)} \cdot u_{2(Hold)} + u_{2(Rot)} \tag{4.12}$$

Controller Architecture

The control architecture for the knee joint controller is depicted in Figure 4.10.

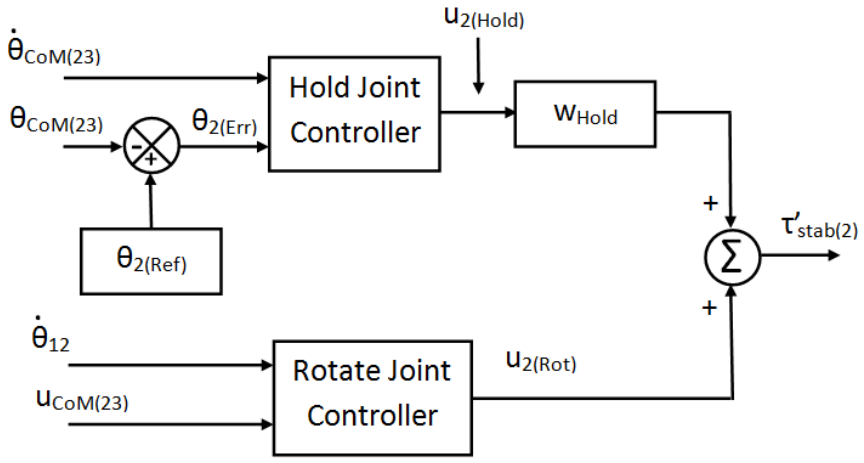

Figure 4.10: Control architecture of the knee joint controller.

4.5.7 Knee Joint Rotational Control

The thigh-HAT composite control directive $u_{CoM(23)}$, together with the limb-segment angular velocity of the thigh, $\dot{\theta}_{12}$, is interpreted by a fuzzy control system to produce the rotary control component, $u_{2(Rot)}$, of the knee joint control action $\tau'_{stab(1)}$.

Action	Symbolic Name	Value
Apply large positive torque	POSLG	1
Apply positive torque	POS	0.5
Apply zero torque	ZERO	0
Apply negative torque	NEG	-0.5
Apply large negative torque	NEGLG	-1

Table 4.7: Control actions and the numeric values/symbolic names used to represent them for the knee joint rotational controller.

Membership Functions

The membership functions associated with the input variables $u_{CoM(23)}$ and $\dot{\theta}_{12}$ are shown in Figure 4.11. $u_{CoM(23)}$ was defined on the universe of discourse $U_1 = [-1, 1]$ (as discussed in Section 4.5.4), while the angular velocity of the thigh, given by $\dot{\theta}_{12}$, was defined on the input space $U_2 = [-25, 25]$ deg/s (or $[-0.4363, 0.4363]$ rad/s). The angular rates ± 25 deg/s, were found to be sufficient in describing the rotational rates of the thigh segment during sit-to-stand.

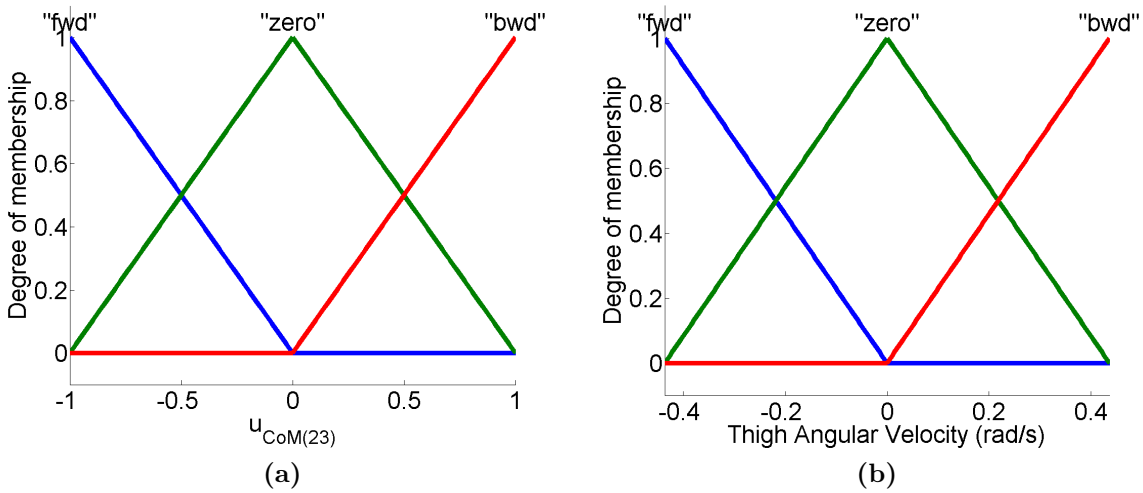

Figure 4.11: Membership functions for the input variables of the knee joint rotational controller.

Control actions associated with the output variable $u_{2(Rot)}$, and the symbolic names and numeric values associated with each, are given in Table 4.7

$u_{2(Rot)}$		$u_{CoM(23)}$		
		"fwd"	"zero"	"bwd"
$\dot{\theta}_{12}$	"fwd"	ZERO	POS	POSLG
	"zero"	NEG	ZERO	POS
	"bwd"	NEGLG	NEG	ZERO

Table 4.8: Knee Joint Rotational Control FAM Table.

FAM Table

Using the definitions provided in Table 4.7, the FAM table for the control of the hold joint controllers is completed as shown in Table 4.8.

The rotational control action $u_{2(Rot)}$ is combined with the hold joint control directive $u_{2(Hold)}$ to produce the knee joint control action $\tau'_{stab(2)}$ as given by Equation 4.12.

4.5.8 Hip Joint Control

Control of the hip joint is approached in a similar manner to control of the knee joint, (i.e., a hold joint action, $u_{3(Hold)}$, is combined with a rotational control component, denoted $u_{3(Rot)} \in [-1, 1]$, to form, in part, the final hip control action $\tau'_{stab(3)}$). Rotational control of the hip joint is dependent upon the thigh-HAT composite control directive $u_{CoM(23)}$, as well as the HAT's orientation, represented by the limb segment angle θ_{123}, and the HAT's angular rate of rotation $\dot{\theta}_{123}$. A fuzzy controller is used to interpret these inputs and output the rotary control action $u_{3(Rot)}$. A separate fuzzy control process is used to monitor the hip joint angle to ensure that the limits defined for its range of motion (RoM) are not being rapidly approached or exceeded. This was necessary for the hip joint because it undergoes a wide range of motion - and tends to develop significant momentum - during the course of the sit-to-stand cycle. The joint RoM controller produces the control action $u_{3(RoM)} \in [-1, 1]$ which effectively serves as a penalty torque at times when the joint RoM limit is being approached or exceeded. The other control actions, $u_{3(Hold)}$ and $u_{3(Rot)}$, are suppressed

at times when the range of motion controller becomes active. This is accomplished by weighting these actions by the factor $w_3(RoM) \in [0, 1]$, calculated as

$$w_{3(RoM)} = 1 - \left|u_{3(RoM)}\right| \tag{4.13}$$

In total three fuzzy controllers are used to produce the final hip joint control action $\tau'_{stab(3)}$:

1. A hold joint controller responsible for producing the control action $u_{3(Hold)}$
2. A rotational joint controller which produces the control action $u_{3(Rot)}$
3. A joint range of motion controller which produces the control action $u_{3(RoM)}$

The control law for the hip joint controller is given by Equation 4.14

$$\tau'_{stab(3)} = w_{3(RoM)} \cdot (w_{(Hold)} \cdot u_{3(Hold)} + u_{3(Rot)}) + u_{3(RoM)} \tag{4.14}$$

where weighting factors $w_{3(RoM)}$ and $w_{(Hold)}$ are given by Equations 4.13 and 4.10 respectively, and $u_{3(Hold)}$ is the control action output by the hip hold joint controller (as discussed in Section 4.5.5).

Controller Architecture

The control architecture for the hip joint controller is depicted in Figure 4.12.

4.5.9 Hip Joint Rotational Control

The thigh-HAT composite control directive $u_{CoM(23)}$, together with the limb-segment angle θ_{123}, and the angular velocity $\dot{\theta}_{123}$, are interpreted by a fuzzy controller to produce the rotary control action $u_{3(Rot)} \in [-1, 1]$.

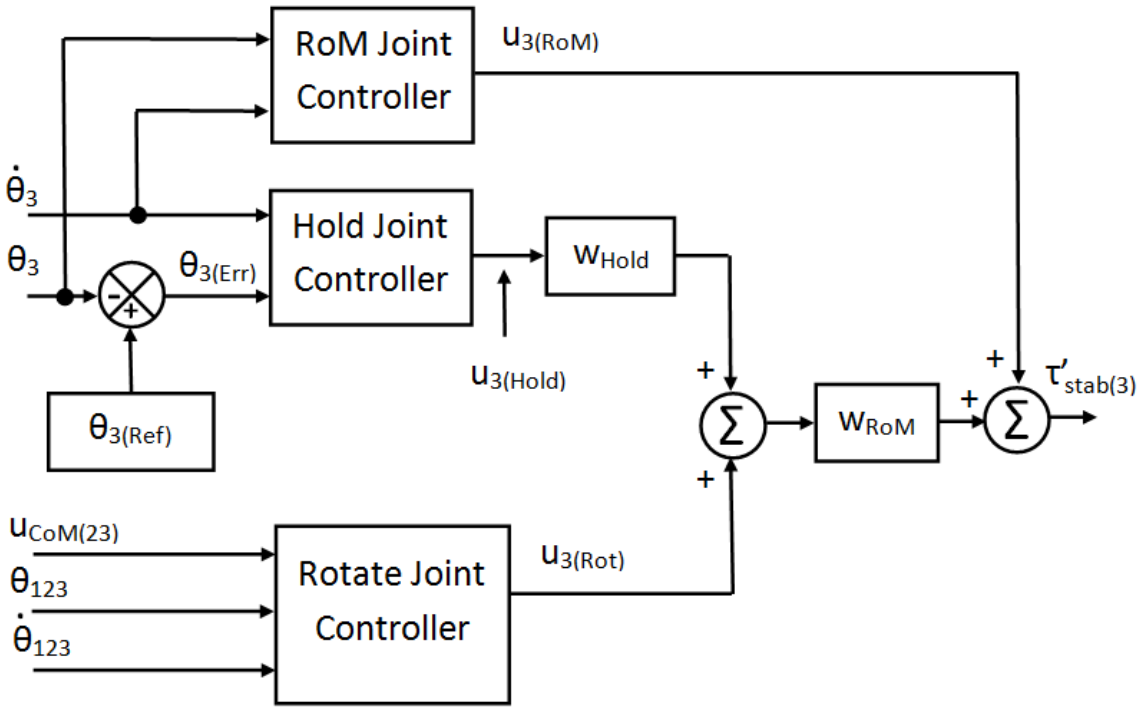

Figure 4.12: Control architecture of the hip joint controller.

Membership Functions

The membership functions associated with the input variables $u_{CoM(23)}$, θ_{123}, and $\dot{\theta}_{123}$ are shown in Figure 4.13. $u_{CoM(23)}$ was defined on the universe of discourse $U_1 = [-1, 1]$ (as discussed in Section 4.5.4). The limb-segment angle θ_{123} was defined on the input space $U_2 = [30, 95]$ deg (or $[0.5236, 1.5708]$ rad). The upper boundary of 95 deg represents the maximum expected backward lean of the HAT (i.e., very little is expected over the course of the movement), while the lower boundary, 30 deg, represents the HAT leaning as far forward as should be possible over the course of the movement. Maximum forward lean of the HAT is expected to occur following seat-off, just prior to vertical ascension.

Unlike the rotational control of the knee joint, which relied only on relative measures (i.e., the angular velocity of the thigh with respect to the control directive $u_{CoM(23)}$), rotational control of the hip joint also includes an absolute measure of the

Action	Symbolic Name	Value
Apply large positive torque	POSLG	1
Apply positive torque	POS	0.5
Apply zero torque	ZERO	0
Apply negative torque	NEG	-0.5
Apply large negative torque	NEGLG	-1

Table 4.9: Control actions and the numeric values/symbolic names used to represent them for the hip joint rotational controller.

HAT's orientation in space. Notions of "forward" and "backward" lean of the HAT were defined for the limb-segment angle θ_{123}. It was decided that no notion of "zero" lean of the HAT was required; therefore, the HAT was - at all times - considered to be leaning forward *and* backward to some degree. Membership functions associated with the angular rate of the HAT were defined on the universe of discourse $U_3 = [-45, 45]$ deg/s (or $[-0.7854, 0.7854]$ rad/s). The angular rates $\pm$ 45 deg/s were reduced from the original estimated values of $\pm$ 75 deg/s over the course of simulated experiments and controller testing. Expert knowledge of the sit-to-stand task provided an excellent starting point, but ultimately these values must be adjusted, or "tuned", by the control engineer to produce the desired result.

Control actions associated with the output variable $u_{3(Rot)}$, and the symbolic names and numeric values associated with each, are summarized in Table 4.9

Controller Guiding Principles

- actuate the hip joint as directed by $u_{CoM(23)}$ unless the HAT is already leaning, or moving, in favor of this action

- if the HAT is leaning in a given direction, and moving in the same direction, take action to avoid exceeding the range of motion limit

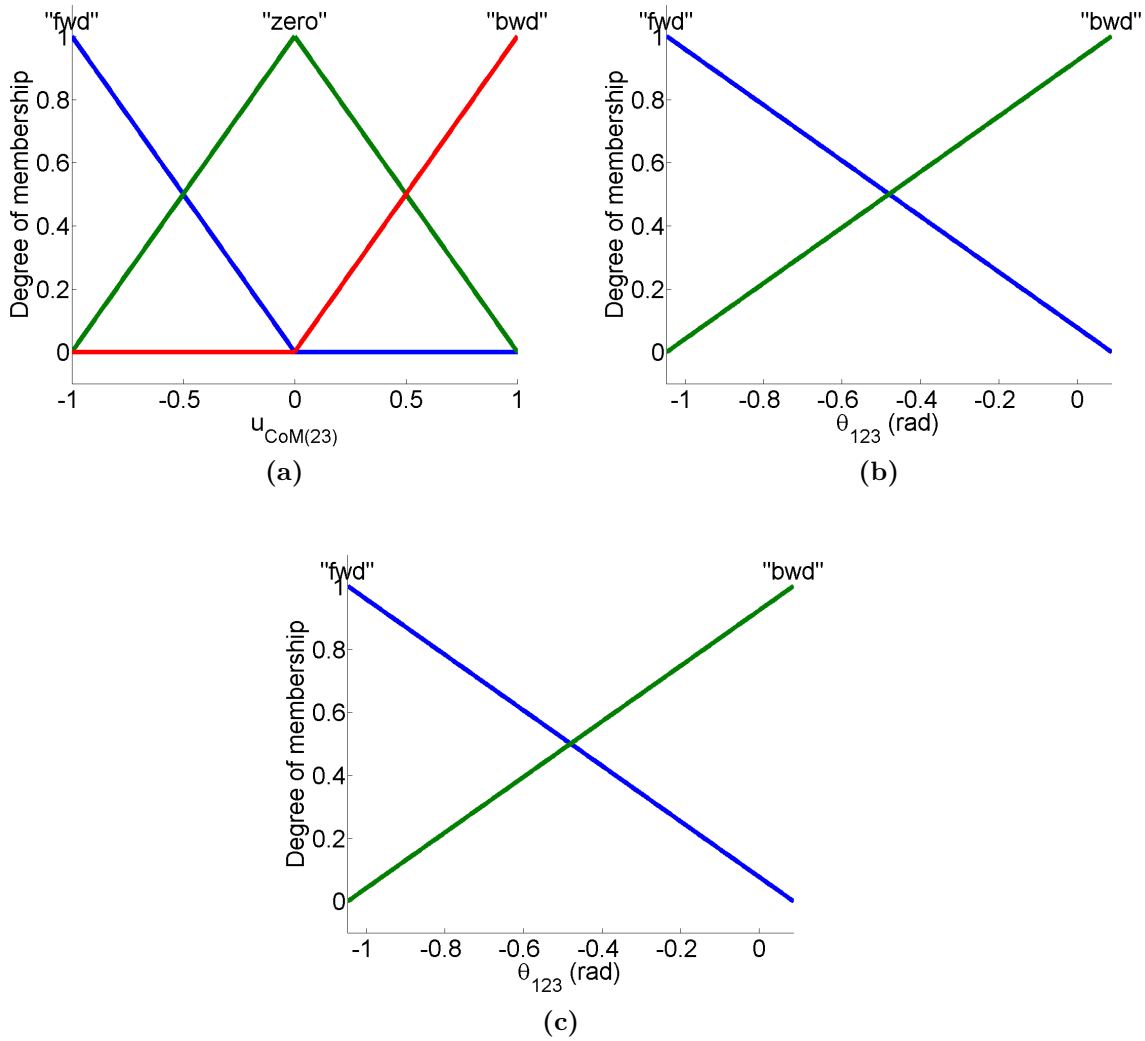

Figure 4.13: Membership functions for the hip joint rotational controller. (a) control directive $u_{CoM(23)}$ output by the thigh-HAT composite controller, (b) the limb-segment angle of the HAT given by θ_{123}, and (c) its associated angular velocity $\dot{\theta}_{123}$.

FAM Table

Using the guiding principles above and the definitions provided in Table 4.9, the FAM table for the control of the hip joint rotational controller is completed as shown in Table 4.10.

$u_{3(Rot)}$		$u_{CoM(23)}$		
θ_{123}	$\dot{\theta}_{123}$	"fwd"	"zero"	"bwd"
"fwd"	"fwd"	POS	POS	POS
	"zero"	ZERO	ZERO	POS
	"bwd"	NEG	NEG	ZERO
"bwd"	"fwd"	POS	POS	POS
	"zero"	ZERO	ZERO	POS
	"bwd"	NEG	NEG	ZERO

Table 4.10: Hip Joint Rotational Control FAM Table.

4.5.10 Hip Joint Range of Motion Control

In the event that the hip joint is rapidly approaching - or has already exceeded - its range of motion limit (as given in Table 3.2), a control action, denoted $u_{3(RoM)}$, is used to produce a penalty force which corrects for this. The hip joint angle, θ_3, existing on the universe of discourse $U_1 = [-135, 0]$ deg (or $[-2.3562, 0.0873]$ rad), and its associated angular rate, $\dot{\theta}_3$, existing on the universe of discourse $U_2 = [-15, 15]$ deg (or $[-0.2618, 0.2618]$ rad), were interpreted by a fuzzy controller to produce the control action $u_{3(RoM)}$. The extents of U_1 are simply the range of motion limits provided in Table 3.2 for the hip joint. A tight tolerance of ± 15 deg/s was placed on $\dot{\theta}_3$, so that even small (i.e., slow) angular rates were considered to be significant in regions where the hip joint approached the limits of its range of motion.

Membership Functions

The membership functions for the input variables of the controller are illustrated in Figure 4.14. Hip joint angles within 2.5 deg (or 0.0436 rad) of the of the joint's range of motion limits were considered to be in "close proximity" the limit. These regions of U_1 are associated with the membership functions labeled as "romprox1" (to do with the hip being fully flexed) and "romprox2" (to do with the hip being fully extended) in the figure.

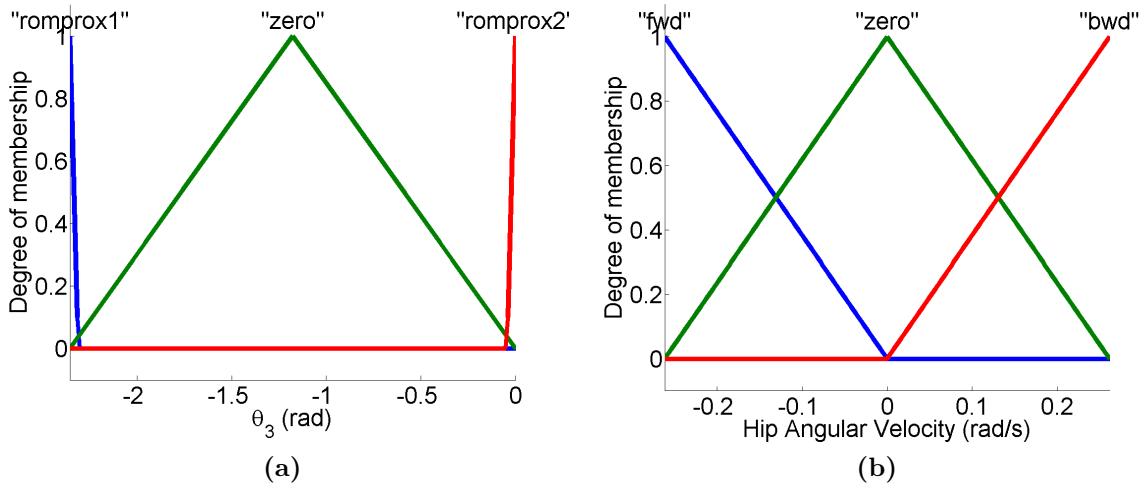

Figure 4.14: Membership functions for the input variables of the hip joint range of motion controller: (a) the hip joint angle given by θ_3, and (b) its associated angular rate $\dot{\theta}_3$.

Action	**Symbolic Name**	**Value**
Apply large positive torque	POSLG	1.0
Apply positive torque	POS	0.5
Apply zero torque	ZERO	0
Apply negative torque	NEG	-0.5
Apply large negative torque	NEGLG	-1.0

Table 4.11: Control actions and the numeric values/symbolic names used to represent them for the hip joint range of motion controller.

Control actions associated with the output variable $u_{3(RoM)}$, and the symbolic names and numeric values associated with each, are summarized in Table 4.11

Controller Guiding Principles

- If the hip joint angle has ventured into a region defined as being in close proximity the joint's range of motion limit, and isn't moving, actuate the hip to a moderate degree to correct for this.

- If the hip joint angle has ventured into a region defined as being in close proximity the joint's range of motion limit, and is moving further into this region, actuate the hip significantly to correct for this.

$u_{3(RoM)}$		θ_3		
		"romprox1"	"zero"	"romprox2"
$\dot{\theta}_3$	"fwd"	POSLG	ZERO	ZERO
	"zero"	POS	ZERO	NEG
	"bwd"	ZERO	ZERO	NEGLG

Table 4.12: Hip Joint Range of Motion Control FAM Table.

- If the hip joint angle has ventured into a region defined as being in close proximity the joint's range of motion limit, and is already moving out of this region, *or*, the joint angle does not fall into one of these regions, no action is required.

FAM Table

Using the guiding principles above and the definitions provided in Table 4.11, the FAM table for the control of the hip joint rotational controller is completed as shown in Table 4.12.

4.5.11 Hip Joint Final Control Action

The rotational control action $u_{3(Rot)}$ is combined with the hold joint control directive $u_{3(Hold)}$ and the range of motion control action $u_{3(RoM)}$ to produce the hip joint control action $\tau'_{stab(3)}$ as given by Equation 4.14.

4.5.12 Stability Controller Output

Degrees of actuation for each joint of the stability controller, contained in $\boldsymbol{\tau}'_{stab}$, are transformed into joint torques (measured in Newton-meters (Nm)) using a simple linear scaling function, given in Equation 4.15

$$\boldsymbol{\tau}_{stab} = K_{stab} \cdot \boldsymbol{\tau}'_{stab} \tag{4.15}$$

where

$$\mathbf{K}_{stab} = \begin{bmatrix} 35 & 25 & 25 \end{bmatrix} (Nm)$$

$\mathbf{K}_{stab}$ is used to scale the normalized control action $\boldsymbol{\tau}'_{stab}$ to a control action appropriate for the joint actuators. These values of $\mathbf{K}_{stab}$ were selected to accommodate a slow controlled movement of the biomechanical model (as is typical in a modern day mobility assist device for mobility impaired persons), while also being large enough to produce an acceptable transient response and to suppress unexpected joint errors (as discussed in Secion 2.3.2). Ideally, gains which serve to critically dampening disturbances in the most active regions of the plant are used. Only through simulated experiment and controller tuning were these gains found to give the desired system performance. The ankle joint is loaded more heavily, and experiences greater inertial resistance, than any other joint in the biomechanical system; therefore it has been assigned a larger control action scaling factor.

4.6 Goal Controller

The goal controller seeks to direct the biomechanical model toward the goal (i.e., standing) configuration, denoted $\boldsymbol{\theta}_f$ (as stated in Section 3.3.3), as directly as possible, giving little, to no, consideration to the stability of the model. The goal configuration is achieved when each limb segment has been rotated into its respective goal configuration orientation (as specified by $\boldsymbol{\theta}_f$). The goal controller, therefore, advances each limb segment toward its goal configuration orientation, but at a rate which also tends to advance the the total-body center of mass toward its final destination located at $\begin{bmatrix} x_{CoM(f)} & y_{CoM(f)} \end{bmatrix}$ (given by Equation 3.29).

The goal controller produces a control action $\boldsymbol{\tau}_{goal}$, where

$$\boldsymbol{\tau}_{goal} = \begin{bmatrix} \tau_{goal(1)} & \tau_{goal(2)} & \tau_{goal(3)} \end{bmatrix}^T$$

and $\tau_{goal(1)}$, $\tau_{goal(2)}$, and $\tau_{goal(3)}$ represent the moments of force applied to the ankle, knee, and hip joint respectively. Just as the stability controller was a conglomeration of three separate joint control processes, so too is the goal controller, (i.e., a separate

fuzzy controller was used to direct the actions of the ankle, knee, and hip joints). The control architecture for the stability controller is depicted in Figure 4.15.

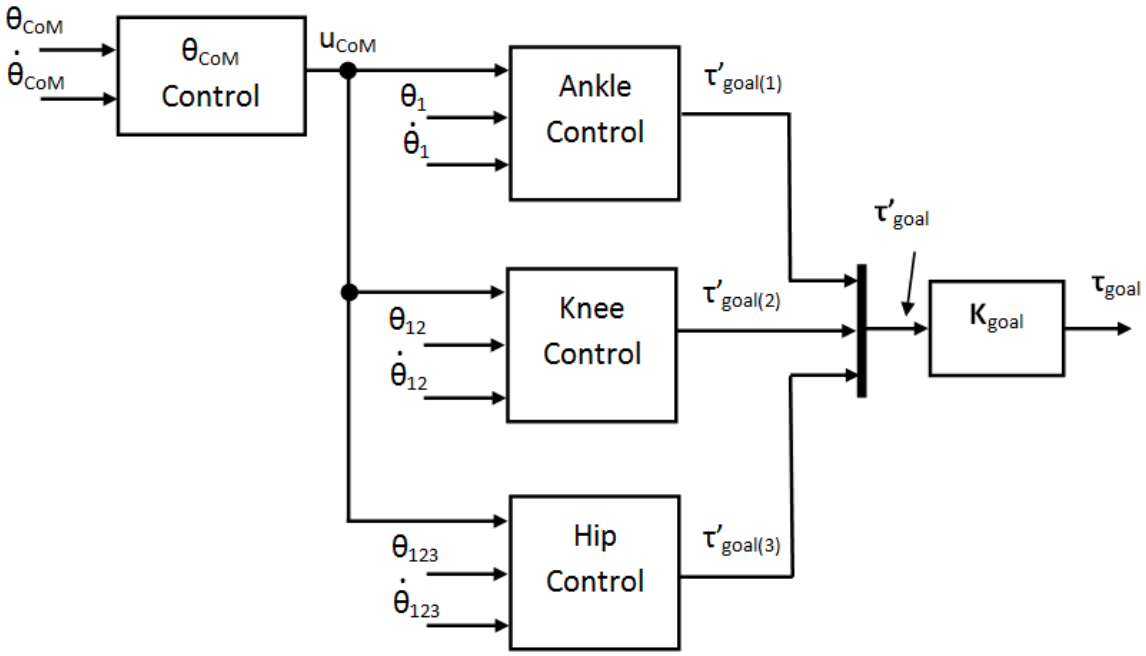

Figure 4.15: Control architecture of the goal controller.

The ankle, knee, and hip joint controllers produced the output $\tau'_{goal(1)}$, $\tau'_{goal(2)}$, and $\tau'_{goal(3)}$ respectively, each of which exists on the range $[-1, 1]$. These control actions were scaled by a factor K_{Goal}, given by Equation 4.16, to yield the goal controller output $\boldsymbol{\tau}_{(goal)}$ in Newton-meters (Nm).

Also in keeping with the control strategy employed by the stability controller, the goal controller used a control preprocess, labeled "θ_{CoM} Control" in Figure 4.15, to influence the control action output by each joint controller. The control preprocess used a fuzzy control system to interpret the error in the inclination of the total body center of mass, given by $\theta_{CoM(Err)}$, and the angular velocity, $\dot{\theta_{CoM}}$, to produce the control directive u_{CoM}, where $\theta_{CoM(Err)}$ is given by Equation 3.11 with $\theta_{CoM(Ref)}$ equal to $\boldsymbol{\theta}_f$ (given by Equation 3.35). This control signal was forwarded to each of the three joint controllers. u_{CoM} is a control action which tends to cause θ_{CoM} to assume its goal configuration value $\theta_{CoM(f)}$; therefore, the control preprocess, labeled "θ_{CoM}

Control," is essentially an inverted pendulum control system whose goal orientation is set to $\theta_{CoM(f)}$. This control process is discussed further in Section 4.6.1.

The operation of the joint controllers is discussed in Section 4.6.2.

4.6.1 θ_{CoM} Control

The "θ_{CoM} control preprocess," introduced in Section 4.6, is an inverted pendulum control process applied to the inclination of the total body center of mass given by θ_{CoM} (given by 3.9). This control process used a fuzzy control system to interpret the error in the inclination of the total body center of mass, given by $\theta_{CoM(Err)}$, and the angular velocity, $\dot{\theta_{CoM}}$, to produce the control directive $u_{CoM} \in [-1, 1]$, where $\theta_{CoM(Err)}$ is given by Equation 3.11 with $\theta_{CoM(Ref)}$ equal to $\boldsymbol{\theta}_f$ (given by Equation 3.35). The control architecture for the θ_{CoM} controller is depicted in Figure 4.16.

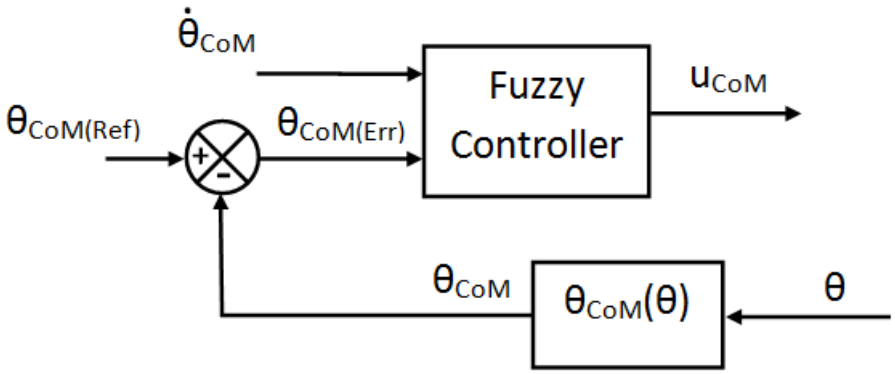

Figure 4.16: Control architecture of the θ_{CoM} control preprocess.

Membership Functions

The membership functions associated with the input variables $\theta_{CoM(Err)}$ and $\dot{\theta}_{CoM}$ are shown in Figure 4.17. $\theta_{CoM(Err)}$ was defined on the universe of discourse $U_1 = [-5, 5]$ deg (or $[-0.0873, 0.0873]$ rad) while the angular rate $\dot{\theta}_{CoM}$ existed on the domain $U_2 = [-15, 15]$ deg/s (or $[-0.2618, 0.2618]$ rad/s). Because the moment of inertia of the biomechanical model about the ankle is quite significant, angular rates given by $\dot{\theta}_{CoM}$ are not expected to be large in magnitude; therefore, the set of angular velocities, ± 15

Action	Symbolic Name	Value
Apply large positive torque	POSLG	1
Apply positive torque	POS	0.5
Apply zero torque	ZERO	0
Apply negative torque	NEG	-0.5
Apply large negative torque	NEGLG	-1

Table 4.13: Control actions and the numeric values/symbolic names used to represent them for the θ_{CoM} controller.

deg/s was used to define the bounds for U_2. To restrict the angular error associated with the inclination of the total body center of mass, given by $\theta_{CoM(Err)}$, the angular bounds ± 5 deg were defined for U_1.

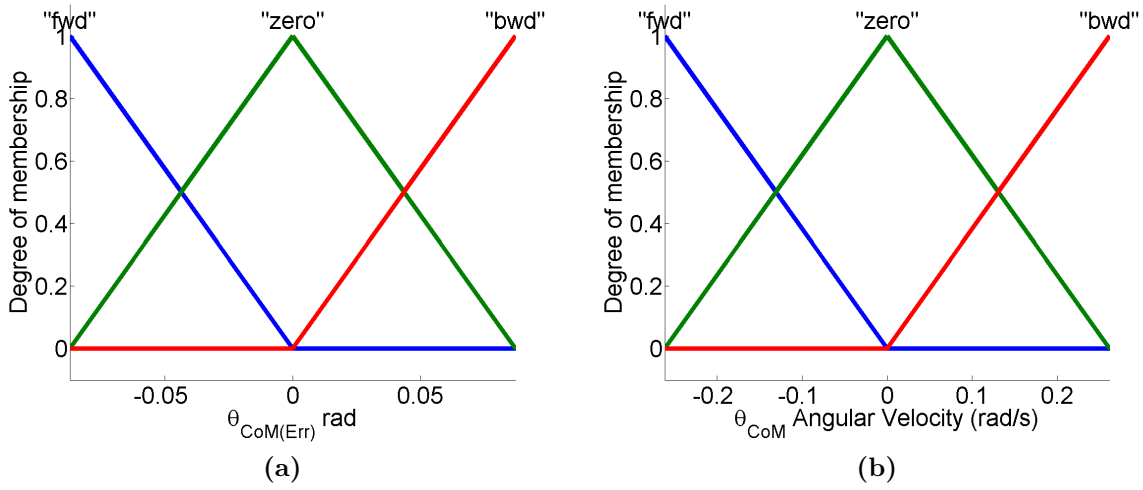

Figure 4.17: Membership functions for the θ_{CoM} controller: (a) error in the inclination of the total body center of mass, given by $\theta_{CoM(Err)}$, and (b) the associated angular velocity given by $\dot{\theta}_{CoM}$.

Control actions associated with the output variable u_{CoM}, and the symbolic names and numeric values associated with each, are summarized in Table 4.13

FAM Table

Using the definitions provided in Table 4.13, the FAM table for the control of the θ_{CoM} controller is completed as shown in Table 4.14.

u_{CoM}		$\theta_{CoM(Err)}$		
$\dot{\theta}_{CoM}$	"fwd"	POSLG	POS	ZERO
	"zero"	POS	ZERO	NEG
	"bwd"	ZERO	NEG	NEGLG

Table 4.14: θ_{CoM} Control FAM Table.

4.6.2 Joint Control

Each joint of the biomechanical model is controlled individually using a dedicated fuzzy control system (as was the case in the stability controller). All three joint controllers implemented the same control architecture, as illustrated in Figure 4.18. u_{CoM}, forwarded by the θ_{CoM} control preprocess, along with the orientation of the limb segment associated with the joint controller, given by θ_x, and the angular velocity of the limb segment, given by $\dot{\theta}_x$, where x = 1, 12, and 123, for the ankle, knee, and hip joint controllers respectively, are interpreted by a fuzzy controller to produce the output $\tau'_{goal(i)}$, where i = 1, 2, and 3, for the ankle, knee, and hip joint controllers respectively. It is the aim of the ankle, knee, and hip joint controllers to position the shank, thigh, HAT respectively, such that, the goal configuration, given by $\boldsymbol{\theta}_f$, is achieved. The goal controller is therefore a conglomeration of three single inverted pendulum control systems seeking to align the rigid body members of the biomechanical model.

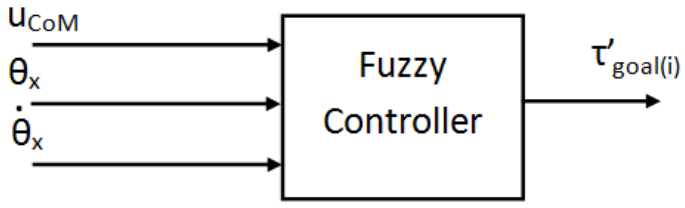

Figure 4.18: Control architecture of the joint controllers.

Membership Functions

The membership functions associated with the input variables u_{CoM}, θ_x, and $\dot{\theta}_x$, where x = 1, 12, and 123, for the ankle, knee, and hip joint controllers respectively,

	Ankle	**Knee**	**Hip**
U_2 (deg)	$[-5, 5]$	$[-5, 5]$	$[-5, 5]$
U_3 (deg/s)	$[-15, 15]$	$[-25, 25]$	$[-25, 25]$

Table 4.15: Definitions for the Universes of Discourse U_2 and U_3.

Action	**Symbolic Name**	**Value**
Apply large positive torque	POSLG	1
Apply positive torque	POS	0.5
Apply zero torque	ZERO	0
Apply negative torque	NEG	-0.5
Apply large negative torque	NEGLG	-1

Table 4.16: Control actions and the numeric values/symbolic names used to represent them for the joint controller.

are shown in Figure 4.17. u_{CoM} existed on the universe of discourse $U_1 = [-1, 1]$, which is in keeping with its definition given in Section 4.6.1). Typical values, suited to the inverted pendulum control of each joint, were used to define the universes of discourse U_2 and U_3, as summarized in Table 4.15. θ_x existed on $U_2 = [-5, 5]$ deg (or $[-0.0873, 0.0873]$ rad), while the angular rate $\dot{\theta}_x$ existed on the domain $U_3 = [-15, 15]$ deg/s (or $[-0.2618, 0.2618]$ rad/s) for the ankle joint controller and $U_3 = [-25, 25]$ deg/s (or $[-0.4363, 0.4363]$ rad/s) for the knee and hip joint controllers. A slightly more restrictive angular rate was defined for the universe of discourse corresponding to the ankle joint velocity as done previously in this work. The ankle joint is simply not expected to require the same angular rate requirements as the knee and hip joints during the course of the sit-to-stand movement.

Control actions associated with the output variable $\tau'_{goal(i)}$, where i = 1, 2, and 3, for the ankle, knee, and hip joint controllers respectively, and the symbolic names and numeric values associated with each control action, are summarized in Table 4.16

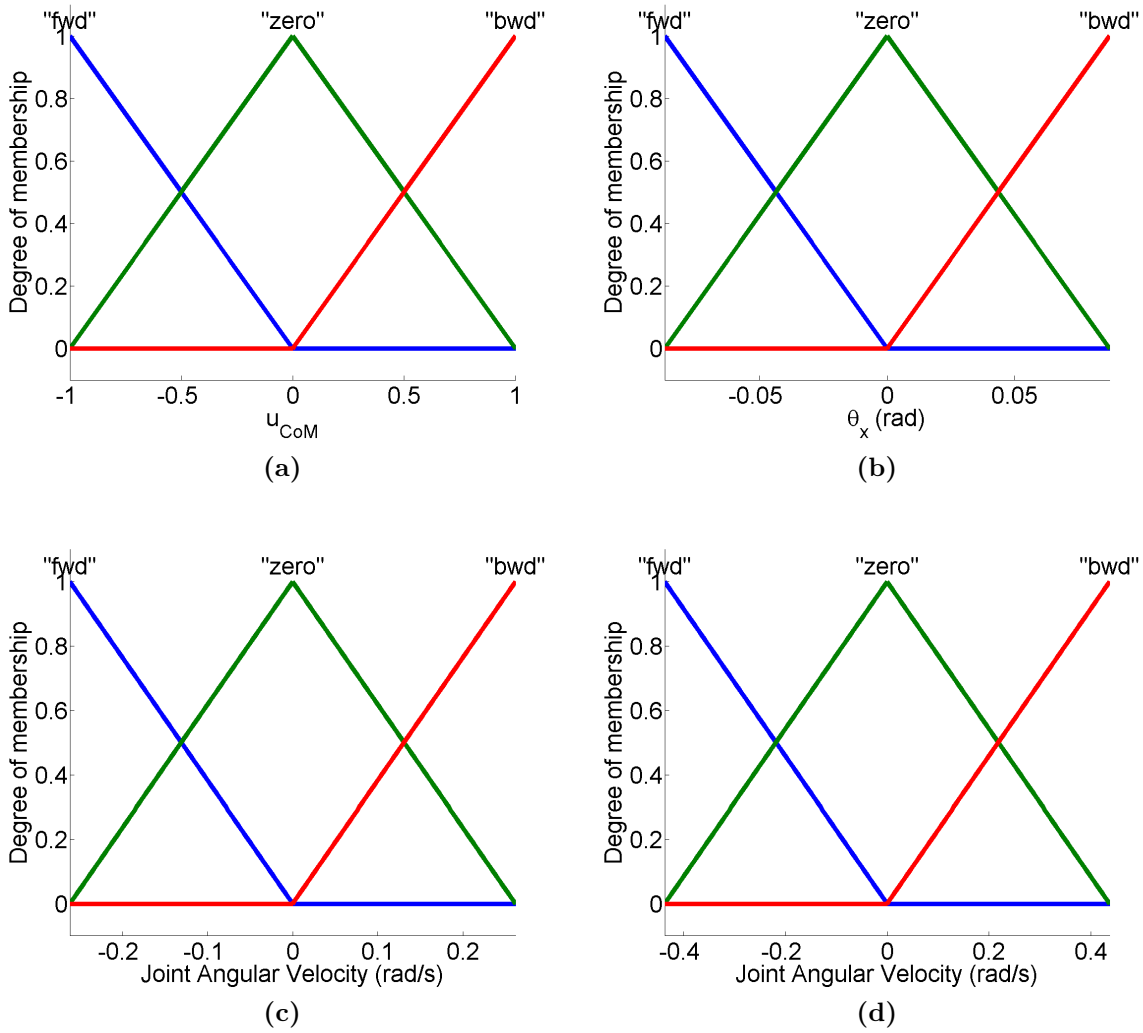

Figure 4.19: Membership functions for (a) u_{CoM}, the θ_{CoM} preprocess control directive, (b) limb segment angle θ_x, where x = 1, 12, and 123 for the ankle, knee, and hip joints respectively, (c) angular velocity of the ankle joint, given by $\dot{\theta}_1$, and (d) angular velocity of the knee and hip joints, given by $\dot{\theta}_2$ and $\dot{\theta}_3$ respectively.

Controller Guiding Principles

- Advance the limb segment toward its goal configuration at a rate which also causes the total-body center of mass to converge on its goal location.

$\tau'_{goal(i)}$		u_{CoM}		
θ_x	$\dot{\theta}_x$	"fwd"	"zero"	"bwd"
"fwd"	"fwd"	POS	POSLG	POSLG
	"zero"	ZERO	POS	POS
	"bwd"	NEG	ZERO	ZERO
"bwd"	"fwd"	ZERO	POS	POS
	"zero"	ZERO	ZERO	ZERO
	"bwd"	NEG	NEG	ZERO
"bwd"	"fwd"	ZERO	ZERO	POS
	"zero"	NEG	NEG	ZERO
	"bwd"	NEGLG	NEGLG	NEG

Table 4.17: Joint Control FAM Table for the Ankle, Knee, and Hip Joints.

FAM Table

Using the guiding principle above, and the definitions provided in Table 4.13, the FAM table for the control of the joint controllers is completed as shown in Table 4.17.

4.6.3 Goal Controller Output

As was done for the stability controller, degrees of actuation for the ankle, knee, and hip joints, contained in $\boldsymbol{\tau}'_{goal}$ are transformed into joint torques using a simple linear scaling function, as given in Equation 4.16.

$$\boldsymbol{\tau}_{goal} = K_{goal} \cdot \boldsymbol{\tau}'_{goal} \tag{4.16}$$

where

$$\mathbf{K}_{goal} = \begin{bmatrix} 25 & 20 & 20 \end{bmatrix} (Nm)$$

As with the stability controller action scaling, given by Equation 4.15, the ankle joint is again favored with a slightly greater scaling factor. This is to accommodate for the greater load and inertial resistance experienced by this joint over the course of the sit-to-stand movement. The same arguments made in Section 4.5.12 for the stability controller also apply here to the goal controller. A set of gains is determined

which give a near critical dampening of disturbances in the most active regions of the plant, while also accommodating a slow controlled movement expected of a mobility support device for persons with a mobility impairment. Also, given that a model of joint friction was not included in the dynamics of the biomechanical model, given by Equation 3.17, a slighly underdamped response, which yields good transient characteristics is desirable. Therefore, through simulated experiment and controller tuning, the values of $\mathbf{K}_{goal}$ which gave the desired level of performance were determined.

4.7 Movement Control By Way of Fuzzy Interpolation

As introduced in Section 4.2, a fuzzy-based control process was used to combine the output of the stability and goal controllers, $\boldsymbol{\tau}_{stab}$ (given by Equation 4.15) and $\boldsymbol{\tau}_{goal}$ (given by Equation 4.16) respectively, to produce the motion control action $\boldsymbol{\tau}'$. This high-level control process used a fuzzy system to assess the stability of the biomechanical model (using the definitions provided in Section 3.2.6) at every instant of the sit-to-stand movement and output a weighting factor, denoted as μ_{stab}, existing on the range $[0, 1]$. μ_{stab} signifies the degree of (biomechanical) stability associated with the biomechanical model's current configuration, given by $\boldsymbol{\theta}$. This weighting factor was applied to the output of the stability and goal controllers so that they may be combined to form the motion control action $\boldsymbol{\tau}'$ as given by Equation 4.17.

$$\boldsymbol{\tau}' = (1 - \mu_{stab}) \cdot \boldsymbol{\tau}_{stab} + \mu_{stab} \cdot \boldsymbol{\tau}_{goal} \tag{4.17}$$

As can be seen in Equation 4.20, the output of the stability and goal controllers were weighted more or less heavily based on the stability of the biomechanical model. The result is a control action which advances the rigid body system toward the goal configuration, given by $\boldsymbol{\theta}_f$ (as discussed in Section 3.3.3), but in a way that promotes (biomechanical) stability.

While seated, the biomechanical model was encouraged to lean forward so that the

total-body center of mass is shifted toward the center of the base of support (referring to the condition illustrated in Figure 3.4a). This was accomplished by weighting the stability controller directive more heavily than that of the goal controller. As the HAT achieved forward lean, control was shifted in favor of the goal controller directive. This caused the biomechanical model to engage in lift-off (or seat-off). At this instant, the biomechanical model achieves is maximum degree of (static) instability, and, no longer seated, the base of support, illustrated in Figure 3.4b, now applies. The output of stability controller is again favored over that of the goal controller, causing the biomechanical model to continue in its forward momentum toward the base of support region, now defined as the linear region from the heel of the foot to the toe of the foot. As the biomechanical model's gravity line enters the base of support, and model stability "improves," control is again shifted in favor of the goal controller's directive so that the goal configuration may be achieved.

If it could be said that the stability controller is primarily responsible for generating forward lean in the biomechanical system, then it could be said the goal controller is primarily responsible for generating vertical rise.

4.7.1 Controller Architecture

The control architecture of the fuzzy system used to assess model stability, and ultimately support the interpolation described in Section 4.7, consisted of a single input and single output (SISO). The input to the fuzzy controller depended on the configuration of the biomechanical model, and specifically, whether it was seated or not. While seated, the limb segment angle associated with the HAT, given by θ_{123}, is interpreted by the fuzzy system to produce the output μ_{stab}; while not seated, the x-component of the location of the total body center of mass, x_{CoM}, is used instead. This is summarized in Equation 4.18. In the seated condition, only the HAT is able to move; therefore, forward/backward lean of the body is directly linked to the the limb segment angle θ_{123}, as is the biomechanical stability of the model. While not

	"seated"	"not seated"
U_1 (deg)	$[55, 90]$	$\left[x_{CoM(0)}, x_{toe}\right]$

Table 4.18: Definitions for the Universes of Discourse U_1.

seated, the gravity line (which crosses the X-Axis at x_{CoM}) provides the most useful measure of biomechanical stability (as discussed in Section 3.2.6).

$$\mu_{stab} = \begin{cases} f_{stab}(\theta_{123}) & \text{while seated,} \\ f_{stab}(x_{CoM}) & \text{otherwise,} \end{cases} \tag{4.18}$$

where $f_{stab}(\cdot)$ is a fuzzy-based evaluation of the stability of the biomechanical model, described in the following sections (namely, sections 4.7.2 and 4.7.3).

4.7.2 Membership Functions

Membership functions for the input variable θ_{123} (i.e., for the "seated" condition) are given in Figure 4.20a, while membership functions for input variable x_{CoM} (i.e., for the "not seated" condition) are illustrated in Figure 4.20b. The input variables existed on the universe of discourse, U_1, whose bounds are given in Table 4.18. While the biomechanical model is in a seated configuration, U_1 is the set of all values associated with input variable θ_{123}; otherwise, U_1 is the set of all values associated with input variable x_{CoM}. The domain of the limb segment angle θ_{123} ranged from its seated upright value of 90 deg (where the "seated upright" configuration is given by $\boldsymbol{\theta}_0$), to a maximum forward lean value of 55 deg, where 55 deg represented a forward lean of the HAT 5 deg beyond (i.e., leaning further forward than) the desired hip-lock value at 60 deg (discussed in Section 4.5.1). The domain of the input variable x_{CoM} ranged from its value in the initial configuration of the biomechanical model, given by $x_{CoM(0)}$ (defined in Equation 3.28), to the X-Axis value which corresponds with the toe of the foot, denoted x_{toe}.

In each case, membership functions were used to describe the input space as being "most stable" and "not stable" to varying degrees of certainty. While seated, the "most stable" point on the input space was defined as the hip-lock angle, given by $\theta_{123} = 60$ deg. Limb segment angles within 5 deg of the hip-lock angle held non-zero membership in the fuzzy set "most stable." In particular, values existing on $U_1 < 60$ deg (which indicated a forward lean beyond the hip-lock angle) held membership in the fuzzy set "most stable" with a of certainty of 1.0. All other values of θ_{123} existing on U_1, outside of the 5 deg span, were characterized as being "not stable," (i.e., held membership in the fuzzy set "not stable," with a certainty of 1.0).

While the biomechanical model was not seated, the "most stable" point on the input space, U_1, was defined as $x_{CoM} = x_{midFoot}$, where $x_{midFoot}$ denotes the X-Axis value which corresponds to the midpoint of the foot (Section 3.2.6 includes a more detailed discussion on bases of support and the justification for this choice). The region of U_1 within the base of support, (i.e., ranging from x_{heel} to x_{toe} and illustrated in Figure 3.4b), held non-zero membership in the fuzzy set "most stable." All other values of x_{CoM} existing on U_1 were characterized as being "not stable," (i.e., held membership in the fuzzy set "not stable," with a certainty of 1.0).

Two "control actions" were associated with the variable μ_{stab}: the "not stable" assessment of the biomechanical model which corresponded to a value of 0, and the "most stable" assessment which corresponded to a value of 1. These values existed as fuzzy singletons on the output space (i.e., the universe of discourse) of the controller.

4.7.3 Fuzzy Rules

Two fuzzy rules were employed by this controller:

1. IF u_1 IS "not stable" THEN $b_1 = 0$

2. IF u_1 IS "most stable" THEN $b_2 = 1$

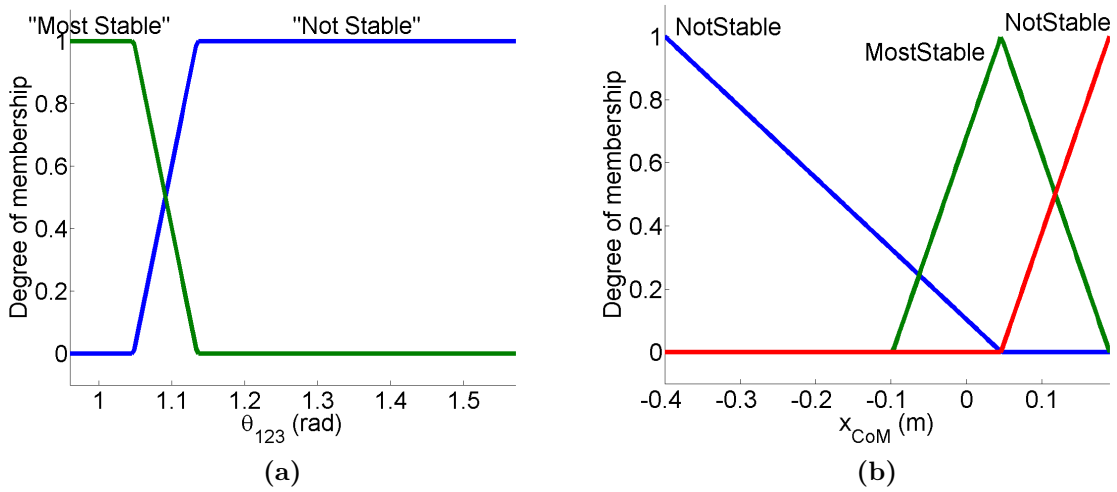

Figure 4.20: Membership functions for the fuzzy system used to assess the stability of the biomechanical model. (a) the seated condition, based upon input variable θ_{123}, and (b) the not seated condition, based upon input variable x_{CoM}.

The fuzzy system performed a nonlinear interpolation between the consequents of the rules, namely, b_1 and b_2, based upon the biomechanical stability associated with the input value given by u_1, where

$$u_1 = \begin{cases} \theta_{123} & \text{while seated,} \\ x_{CoM} & \text{otherwise,} \end{cases} \tag{4.19}$$

to form the output of the controller given by μ_{stab}.

4.7.4 Fuzzy Interpolator Output

The fuzzy interpolator, depicted in Figure 4.1, produced the movement control action, $\boldsymbol{\tau}'$, by combining the stability and goal controller outputs as given in Equation 4.17. Stability of the biomechanical model determined how much of each control directive, (i.e., the goal and stability controller output), was

4.8 Final Control Action

The gravity compensation control action, $\hat{\mathbf{G}}$, (given by Equations 4.3 and 4.1) was combined with the motion control action, $\boldsymbol{\tau}'$, (given by Equation 4.17) to form the final control action delivered to the plant (i.e., the three-link biomechanical model), $\boldsymbol{\tau}$, given by Equation 4.20.

$$\boldsymbol{\tau} = \hat{\mathbf{G}} + \boldsymbol{\tau}' \tag{4.20}$$

4.9 Controller Tuning

Expert knowledge of a control process, in this case, the sit-to-stand operation, typically provides an excellent starting point for fuzzy controller design and implementation, but it is the responsibility of the control engineer to revise the design so that the expected level of controller performance is realized. In this work, several universes of discourse, and membership functions definitions, were adjusted from their original values so that the desired controller response was achieved. Some examples of controller tuning were provided in Sections 4.5.3 and 4.5.8. Typically, an overestimation of values occurred, where the bounds of an input variable, such as the maximum angular rate defined for a joint, was too great and needed to be constricted to improve controller response. Shifting the midpoint of triangular membership functions on a universe of discourse is also a common occurrence in the tuning of fuzzy control systems [19].

4.10 Chapter Summary

Fuzzy logic-based control was used to develop a control system which artificially reproduced the sit-to-stand movement using the biomechanical model described in Chapter 3. Fuzzy logic provided a well structured and intuitive approach to control system design. The use of linguistic terms such as “not stable” or “most stable” made for an intuitive rule-base construction process. Leveraging expert semantic

knowledge of the control process meant that the use of model-based parameters, as part of the control strategy, could generally be kept to a minimum. This is because good control is possible without the use of a detailed mathematical model of the plant when a wealth of semantic knowledge about the process is available. If a detailed biomechanical model does not need to be constructed for every individual requiring a control solution, the controller tuning process (where the control system is adapted to meet the needs of a specific individual) is simplified, making for a - potentially - cost effective solution.

A basic gravity model of the plant was included in the control law of the controller (given by Equations 4.3 and 4.1), as is done by some robotics manufacturers. This model, denoted $\hat{\mathbf{G}}$, served as a "best guess" at the joint torques required to maintain a static configuration of the biomechanical model. Movement control was established by combining the output from two separate fuzzy control processes. The first a stability controller which sought to move the model into the most stable configuration, and the second, a goal controller which sought to move the model toward the desired goal configuration (namely, standing). These controllers operated within the feedback path of the control system depicted in Figure 4.1. The stability and goal controller output were combined using a third fuzzy system which weighted one controller's output more or less heavily than the other, based upon the stability of the biomechanical model. The gravity compensation action, $\hat{\mathbf{G}}$, was summed with the motion control directive, $\boldsymbol{\tau}$', to produce the final control action, $\boldsymbol{\tau}$, delivered to the plant (as given in Equation 4.20).

Chapter 5

Simulation Results

5.1 Introduction

This chapter presents the simulation results of the sit-to-stand control system developed in Chapter 4. Results for the stability, goal, and fuzzy interpolator control systems are presented separately. The software simulation of the control systems, and the biomechanical model discussed in Chapter 3, were carried out using Mathwork's MATLAB^{TM} . As discussed in Section 3.3.6, a simulation time step of 0.0286 s (corresponding to an update rate of 35 Hz) was used. The movement produced by the automated sit-to-stand controller was compared against exemplars of the human sit-to-stand process collected using a Vicon^{TM} motion capture system (the details of which are included in Appendix C).

5.2 Criteria for Success

5.2.1 Goal and Sit-to-Stand Controllers

Movement sequences, which involved the goal controller, were expected to guide the biomechanical model into the "quiet standing" configuration, where, as stated in Section 1.8, "quiet standing" is defined as the configuration of the model such that:

1. Each joint angle of the biomechanical model, given by θ_1, θ_2, and θ_3 respectively,

falls within 1 degree of its end-target configuration value, given by $\boldsymbol{\theta}_f$ (defined in Equation 3.35).

2. The angular velocity of each joint, given by $\dot{\theta}_1$, $\dot{\theta}_2$, and $\dot{\theta}_3$ respectively, is less than 1 degree/s, (i.e., the biomechanical model has effectively come to rest).

Item (1) above may be restated in terms of the joint angle error, denoted $\boldsymbol{\theta}_{Err}$, as: "the error in each joint, given by $\boldsymbol{\theta}_{Err}$, is less than 1 degree," where

$$\boldsymbol{\theta}_{Err}(t) = \boldsymbol{\theta}_f - \boldsymbol{\theta}(t) \tag{5.1}$$

and $\boldsymbol{\theta}(t)$ is the set of joint angles as given in Equation 3.15.

For movement sequences, involving the goal controller, to be considered "successful," the biomechanical model must achieve quiet standing at some time $t = t_{success}$, and remain in quiet standing for all times $t > t_{success}$. Therefore, the criteria for success may be stated as

$$\left|\boldsymbol{\theta}_{(Err)}(t)\right| < 1 \text{ deg, for } t \geq t_{success} \tag{5.2a}$$

$$\left|\dot{\boldsymbol{\theta}}(t)\right| < 1 \text{ deg/s, for t } \geq t_{success} \tag{5.2b}$$

where $\dot{\boldsymbol{\theta}}(t)$ is the set of joint angle velocities as given in Equation 3.16.

5.2.2 Stability Controller

The purpose of the stability controller was to bring the biomechanical model into the "most stable" configuration, as discussed in Section 4.5. Therefore, movement sequences involving only the stability controller, are expected to terminate with the biomechanical model having achieved a highly stable configuration. The criteria for success, for movement involving only the stability controller, are given in Equation

5.3.

$$\left|\theta_{Com(Ref)} - \theta_{Com}(t)\right| < 1 \text{ deg, for } t \geq t_{success} \tag{5.3a}$$

$$\left|\dot{\boldsymbol{\theta}}(t)\right| < 1 \text{ deg/s, for t } \geq t_{success} \tag{5.3b}$$

where θ_{Com} is the inclination of the total body center of mass (given in Equation 3.9, $\theta_{Com(Ref)}$ is the desired inclination given by Equation 4.5, and $\dot{\boldsymbol{\theta}}(t)$ is the set of joint angle velocities (as given in Equation 3.16).

Specific to the stability controller, $\theta_{Com(Ref)}$ is calculated using Equation 4.5 as

$$\theta_{CoM(Ref)} = arccos\left(\frac{x_{midFoot}}{R_{CoM}}\right)$$

$$= arccos\left(\frac{0.04600}{1.000}\right)$$

$$= 86.90 \text{ deg}$$

where the distance to the total body center of mass given by R_{CoM} is 1.00 m (a value found to be typical for this biomechanical model), and

$$x_{midFoot} = b - \frac{1}{2} \cdot l_{foot}$$

where b is given by Equation 3.7, and l_{foot} is given by Equation 3.8.

Criterion (1), given as Equation 5.3a, bounds the error between the desired total body center of mass inclination and its current value for all times $t \geq t_{success}$. The error, denoted $\theta_{Com(Err)}$, is explicitly stated in Equation 5.5.

$$\theta_{Com(Err)}(t) = \theta_{Com(Ref)} - \theta_{Com}(t) \tag{5.5}$$

Criterion (2), given as Equation 5.3b, essentially states that the biomechanical model has come to rest.

5.3 Test Case Scenarios

Three test cases were used to investigate the response of the control systems developed in this work. They differ in how the biomechanical model was configured at the onset of the movement, as follows:

1. **Initially seated**. The biomechanical model began in "quiet sitting," (i.e., at rest, in a seated upright configuration), at the onset of the movement.

2. **Seat-off**. The biomechanical model began in a worst case (i.e., highly statically unstable) configuration where it hovered, unmoving, just above the chair's surface. Normally during seat-off, a forward momentum, developed in the initiation phase of the movement, would be present to help carry the biomechanical model forward. This was intentionally neglected in this test case.

3. **Near standing**. The biomechanical model began, at rest, in a configuration near standing, given by $\boldsymbol{\theta}_{ns} = \begin{bmatrix} 63.91 & 55.09 & -59.38 \end{bmatrix}^T$ (deg).

Test case #1 provided the typical starting configuration of a individual about to undergo the sit-to-stand movement. Test case #2 provided a highly statically unstable configuration of the biomechanical model. Test case #3 was used to ensure that the control system being tested did in fact cause the biomechanical model to converge on the desired configuration when in the neighborhood of the solution.

Time t = 0 s coincided with the application of the first control action to the biomechanical system, (i.e., the onset of the sit-to-stand movement).

Quantity	Expected Value	Measured Value	Error
θ_{CoM} (deg)	86.90	86.55	-0.35
$\dot{\boldsymbol{\theta}}$ (deg/s)	0	-0.42	-0.42
	0	0.95	0.95
	0	0.50	0.50
W (J)	-	179	-

Table 5.1: Simulation Results for Stability Controller Test Case #1.

5.4 Stability Controller Simulation Results

The motion control action, given by $\boldsymbol{\tau}'$, consisted of only the stability control action $\boldsymbol{\tau}_{stab}$ for the tests conducted in this section, such that

$$\boldsymbol{\tau}' = \boldsymbol{\tau}_{stab}$$

and the control action delivered to the plant (i.e., the three-link biomechanical model), $\boldsymbol{\tau}$, is given by Equation 4.20. Thus the plant is actuated using only the stability control action, $\boldsymbol{\tau}_{stab}$, and the gravity compensation action, $\hat{\mathbf{G}}$.

The criteria for success for this controller are outlined in Section 5.2.2.

5.4.1 Test Case #1: Initially Seated

Beginning in the seated upright configuration, given by $\boldsymbol{\theta}_0$ and illustrated in Figure 5.1a, the stability controller was used to move the biomechanical model into the "most stable" configuration, as depicted in Figure 5.1a. The success criteria were met at simulation time t = 6.25 s. Results of this test, at t = 6.25 s, are summarized in Table 5.1.

The initial and final configurations of the biomechanical model, as well as the path traversed by the center of mass are given in Figure 5.1a, the control actions applied to the joints of the biomechanical model are depicted in 5.1b, and the joint angles plotted over the course of the movement are given in Figure 5.2. From Table 5.1 it can be seen that the biomechanical model comes to rest (i.e., all three joint

angle velocities, given by $\dot{\boldsymbol{\theta}}$, are less than 1 deg/s) in a stable configuration, with the inclination of the total body center of mass falling within 0.35 deg of its target value. An estimate for the total work done by all three joint actuators over the course of the movement (found using Equation 3.26) is also given in the table.

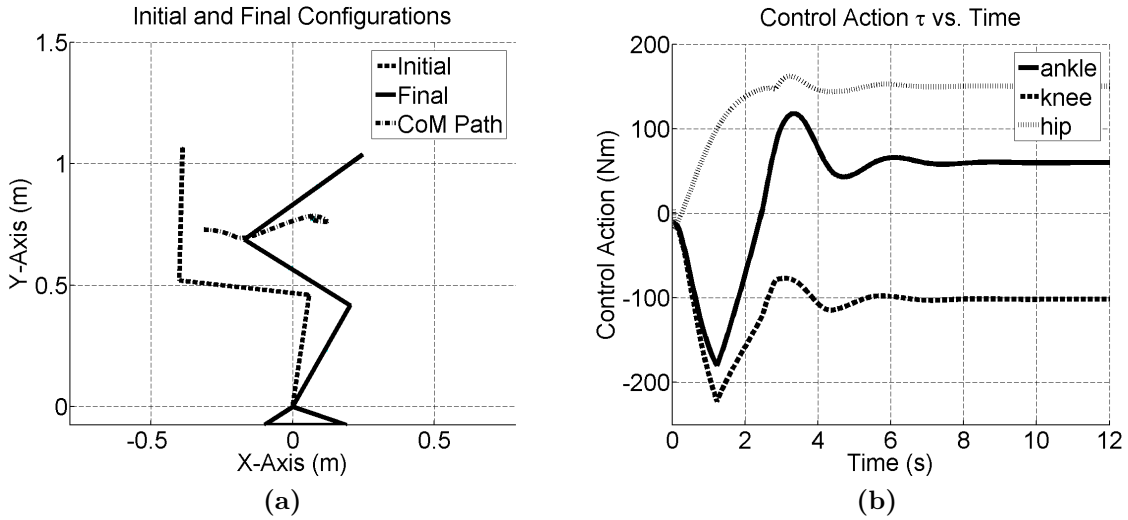

Figure 5.1: Simulation results for stability controller test case #1. (a) initial and final configurations of the biomechanical model along with the path traversed by the center of mass (CoM), and (b) the control actions of each joint given by $\boldsymbol{\tau}$.

Looking at Figure 5.1a, the path traversed by the total body center of mass is a relatively direct path forward. The total body center of mass is moved from its initial position to the "most stable" position while seated, to "most stable" position while not seated (as discussed in Sections 3.2.6 and 4.5.1). The primarily horizontal movement of the total body center of mass is in keeping with the expectation that the stability controller will provide the majority of the forward lean component of the sit-to-stand movement. A small underdamped response is observed in the joint angle plots of Figure 5.2. While a critically damped response is ideal, no model of joint friction was included in the dynamic equation for the biomechanical model (given by Equation 3.17); therefore, the slightly underdamped response observed in the results above would likely be negated, (i.e., dampened), in a physical realization of the system.

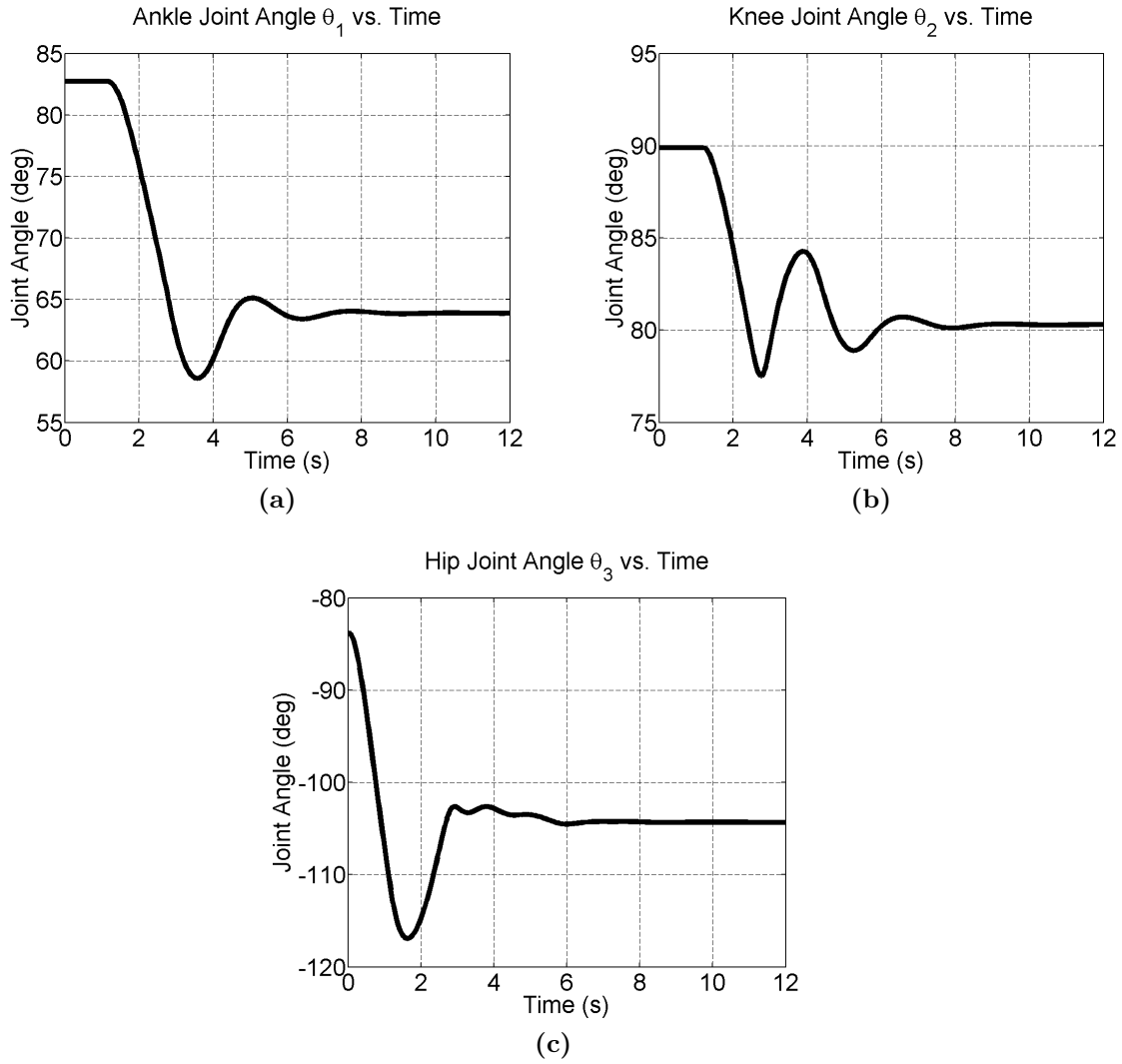

Figure 5.2: Joint angle plots for stability controller test case #1. (a) ankle, (b) knee, and (c) hip.

The results shown in Figures 5.1 and 5.2 were intentionally plotted beyond time $t_{success}$ to demonstrate the steady state achieved by the biomechanical model for times $t > 6.25$ s. Steady state values after a long simulation time (i.e., $t = 12$ s) are given in Table 5.2.

5.4.2 Test Case #2: Seat-off

Test case #2 begins with the biomechanical model in a highly statically unstable configuration typical of seat-off in the sit-to-stand movement; the difference, in this

Quantity	Expected Value	Measured Value	Error
θ_{CoM} (deg)	86.90	86.90	0.00
$\dot{\boldsymbol{\theta}}$ (deg/s)	0	0.01	0.01
	0	0.00	0.00
	0	0.00	0.00
W (J)	-	179.0	-

Table 5.2: Steady State Values for Stability Controller Test Case #1.

Quantity	Expected Value	Measured Value	Error
θ_{CoM} (deg)	86.90	86.58	-0.32
$\dot{\boldsymbol{\theta}}$ (deg/s)	0	-0.47	-0.47
	0	0.95	0.95
	0	0.46	0.46
W (J)	-	127	-

Table 5.3: Simulation Results for Stability Controller Test Case #2.

case however, is that the model begins at rest. The success criteria were met (i.e., the stability controller moved the biomechanical model into the "most stable" configuration) at simulation time t = 5.17 s. Results of this test, at t = 5.17 s, are summarized in Table 5.3.

The initial and final configurations of the biomechanical model, as well as the path traversed by the center of mass are given in Figure 5.3a, the control actions applied to the joints of the biomechanical model are depicted in 5.3b, and the joint angles plotted over the course of the movement are given in Figure 5.4. From Figure 5.3a it can be seen that the stability controller drove the biomechanical model forward, until such time, the total body center of mass came to be in the middle of the base of support (defined for the "not standing" condition, as discussed in Section 3.2.6).

5.4.3 Test Case #3: Near Standing

In the third test case, the biomechanical model began in a near standing configuration. The stability controller was once again used to move the biomechanical model into the "most stable" configuration, as depicted in Figure 5.5a. This test case was used to investigate the response of the stability controller in the region of operation near the

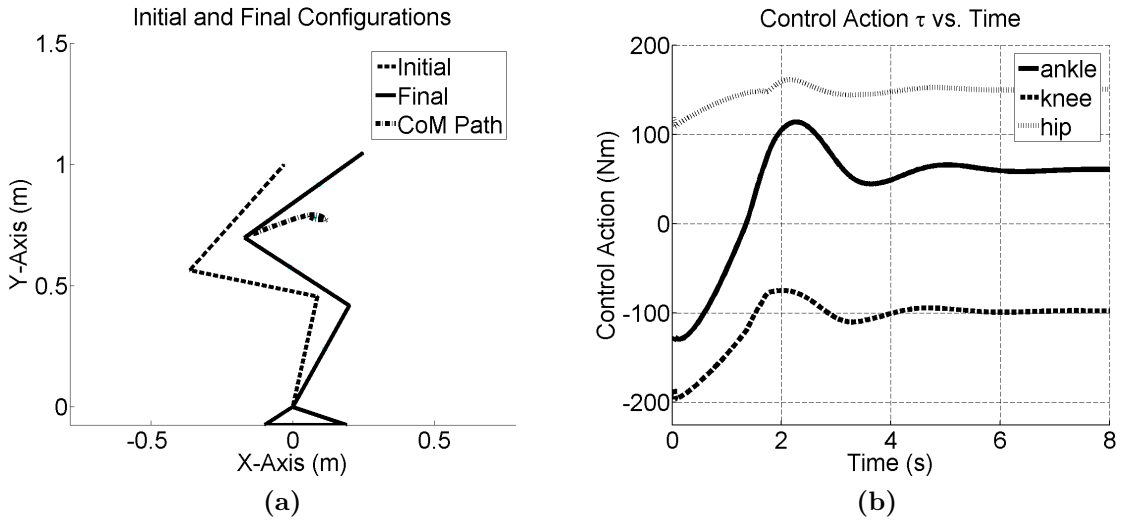

Figure 5.3: Simulation results for stability controller test case #2. (a) initial and final configurations of the biomechanical model along with the path traversed by the center of mass (CoM), and (b) the control actions of each joint given by $\boldsymbol{\tau}$.

Quantity	Expected Value	Measured Value	Error
θ_{CoM} (deg)	86.90	86.45	-0.45
$\dot{\boldsymbol{\theta}}$ (deg/s)	0	-0.49	-0.49
	0	0.99	0.99
	0	0.25	0.25
W (J)	-	36	-

Table 5.4: Simulation Results for Stability Controller Test Case #3.

end-goal configuration (i.e., standing). The success criteria were met at simulation time t = 3.31 s. Results of this test, at t = 3.31 s, are summarized in Table 5.4.

The initial and final configurations of the biomechanical model, as well as the path traversed by the center of mass are given in Figure 5.5a, the control actions applied to the joints of the biomechanical model are depicted in 5.5b, and the joint angles plotted over the course of the movement are given in Figure 5.6. From Figure 5.5a, it can be seen that the stability controller caused the total body center of mass to move directly to its goal position, thereby achieving the "most stable" configuration defined for the "not seated" condition (as discussed in Section 3.2.6).

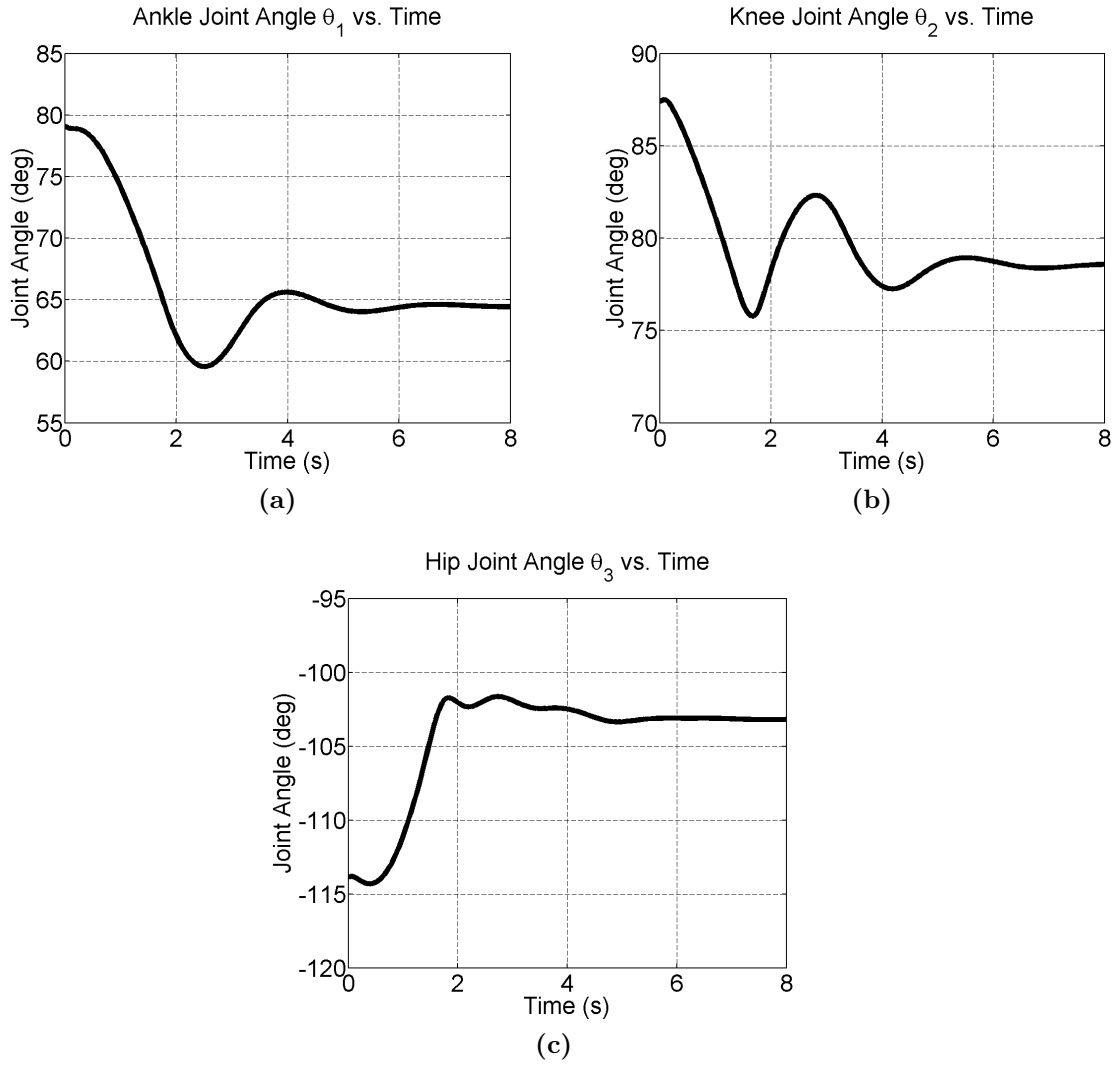

Figure 5.4: Joint angle plots for stability controller test case #2. (a) ankle, (b) knee, and (c) hip.

5.4.4 Stability Controller Conclusions

Test cases #1, #2, and #3 demonstrated that the stability controller was able to direct the biomechanical model from various initial configurations to a stable configuration where the total-body center of mass was placed directly over the middle of the base of support. A strong horizontal movement component was observed in all three cases - an expected result given the stability controller was designed to move

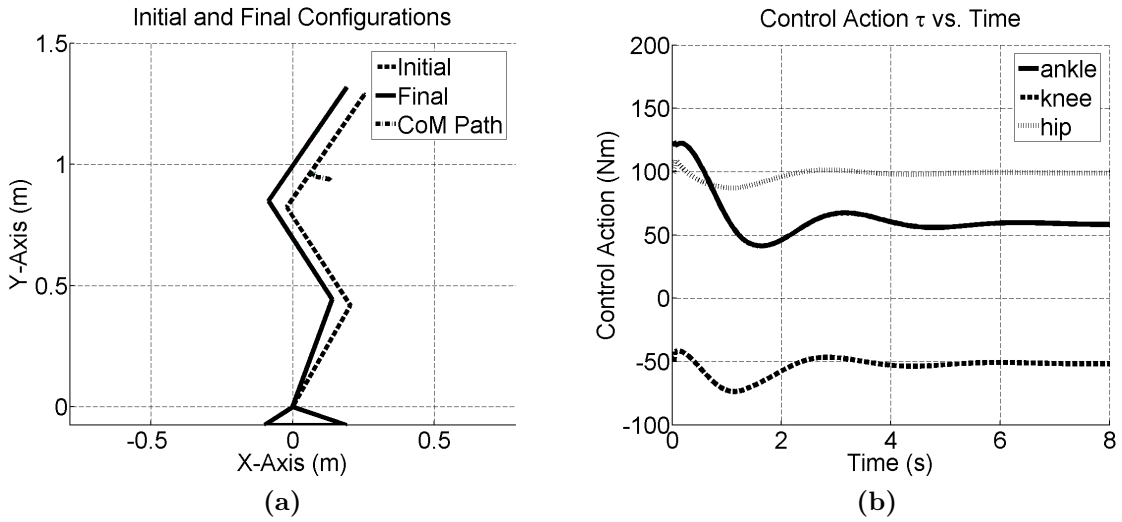

Figure 5.5: Simulation results for stability controller test case #3. (a) initial and final configurations of the biomechanical model along with the path traversed by the center of mass (CoM), and (b) the control actions of each joint given by $\boldsymbol{\tau}$.

the total-body center of mass into the region of the base of support as directly as possible.

5.5 Goal Controller Simulation Results

The purpose of the goal controller was to move the biomechanical model into the goal (i.e., standing) configuration, given by $\boldsymbol{\theta}_f$ in Equation 3.27. Test cases #2 and #3, as discussed in Section 5.3, were used to investigate the response of the goal controller. Test case #1 was omitted as the goal controller is not active during the initiation or seat-off phases of the sit-to-stand movement (save an instant at hip-lock where the ankle and knee joint torques contribute momentarily, discussed further in Section 5.6.1). The criteria for success for this controller, described in Section 5.2.1, require that the biomechanical model comes to rest in the standing configuration, where it is to remain in quiet standing.

The motion control action, given by $\boldsymbol{\tau}'$, consisted of only the goal control action

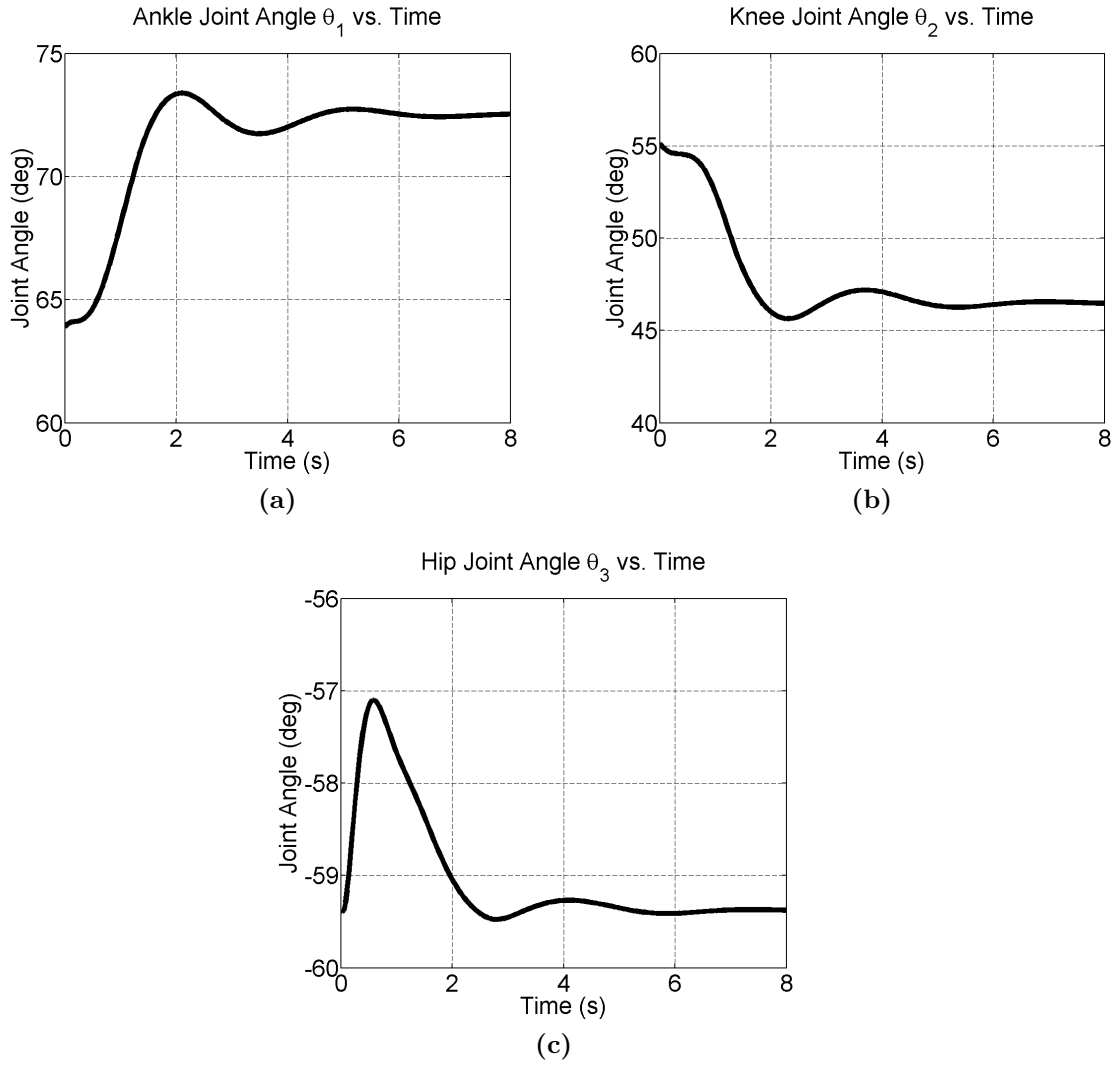

Figure 5.6: Joint angle plots for stability controller test case #3. (a) ankle, (b) knee, and (c) hip.

$\boldsymbol{\tau}_{goal}$ for the tests conducted in this section, such that

$$\boldsymbol{\tau}' = \boldsymbol{\tau}_{goal}$$

and the control action delivered to the plant (i.e., the three-link biomechanical model), $\boldsymbol{\tau}$, is given by Equation 4.20. Thus the plant is actuated using only the goal control action, $\boldsymbol{\tau}_{goal}$, and the gravity compensation action, $\hat{\mathbf{G}}$.

Quantity	Expected Value	Measured Value	Error
θ_{CoM} (deg)	88.7	89.18	0.5
$\boldsymbol{\theta}$ (deg)	85	85.03	0.03
	10	10.99	0.99
	-10	-10.51	-0.51
$\dot{\boldsymbol{\theta}}$ (deg/s)	0	0.30	0.30
	0	-0.65	-0.65
	0	0.24	0.24
W (J)	-	313	-

Table 5.5: Simulation Results for Goal Controller Test Case #1.

5.5.1 Test Case #1: Seat-off

In this test case, the goal controller is forced to recover from the highly unstable seat-off condition and move the biomechanical model into the goal configuration, given by $\boldsymbol{\theta}_f$. The criteria for success were met at simulation time $t = 10.37$ s. Results of this test, at t = 10.37 s, are summarized in Table 5.5. The time required to achieve the success criteria in this test case was expected to be greater in duration than other test case scenarios involving the goal controller, given: 1) the highly unstable nature of this test case, and 2) the fact that the goal controller does not have a strong horizontal, stability correction component to its actions.

The initial and final configurations of the biomechanical model, as well as the path traversed by the center of mass are given in Figure 5.7a, the control actions applied to the joints of the biomechanical model are depicted in 5.7b, and the joint angles plotted over the course of the movement are given in Figure 5.8. In each joint angle plot of Figure 5.8, the desired angular position of the joint, as given by $\boldsymbol{\theta}_f$, is represented by a dashed line. As can be seen in Figure 5.7a the path traversed by the total body center of mass demonstrated a strong vertical rise component in its motion (more so at the onset of the movement), before coming to rest at its final location.

Steady state values of the biomechanical system achieved after a long simulation

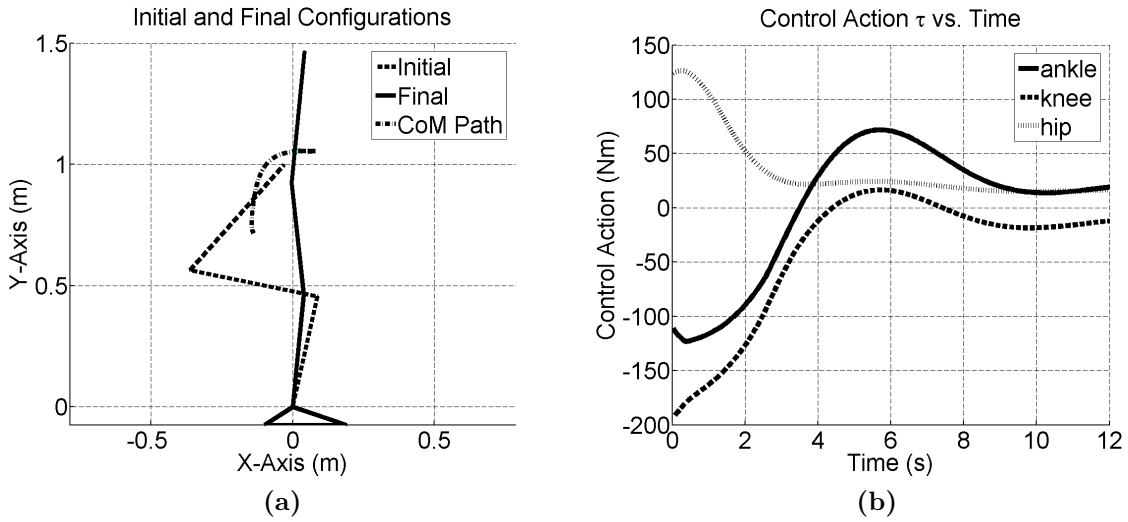

Figure 5.7: Simulation results for goal controller test case #1. (a) initial and final configurations of the biomechanical model along with the path traversed by the center of mass (CoM), and (b) the control actions of each joint given by $\boldsymbol{\tau}$.

Quantity	Expected Value	Measured Value	Error
θ_{CoM} (deg)	88.7	88.88	0.2
$\boldsymbol{\theta}$ (deg)	85	85.10	0.10
	10	10.18	0.18
	-10	-10.10	-0.10
$\dot{\boldsymbol{\theta}}$ (deg/s)	0	-0.15	-0.15
	0	-0.28	-0.28
	0	0.21	0.21
W (J)	-	313	-

Table 5.6: Steady State Values for Goal Controller Test Case #1.

time (i.e., $t = 12$ s) are given in Table 5.6. As can be seen from the table, the measured values generally approached their expected values even more closely than the results given in Table 5.5 (when the criteria for success were first achieved).

5.5.2 Test Case #2: Near Standing

The second test case used to investigate the response of the goal controller involved initializing the biomechanical model in a near standing configuration, (i.e., a configuration in the neighborhood of the solution). This test case was used to ensure that the goal controller caused the model to converge on the desired configuration as

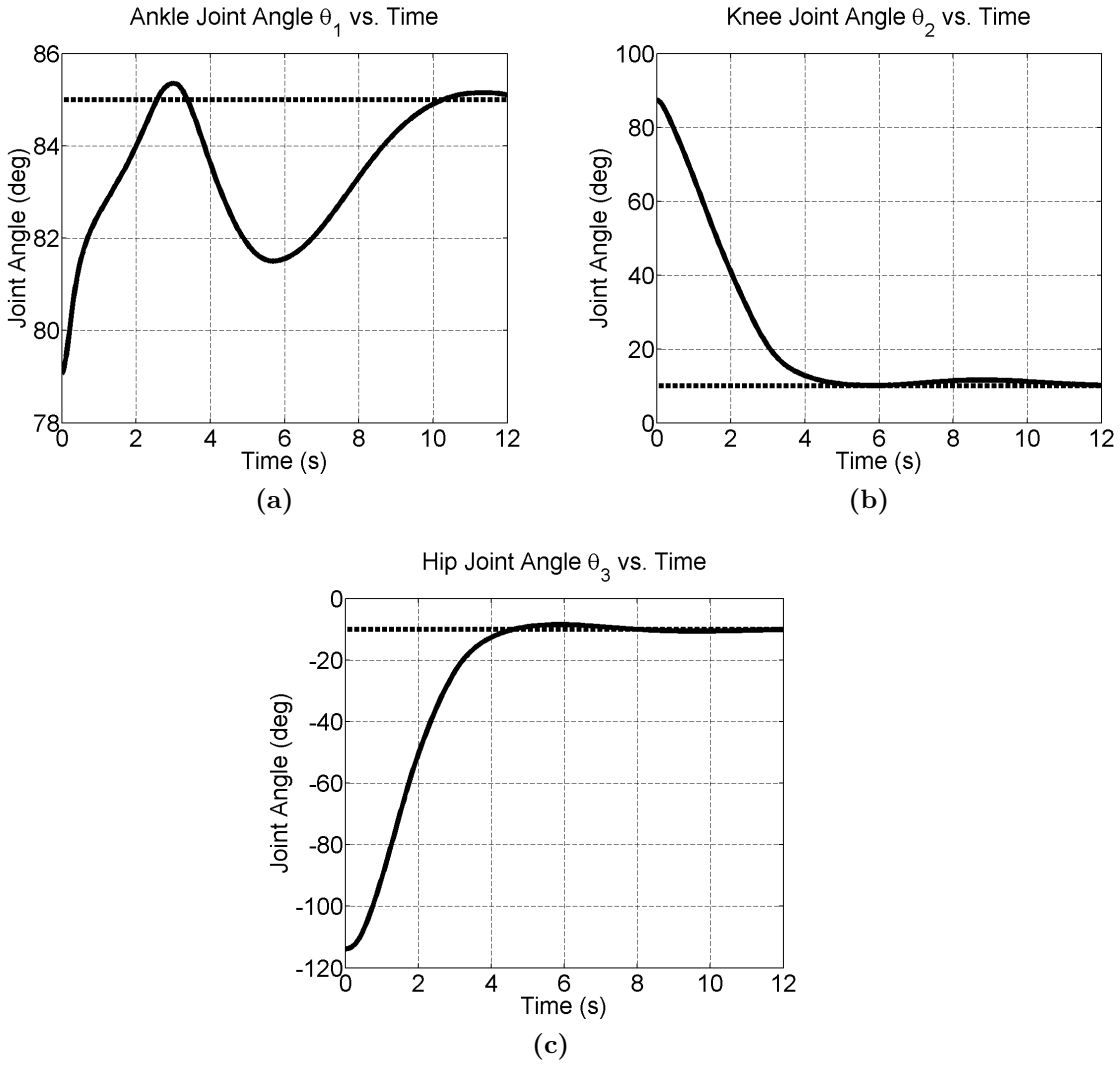

Figure 5.8: Joint angle plots for goal controller test case #1. (a) ankle, (b) knee, and (c) hip.

expected. The criteria for success were met at simulation time $t = 5.63$ s. Results of this test, at t = 5.63 s, are summarized in Table 5.7.

The initial and final configurations of the biomechanical model, as well as the path traversed by the center of mass are given in Figure 5.9a, the control actions applied to the joints of the biomechanical model are depicted in 5.9b, and the joint angles plotted over the course of the movement are given in Figure 5.10. As can be seen in Figure 5.9a, the path traversed by the total body center of mass again

Quantity	Expected Value	Measured Value	Error
θ_{CoM} (deg)	88.7	89.59	0.9
$\boldsymbol{\theta}$ (deg)	85	85.67	0.67
	10	10.58	0.58
	-10	-10.52	-0.52
$\dot{\boldsymbol{\theta}}$ (deg/s)	0	-0.61	-0.61
	0	-0.98	-0.98
	0	0.81	0.81
W (J)	-	103	-

Table 5.7: Simulation Results for Goal Controller Test Case #2.

demonstrated a strong vertical rise component in its motion, before coming to rest at its final location.

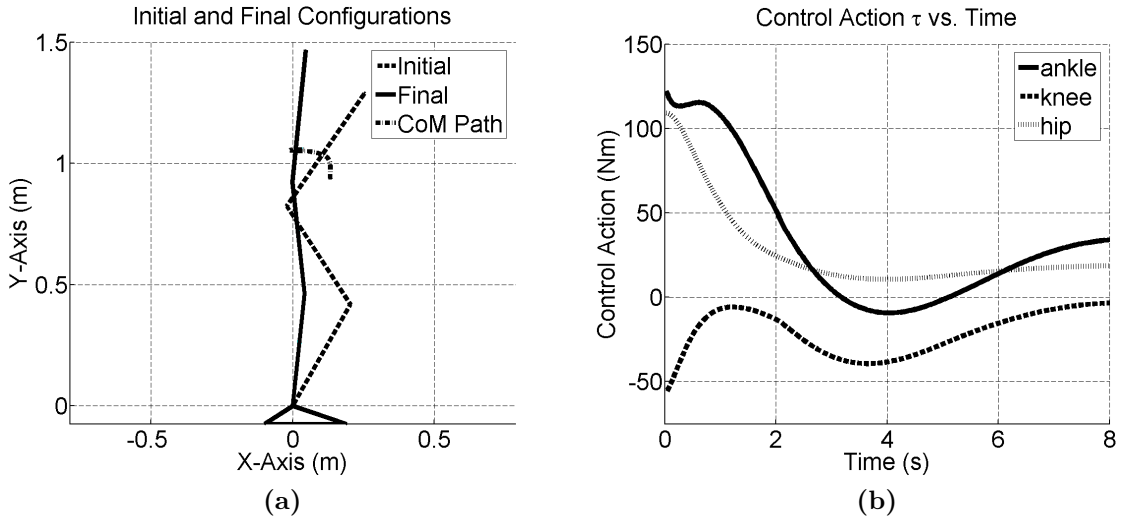

Figure 5.9: Simulation results for goal controller test case #2. (a) initial and final configurations of the biomechanical model along with the path traversed by the center of mass (CoM), and (b) the control actions of each joint given by $\boldsymbol{\tau}$.

5.5.3 Goal Controller Conclusions

As demonstrated by the results for test cases #1 and #2, the goal controller brought the biomechanical model to rest in the desired (standing) configuration. In each test case, the path traversed by the total body center of mass indicated that, at the onset of the movement, the biomechanical model underwent a phase of strong vertical rise before coming to rest in the desired configuration. This observation is in keeping

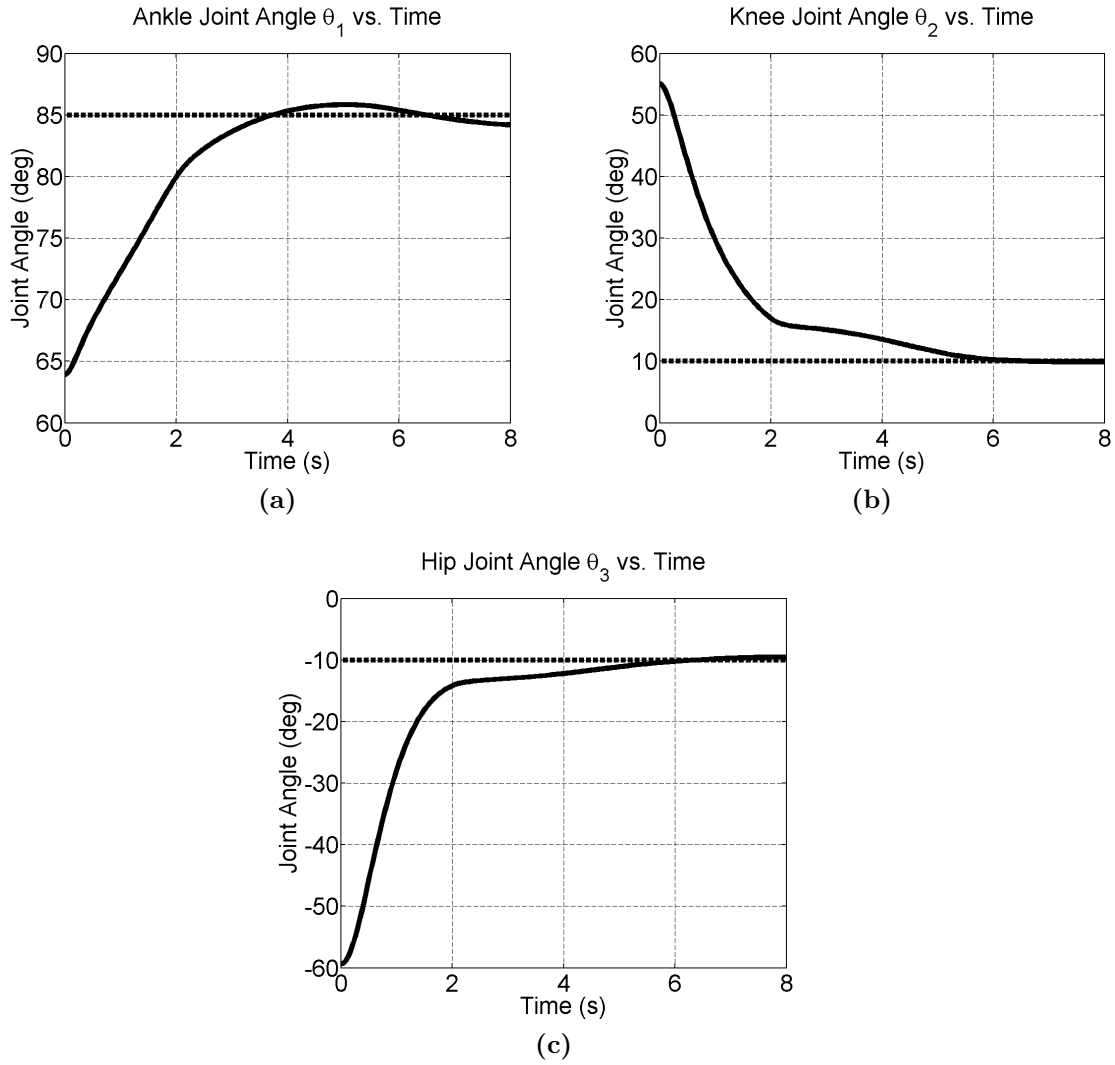

Figure 5.10: Joint angle plots for goal controller test case #2. (a) ankle, (b) knee, and (c) hip.

with the expectation that the goal controller will provide the majority of vertical rise in the sit-to-stand movement.

5.6 Full Sit-to-Stand Controller Simulation Results

Having tested the stability and goal controllers separately in Sections 5.4 and 5.5 respectively, their actions were combined using a fuzzy interpolator, as depicted in Figure 4.1, to form the motion control action $\boldsymbol{\tau}'$. The fuzzy interpolator combined the output of the stability and goal controllers based on the stability of the biomechanical

Quantity	Expected Value	Measured Value	Error
θ_{CoM} (deg)	88.7	89.44	0.8
$\boldsymbol{\theta}$ (deg)	85	85.36	0.36
	10	10.99	0.99
	-10	-10.86	-0.86
$\dot{\boldsymbol{\theta}}$ (deg/s)	0	-0.55	-0.55
	0	-0.99	-0.99
	0	0.97	0.97
W (J)	-	336	-

Table 5.8: Simulation Results for Sit-to-Stand Controller Test Case #1.

model, as discussed in Section 4.7. The motion control action is combined with the gravity compensation action, $\hat{\mathbf{G}}$, to form the final control action delivered to the plant, $\boldsymbol{\tau}$, as give by Equation 4.20. The three test cases outlined in Section 5.3 were used to investigate the response of the sit-to-stand control system. The criteria for success for this controller are stated in Section 5.2.1.

5.6.1 Test Case #1: Initially Seated

In this test case, the sit-to-stand controller was used to guide the biomechanical model from a seated configuration to the goal (i.e., standing) configuration. This test case provides the primary results of interest for this work. The criteria for success were met at simulation time $t = 8.34$ s. Results of this test, at t = 8.34 s, are summarized in Table 5.8.

The initial and final configurations of the biomechanical model, as well as the path traversed by the center of mass are given in Figure 5.11a, the control actions applied to the joints of the biomechanical model are depicted in 5.11b, and the joint angles plotted over the course of the movement are given in Figure 5.12.

The movement progressed as expected: the HAT was rotated clockwise into forward lean. Seat-off quickly followed engaging the entire rigid body system in a forward lean activity. As the total body center of mass moved into the base of support (through the heel), the biomechanical model ascended vertically. Nearing full exten-

sion, the model engaged in balance recovery coming to rest in the desired standing configuration.

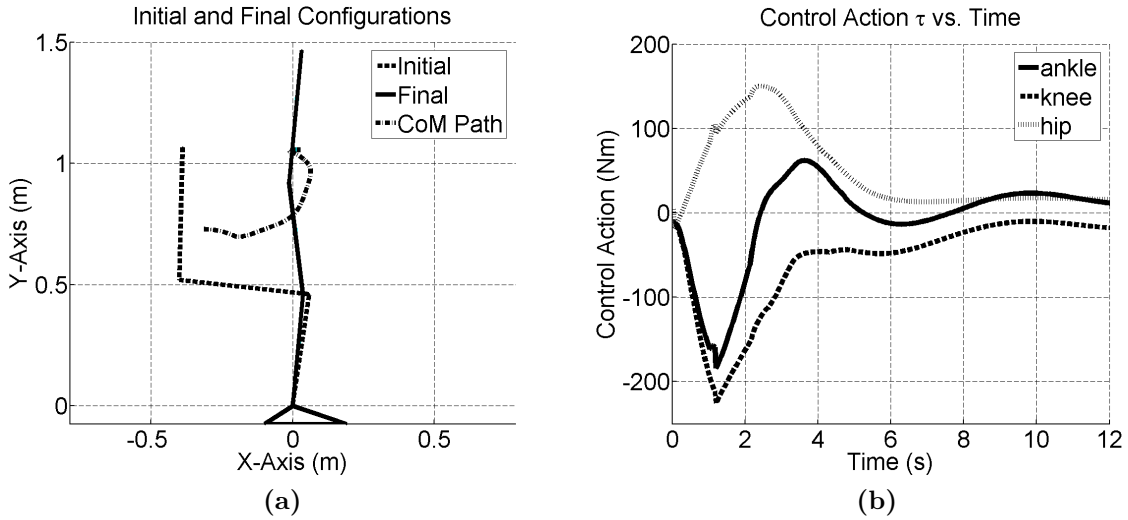

Figure 5.11: Simulation results for sit-to-stand controller test case #1. (a) initial and final configurations of the biomechanical model along with the path traversed by the center of mass (CoM), and (b) the control actions of each joint given by $\boldsymbol{\tau}$.

Graphs showing the joint angles and path traversed by the center of mass for the motion capture data provided in Appendix C are reproduced in Figure 5.13 for comparison purposes. The sit-to-stand movement for a single healthy male subject was captured using a Vicon$^{\text{TM}}$ optical tracking system.

In comparing the joint angle plots derived from the motion tracking data (given in Figure 5.13) to the those included as part of the simulation results (depicted in Figure 5.12), they appear to be quite similar. It should be noted that the sit-to-stand movement in Figure 5.13) is completed in approximately 3 s, while the simulated movement progressed at almost one third this rate, given the success criteria were met at 8.34 s. Producing a slower controlled movement was intentional. The gains K_{stab} and K_{goal} (discussed in Sections 4.5.12 and 4.6.3 respectively) were selected so that a movement appropriate for assisting an invidividual with a mobility impairment would result. This is believed to be approximately one third of the rate of a heathly individual. But more importantly, it should be noted that the controller may be

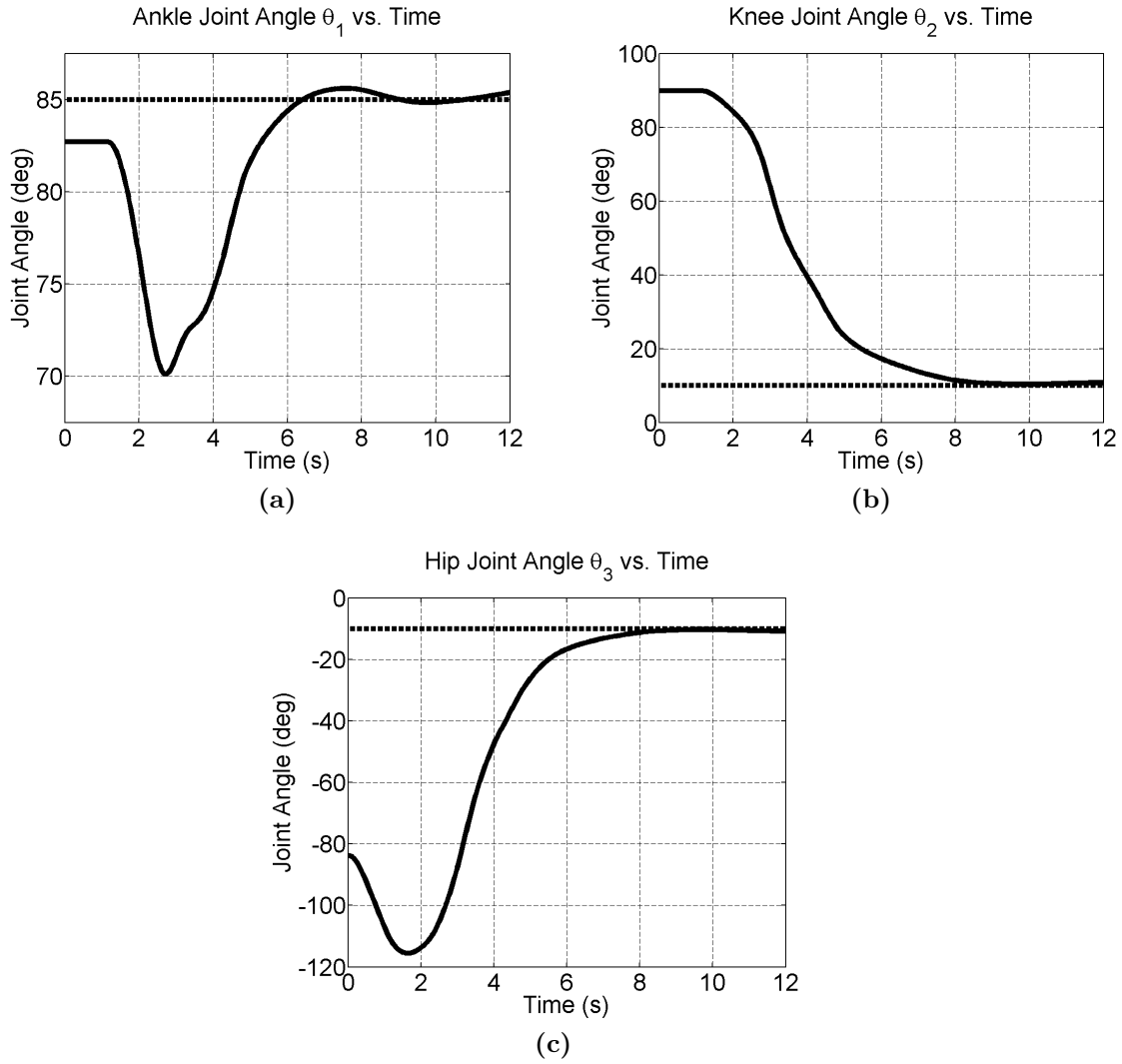

Figure 5.12: Joint angle plots for sit-to-stand controller test case #1. (a) ankle, (b) knee, and (c) hip.

tuned to meet any desired rate of movement, limited only by the capability of the physical device (i.e., the actuators included as part the advanced mobility support device).

The paths traversed by the center of mass (shown in Figures 5.13d and 5.11a respectively) are also quite similar. Some variation is to be expected when comparing a biomechanical model restricted to three degrees of freedom versus the unconstrained motion of of a healthy male subject. In comparing Figures 5.13d and 5.11a, a minor premature plantarflexion of the ankle is observed during the recovery phase (i.e., just

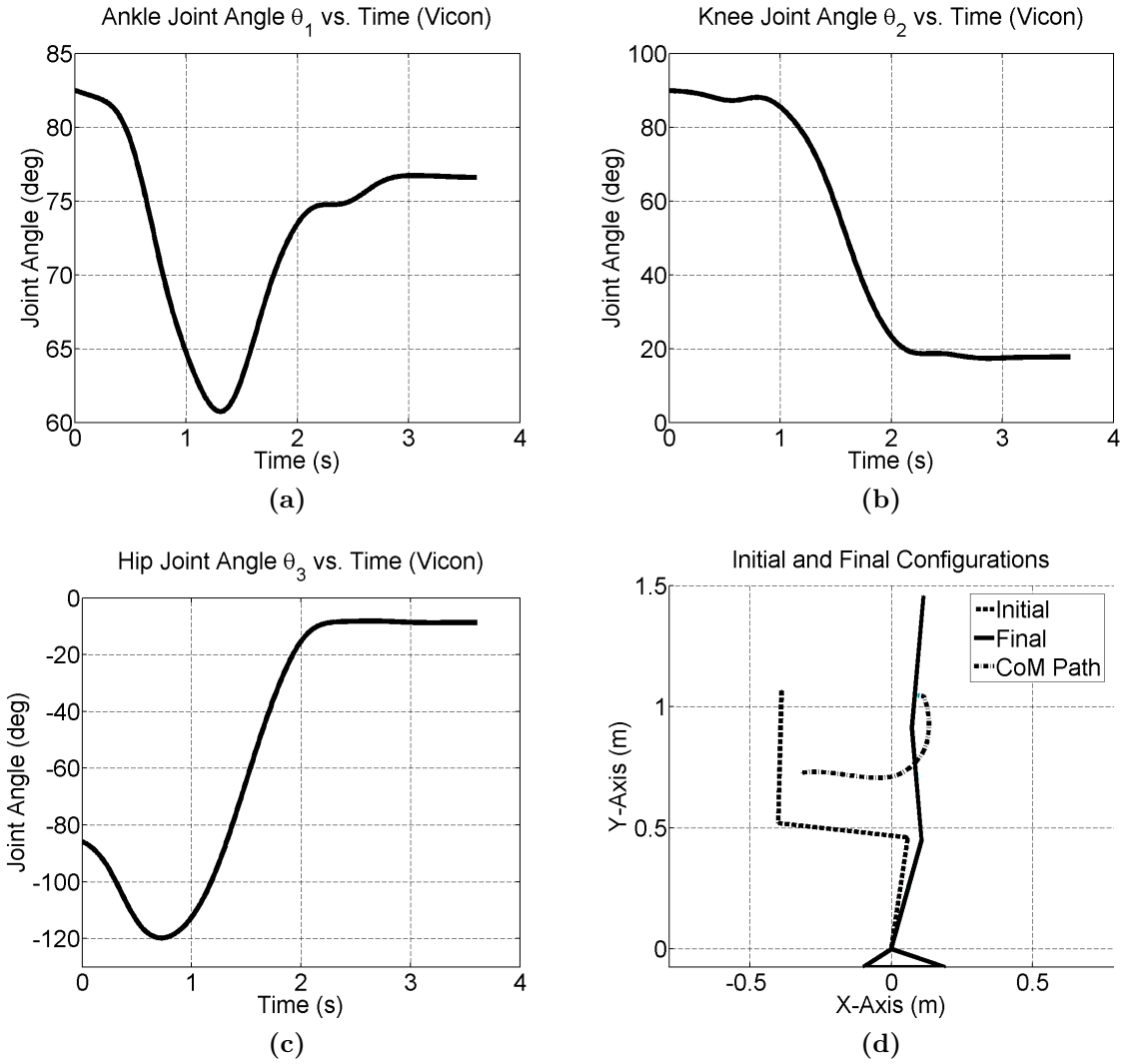

Figure 5.13: Joint angles and the path traversed by the center of mass captured using a motion tracking system. (a) ankle, (b) knee, (c) hip, and (d) path traversed by the center of mass.

prior to the total body center of mass settling in its final location) in the simulation results versus the motion capture data.

The weighting factor used to interpolate between stability and goal controller output, μ_{stab} (as discussed in Section 4.7), was plotted over the course of the simulation, labeled in Figure 5.14a as "Goal Controller Weighting." Figure 5.14a depicts the weighting factor, μ_{stab}, as it is applied directly to the goal controller output (as

indicated in Equation 4.17). Figure 5.14b, depicts the weighting factor $(1 - \mu_{stab})$, as applied directly to the stability controller output over the course of the simulation.

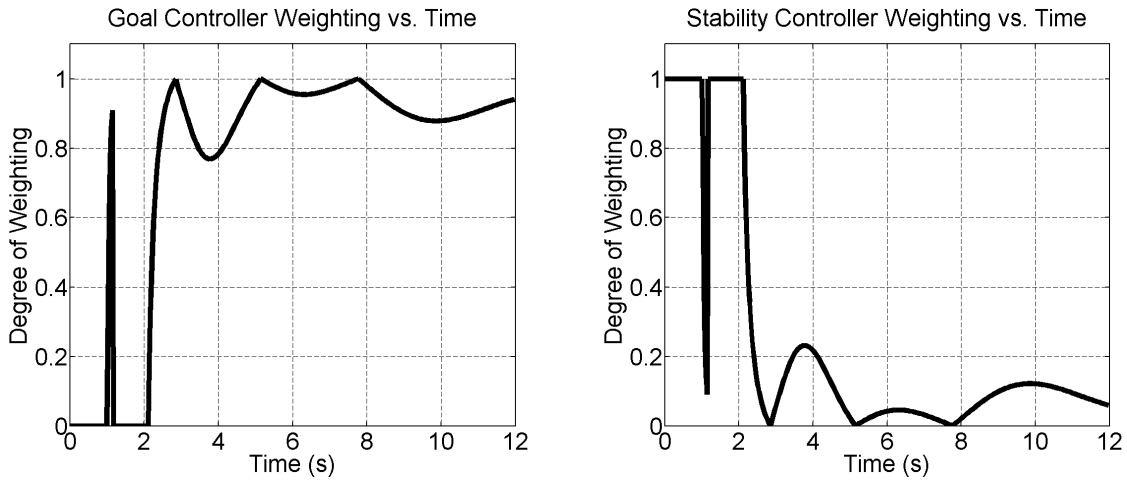

Figure 5.14: Weighting factors applied to stability and goal controller output. (a) μ_{stab} corresponding to the weight factor applied to the output of the goal controller, and (b) $(1 - \mu_{stab})$ applied to the output of the the stability controller.

It can be seen from Figure 5.14 that the sit-to-stand controller relied heavily on the stability controller input during the initiation phase (i.e., while seated). Only at the instant where the HAT achieved the desired degree of forward lean did the sit-to-stand controller suddenly favor the goal controller output. Once the biomechanical model engaged in seat-off, (i.e., assumed a highly statically unstable configuration), the stability controller output was quickly favored once again. As the total body center of mass (or rather the "gravity line") enters the base of support (at the heel of the foot), control is shifted in favor of the goal controller so that it may direct the biomechanical model into the standing configuration.

Steady state values of the biomechanical system achieved after a long simulation time (i.e., $t = 12$ s) are given in Table 5.9. As can be seen from the table, over a longer simulation time, the error associated with $\boldsymbol{\theta}$, (i.e., the joint angles), and the total body center of mass (θ_{CoM}) decreased slightly from their values when the criteria for success were first achieved (given in Table 5.8); however, the reduction in the errors

Quantity	Expected Value	Measured Value	Error
θ_{CoM} (deg)	88.7	89.35	0.7
$\boldsymbol{\theta}$ (deg)	85	85.38	0.38
	10	10.78	0.78
	-10	-10.77	-0.77
$\dot{\boldsymbol{\theta}}$ (deg/s)	0	0.30	0.30
	0	0.03	0.03
	0	-0.08	-0.08
W (J)	-	336	-

Table 5.9: Steady State Values for Sit-to-Stand Controller Test Case #1.

associated with $\dot{\boldsymbol{\theta}}$, (i.e., the joint angular rates), was much more substantial. This indicates that the desired standing configuration was achieved and, for all intents and purposes, the model had come to rest.

5.6.2 Test Case #2: Seat-off

The highly statically unstable test case, presented by test case #2, was used to ensure that the stability controller action was utilized during periods of high (biomechanical) instability, and that the goal controller was used to reach the desired configuration. The criteria for success were met at simulation time $t = 7.26$ s. Results of this test, at t = 7.26 s, are summarized in Table 5.10. The time required to meet the success criteria in this test case falls almost exactly in the middle of the times recorded for the stability and goal controllers for the same test case. This is because the stability controller is utilized at the onset of the movement to quickly move the biomechanical model toward a stable configuration. Once the model enters a region of stability, control is intertwined with the goal controller to bring the model into the standing configuration.

The initial and final configurations of the biomechanical model, as well as the path traversed by the center of mass are given in Figure 5.15a, the control actions applied to the joints of the biomechanical model are depicted in 5.15b, and the joint angles plotted over the course of the movement are given in Figure 5.16. All three

Quantity	Expected Value	Measured Value	Error
θ_{CoM} (deg)	88.7	89.46	0.8
$\boldsymbol{\theta}$ (deg)	85	85.37	0.37
	10	10.99	0.99
	-10	-10.83	-0.83
$\dot{\boldsymbol{\theta}}$ (deg/s)	0	-0.42	-0.42
	0	-0.97	-0.97
	0	0.85	0.85
W (J)	-	287	-

Table 5.10: Simulation Results for Sit-to-Stand Controller Test Case #2.

joint angles depicted in Figure 5.16 demonstrate a smooth rotation of the joint from their initial positions to their goal positions.

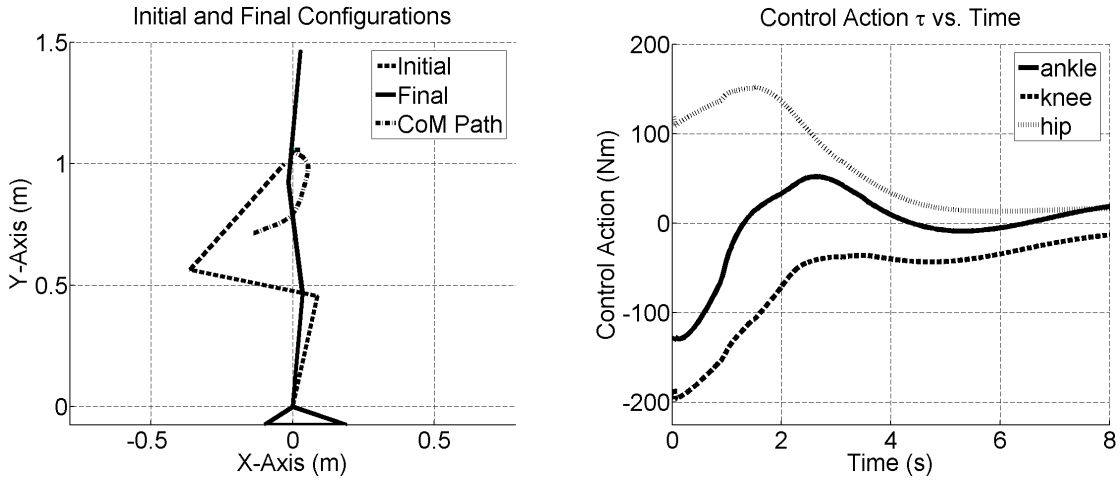

Figure 5.15: Simulation results for sit-to-stand controller test case #2. (a) initial and final configurations of the biomechanical model along with the path traversed by the center of mass (CoM), and (b) the control actions of each joint given by $\boldsymbol{\tau}$.

The weighting factor used to interpolate between stability and goal controller output, μ_{stab} (as discussed in Section 4.7), was plotted over the course of the simulation, labeled in Figure 5.17a as "Goal Controller Weighting." Figure 5.17b, depicts the weighting factor $(1 - \mu_{stab})$, as applied directly to the stability controller output over the course of the simulation.

As can be seen from Figure 5.17, the stability controller output was relied upon

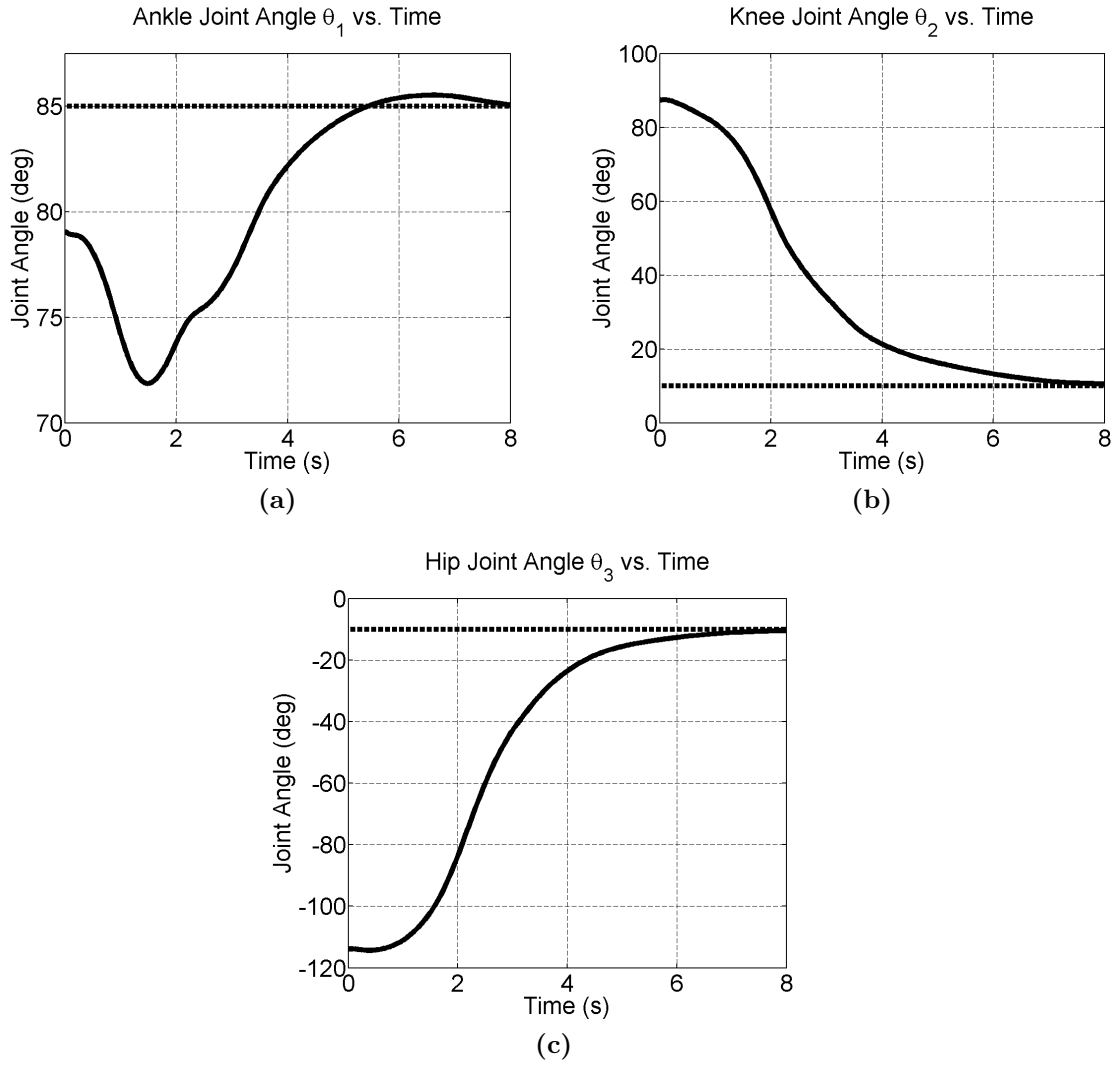

Figure 5.16: Joint angle plots for sit-to-stand controller test case #2. (a) ankle, (b) knee, and (c) hip.

exclusively at the onset of the movement to facilitate stability recovery. The biomechanical model was quickly moved into the base of support region where vertical ascension could then be safely engaged using the control directives of the goal controller. Thus, the two controllers were utilized as required to promote biomechanical stability of the model and to achieve the goal configuration.

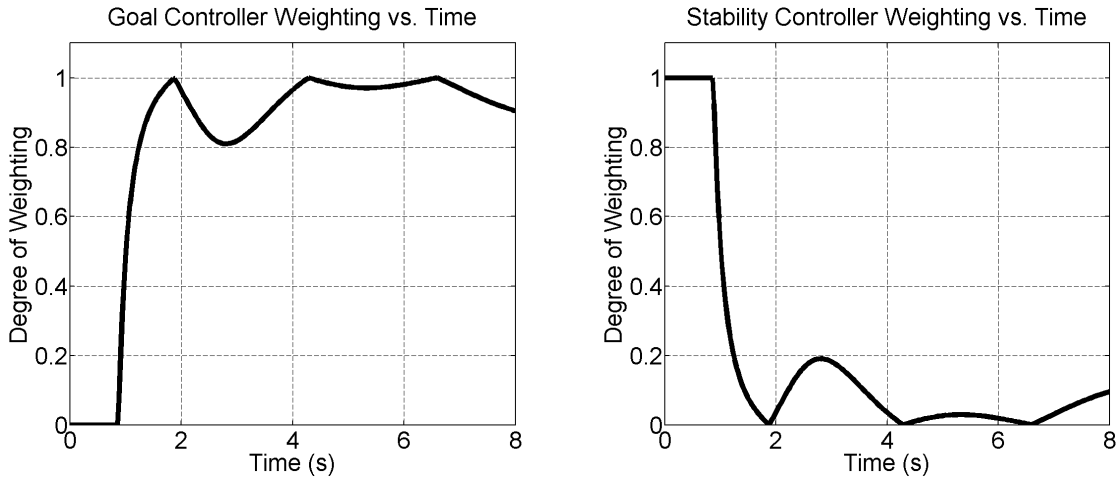

Figure 5.17: Weighting factors applied to stability and goal controller output for sit-to-stand controller test case #2. (a) μ_{stab} corresponding to the weight factor applied to the output of the goal controller, and (b) $(1 - \mu_{stab})$ applied to the output of the the stability controller.

5.6.3 Test Case #3: Near Standing

The third test case investigated the response of the sit-to-stand controller in the neighborhood of the solution (i.e., standing configuration). The biomechanical model began in a configuration near standing, as discussed in Section 5.3. This test case was used to ensure that the goal controller caused the biomechanical model to converge on the desired (standing) configuration as expected. The criteria for success were met at simulation time $t = 9.71$ s. They were nearly met at time $t = 6.08$ s, but the stability control directive bringing the biomechanical model back toward the middle of the base of support, and a minor premature ankle plantarflexion action from the goal controller (previously identified in Section 5.6.1), caused the biomechanical model to diverge slightly from the definition laid out for quiet standing in Section 5.2.1, as can be seen in Figure 5.18a. Results of this test, at t = 9.71 s, are summarized in Table 5.11.

The initial and final configurations of the biomechanical model, as well as the path traversed by the center of mass are given in Figure 5.18a, the control actions

Quantity	Expected Value	Measured Value	Error
θ_{CoM} (deg)	88.7	89.76	1.1
$\boldsymbol{\theta}$ (deg)	85	85.69	0.69
	10	10.99	0.99
	-10	-10.92	-0.92
$\dot{\boldsymbol{\theta}}$ (deg/s)	0	0.20	0.20
	0	-0.50	-0.50
	0	0.26	0.26
W (J)	-	108	-

Table 5.11: Simulation Results for Sit-to-Stand Controller Test Case #3.

applied to the joints of the biomechanical model are depicted in 5.18b, and the joint angles plotted over the course of the movement are given in Figure 5.19.

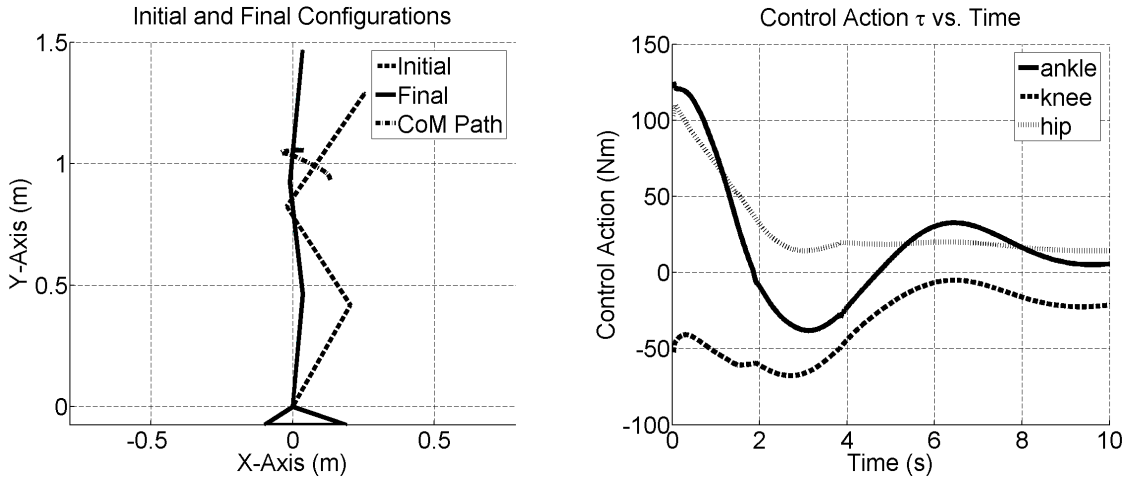

Figure 5.18: Simulation results for sit-to-stand controller test case #3. (a) initial and final configurations of the biomechanical model along with the path traversed by the center of mass (CoM), and (b) the control actions of each joint given by $\boldsymbol{\tau}$.

The weighting factor used to interpolate between stability and goal controller output, μ_{stab} (as discussed in Section 4.7), was plotted over the course of the simulation, labeled in Figure 5.20a as "Goal Controller Weighting." Figure 5.20b, depicts the weighting factor $(1 - \mu_{stab})$, as applied directly to the stability controller output over the course of the simulation. It can be seen from Figure 5.20, that the stability controller output was weighted more than that of the goal controller only very

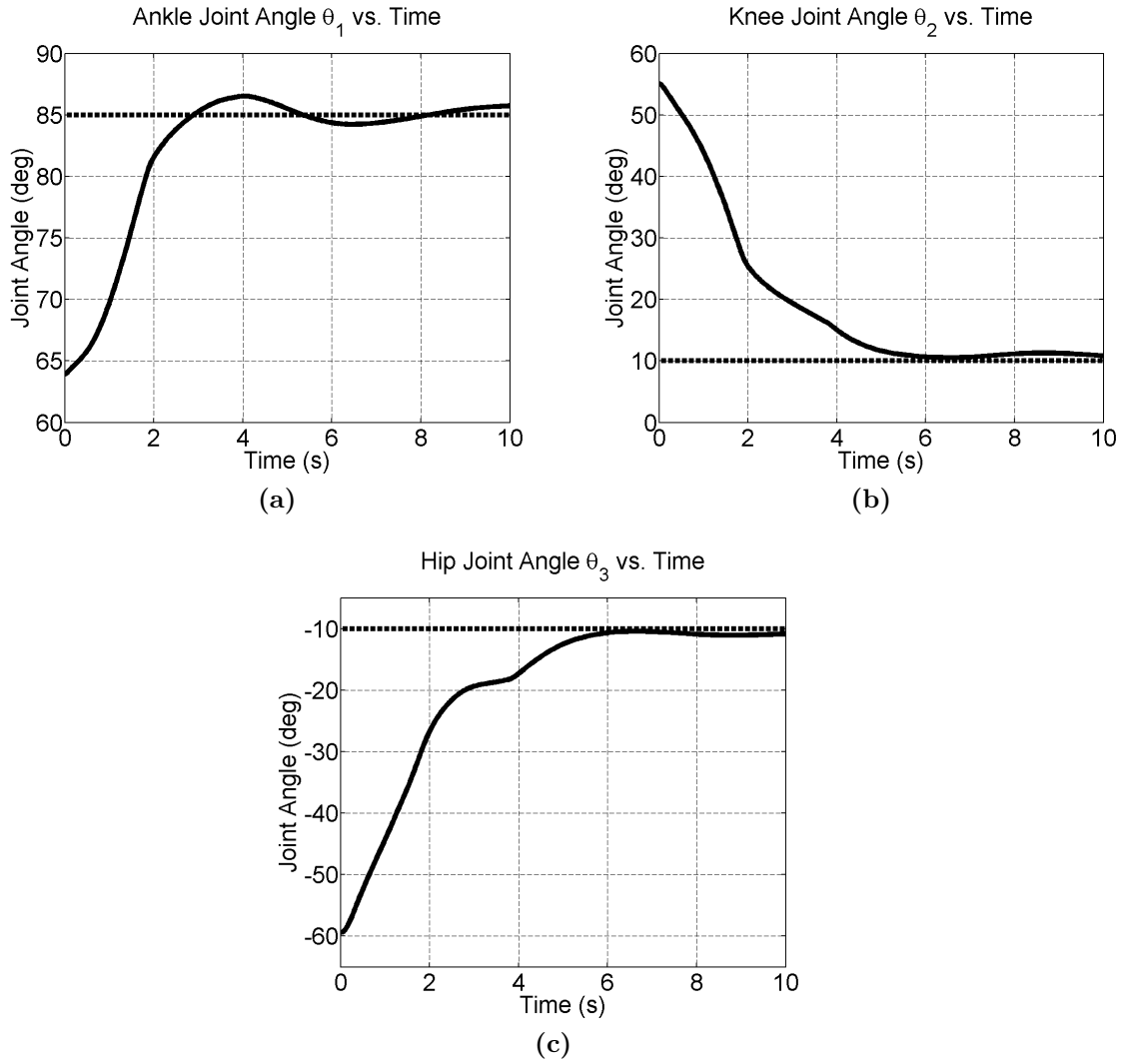

Figure 5.19: Joint angle plots for sit-to-stand controller test case #3. (a) ankle, (b) knee, and (c) hip.

briefly at the onset of the movement. This was necessary for shifting the gravity line of the biomechanical model back toward the middle of the base of support. For the remainder of the movement the goal controller output was favored so that the biomechanical model could be brought into the goal configuration associated with standing. This weighting scheme is exactly as should be expected given the operating point of the plant, (i.e., the biomechanical model), began in close proximity to the goal configuration.

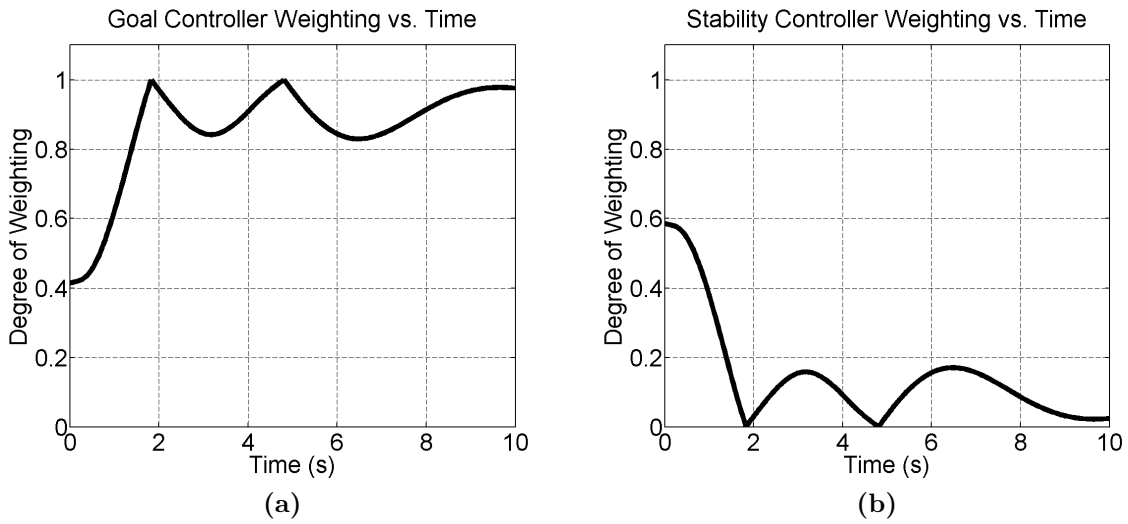

Figure 5.20: Weighting factors applied to stability and goal controller output for sit-to-stand controller test case #3. (a) μ_{stab} corresponding to the weight factor applied to the output of the goal controller, and (b) $(1 - \mu_{stab})$ applied to the output of the the stability controller.

5.6.4 Sit-to-Stand Controller Conclusions

In all three test cases used to investigate the response of the sit-to-stand control system, it was able to bring the model to rest in the goal (standing) configuration. As expected, in regions of operation where the biomechanical model displayed relative instability, the stability controller output was weighted more heavily, or even used exclusively, by the sit-to-stand controller until (biomechanical) stability of the model was achieved. Over the course of the sit-to-stand movement, the stability controller was shown to primarily contribute to forward (and when necessary, backward) lean of the biomechanical model, while the goal controller generated the majority of the vertical rise component. Using a third fuzzy system to interpolate between these control actions - based upon stability of the biomechanical model - yielded a realistic, and stable, sit-to-stand movement.

A comparison was made between the motion capture data presented in Appendix C for a single healthy male subject, to the simulation results presented in Section 5.6.1. The simulation results proved to be very similar in appearance to that of the

motion capture data, both in terms of the joint angle plots (illustrated in Figures 5.12 and 5.13) and the path traversed by the total body center of mass (illustrated in Figures 5.11a and 5.13d). Joint angle plots are very commonly used by clinicians to evaluate human movement activities [20,34]. Therefore, based upon these results, it may be stated that a realistic movement has been realized. Furthermore, a video compiled from snapshots of the biomechanical model's configuration over the course of the simulated sit-to-stand movement (for sit-to-stand controller test case #1) further validated this claim. The argument was made in Section 4.1 of this work, that if a realistic sit-to-stand movement could be mimicked, then an energy efficient solution is likely to result. Based upon this argument, and the claim that a realistic movement had been observed in the simulated results of Section 5.6.1, then it follows that the movement produced by the sit-to-stand controller is likely reasonably energy efficient.

A minor premature plantarflexion of the ankle joint was observed in the operation of the goal controller as discussed in Section 5.6.1. For the most part, this undesired effect only affected the time required to meet the success criteria laid out for the sit-to-stand controller in test case #3 (Section 5.6.3).

5.7 The Effects of Varying Model Parameter m_3

As discussed in Section 3.2.5, the mass of the HAT, given by m_3, is by far the most influential mass of the three-link biomechanical model used in this work. It is also the rigid body member whose mass is most likely to be incorrectly assessed, given it represents the whole of the head, arms, and trunk. Estimates for this mass parameter are given by Equation 3.4, where the parameter $\alpha \in \{-0.25, 0, 0.25\}$ was varied to produce over- and underestimates for the mass of the HAT, denoted $\hat{m}_3$. Since the estimated location of the total-body center of mass is a function of the mass parameters m_1, m_2, and $\hat{m}_3$ (given by Equation 3.6), and it plays a vital role in the

Quantity	Expected Value	Measured Value	Error
θ_{CoM} (deg)	88.7	89.44	0.8
$\boldsymbol{\theta}$ (deg)	85	85.34	0.34
	10	10.97	0.97
	-10	-10.84	-0.84
$\dot{\boldsymbol{\theta}}$ (deg/s)	0	-0.56	-0.56
	0	-0.97	-0.97
	0	0.96	0.96
W (J)	-	338	-

Table 5.12: Simulation Results for Sit-to-Stand Controller m_3 Mass Overestimate.

sit-to-stand control system (as discussed in Chapter 4), two test cases were used to investigate the effects of varying mass parameter $\hat{m}_3$ using parameter α.

5.7.1 Test Case #1: Mass Parameter m_3 Overestimate

The mass parameter m_3 was overestimated using Equation 3.4 with $\alpha = 0.25$, such that

$$\begin{aligned} \hat{m}_3 &= m_3 + m_3 \cdot 0.25 \\ &= 1.25 \cdot m_3 \end{aligned}$$

where m_3 is the actual mass of the HAT rigid body segment.

The sit-to-stand movement was simulated using the overestimated value of m_3 and sit-to-stand controller test case #1 (Section 5.6.1). The criteria for success were met at simulation time $t = 8.37$ s. This represents an additional time of 0.03 s over the time required by the sit-to-stand controller where a mass parameter overestimate was not used. Results of this test, at $t = 8.37$ s, are summarized in Table 5.12.

Comparing the results from Table 5.12 with the simulation results from Table 5.8, no appreciable difference is observed. For all intents and purposes the results are identical. Therefore, a 25% overestimate of mass parameter m_3 had no appreciable effect on the sit-to-stand controller performance.

Quantity	Expected Value	Measured Value	Error
θ_{CoM} (deg)	88.7	89.37	0.7
$\boldsymbol{\theta}$ (deg)	85	85.34	0.34
	10	10.98	0.98
	-10	-10.82	-0.82
$\dot{\boldsymbol{\theta}}$ (deg/s)	0	-0.54	-0.54
	0	-0.95	-0.95
	0	0.90	0.90
W (J)	-	337	-

Table 5.13: Simulation Results for Sit-to-Stand Controller m_3 Mass Underestimate.

5.7.2 Test Case #2: Mass Parameter m_3 Underestimate

The mass parameter m_3 was underestimated using Equation 3.4 with $\alpha = -0.25$, such that

$$\begin{aligned} \hat{m}_3 &= m_3 + m_3 \cdot (-0.25) \\ &= 0.75 \cdot m_3 \end{aligned}$$

where m_3 is the actual mass of the HAT rigid body segment.

The sit-to-stand movement was simulated using the underestimated value of m_3 and again with sit-to-stand controller test case #1. The criteria for success were met at simulation time $t = 8.37$ s, (i.e., identical to the time recorded for test case #1 in Section 5.7.1). Results of this test, at $t = 8.37$ s, are summarized in Table 5.13.

Again comparing the results from Table 5.13 with the simulation results from Table 5.8, no appreciable difference is observed. As with the case of the mass parameter overestimate, for all intents and purposes the results are identical. Thus, a 25% underestimate of mass parameter m_3 had no appreciable effect on sit-to-stand controller performance.

5.7.3 Mass Parameter Variation Conclusions

The results summarized in Tables 5.12 and 5.13, show that no appreciable affect was observed on the performance of the sit-to-stand controller in the event of an over- or underestimate of mass parameter m_3. It was expected that the vector projected to the total body center of mass (and therefore the inclination of the total body center of mass given by θ_{CoM}), depicted in Figure 3.5, would change only slightly in the presence of a 25% over- or underestimate of this mass parameter. This is because, at 67.8% of the total body mass (as given in Table 3.1), the HAT already greatly determines the location of the total body center of mass. Therefore, measures of importance to the sit-to-stand controller, such as θ_{CoM}, are tolerant to significant over- and underestimates of the HAT's mass. This is desirable, because, as stated previously, the HAT is the most influencial mass of the biomechanical system and it is the one most likely to be incorrectly assessed. Moreover, the mass of the HAT is the rigid body most likely to vary between individuals; hence, an insensitivity to mass parameter m_3 is a highly desirable controller property.

5.8 Impulse Response Testing

Due the highly nonlinear nature of the fuzzy-based control system developed in this work, conventional stability analysis methods cannot be used. Instead, the impulse response testing strategy used in [19] was adopted. Impulse response is a standard test used to investigate the stability, and generally characterize the response, of a control system. A large momentary disturbance is applied to the plant so that the controller's response may be observed. The disturbance is modelled as a set of joint torques, as was done in [19], denoted as $\mathbf{u}_{dist}$, where

$$\mathbf{u}_{dist} = \begin{bmatrix} 400 & 300 & 200 \end{bmatrix}^T Nm \tag{5.8}$$

$\mathbf{u}_{dist}$ was interjected into the control path as shown in Figure 5.21. The disturbance impulse is applied for one time step of the simulation, (i.e., a duration of 0.0286 s), from times t_1 to t_2. The control action delivered to the plant, at any given time t, may then be stated as

$$\boldsymbol{\tau}(t) = \begin{cases} \boldsymbol{\tau}(t) + \mathbf{u}_{dist}, & t_1 \leq t \leq t_2 \\ \boldsymbol{\tau}(t), & \text{otherwise} \end{cases}$$

The disturbance action, $\mathbf{u}_{dist}$, represents a set of joint torques greater in magnitude than the maximum values normally experienced by the joints during sit-to-stand (where Figure 5.11b constitutes a set of normal values). The ankle disturbance action (400 Nm) is over double the maximum value normally experienced by the ankle joint, directly affecting the lean of the entire biomechanical system. $\mathbf{u}_{dist}$ essentially acts as a large backward push at approximately chest height on the model.

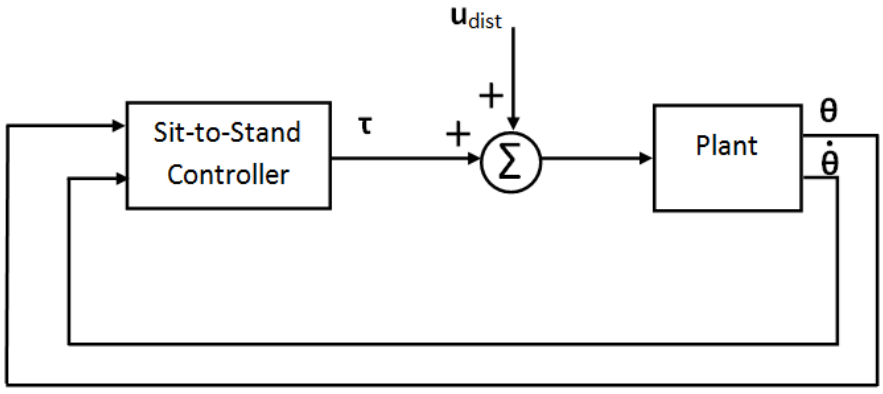

Figure 5.21: Control path with disturbance.

5.8.1 Impulse Response: Test Case #1

The biomechanical model began at rest in a standing configuration, given by $\boldsymbol{\theta}_f$. It was then perturbed by $\mathbf{u}_{dist}$ for the equivalent of one time step from t = 0 to t = 0.0286 s, effectively pushing the model suddenly backward. The sit-to-stand controller responded to the disturbance with the set of control actions shown in

Figure 5.22b returning the biomechanical model to quiet standing. The initial and final configurations of the biomechanical model, as well as the path traversed by the total body center of mass are illustrated in Figure 5.22a. In the figure, it can be seen that the center of mass was perturbed horizontally backward, then returned along the same path to overshoot slightly before coming to rest at the desired standing configuration. This indicates that the sit-to-stand controller responded directly to the errors which developed in the configuration of the biomechanical model as a result of the disturbance.

One of the more useful measures in analyzing the control system's response is to look at the weights assigned to the stability and goal controller output over the course of the simulation. These are illustrated in Figures 5.22d and 5.22c respectively. Looking at Figure 5.22, it can be seen that, after some delay (for the disturbance to take effect), the stability controller output was weighted more heavily than the goal controller to promote balance recovery. As the gravity line, projected from the total body center of mass, returned to the base of support region, the goal controller output was once again favored. A damped oscillatory (i.e., underdamped) response is seen in the weighting of the stability and goal controller output, and is also visible in the control actions of Figure 5.22b.

The success criteria (given in Section 5.2.1, were once again met at time $t = 8.40$ s (i.e., $t_{success}$), following the disturbance at time t = 0. These results are summarized in Table 5.14. Given that the sit-to-stand controller required 9.71 s (and nearly 6.08 s) to recover from the near standing test case described in Section 5.6.3, a recovery time of 8.40 s following a large perturbation from a standing configuration is not unreasonable.

5.8.2 Impulse Response: Test Case #2

In test case #2, the biomechanical model began in a seated configuration, given by $\boldsymbol{\theta}_i$, and progressed through the sit-to-stand movement. The disturbance $\mathbf{u}_{dist}$ was

Time of Disturbance t_1 (s)	**Time of Success** $t_{success}$ (s)	**Recovery Period** $t_{success}$ - t_1 (s)	**Work Done** (J)
0	8.40	8.40	138

Table 5.14: Simulation Results for Impulse Response Test Case #1.

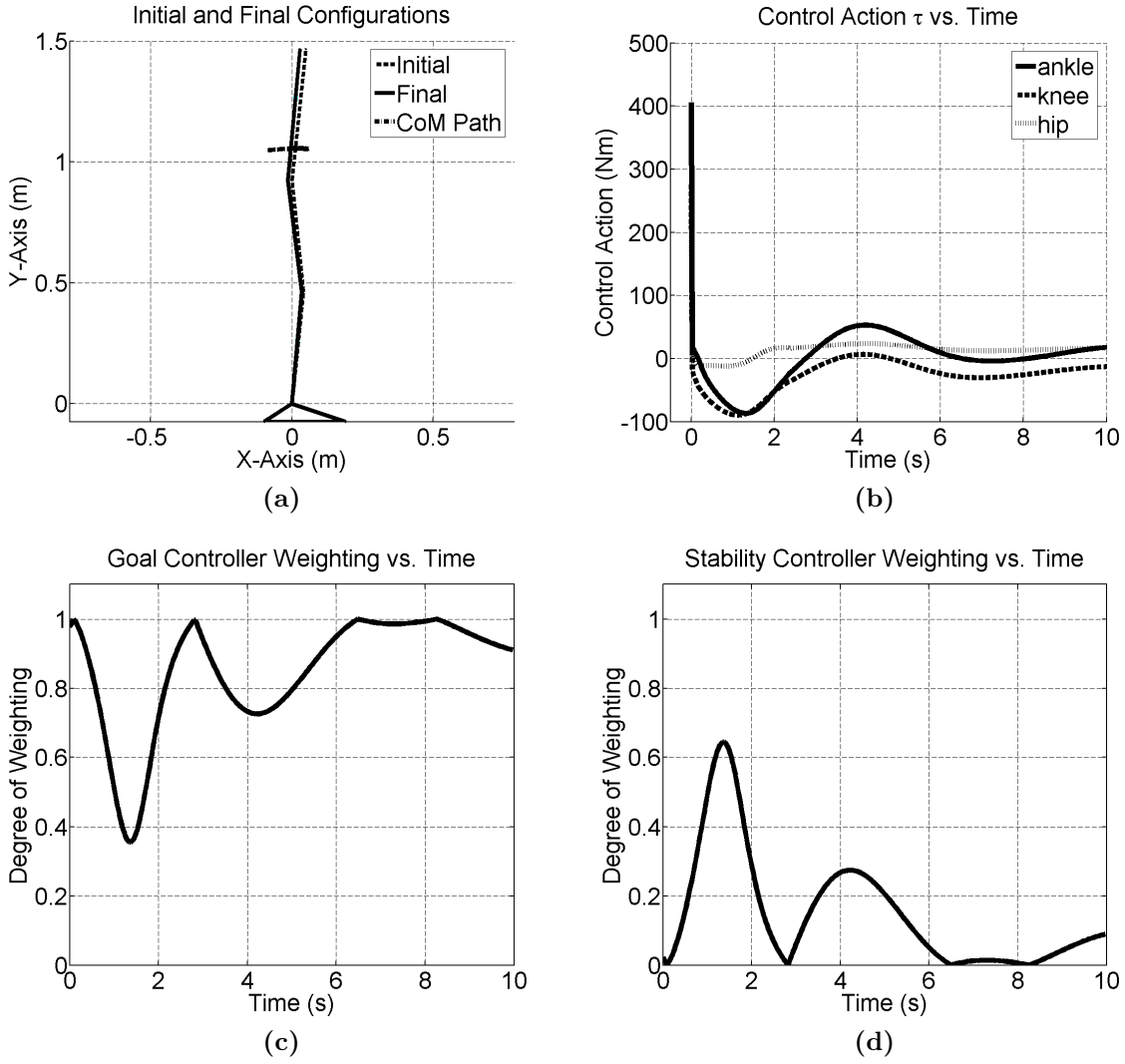

Figure 5.22: Simulation results for disturbance test case #1. (a) the initial and final configurations of the biomechanical model, (b) the control actions produced by the sit-to-stand controller plus disturbance $\mathbf{u}_{dist}$, (c) the weighting factor, μ_{stab}, applied to the goal controller output, and (d) the weighting factor, $(1-\mu_{stab})$, applied to the stability controller output.

applied during seat-off - the most statically unstable phase of sit-to-stand. This test case presented a worst case scenario in terms of exploiting biomechanical instability

Time of Disturbance t_1 (s)	**Time of Success** $t_{success}$ (s)	**Additional Time** $t_{success}$ - 8.34 (s)	**Work Done)** (J)
2	10.26	1.92	359

Table 5.15: Simulation Results for Impulse Response Test Case #2.

and the need for balance recovery. The disturbance was applied at time $t_1 = 2$ s for a duration of 0.0286 s. The criteria for success were met at time $t = 10.26$ s (i.e., $t_{success}$). Results of this test are summarized in Table 5.15.

The column "Additional Time" presents the difference between the time required to achieve the success criteria in the presence of a disturbance $\mathbf{u}_{dist}$ versus without (as presented in Table 5.8 of Section 5.6.1). Therefore, it can be seen from Table 5.15, in this test case, an additional 1.92 s was required to complete the sit-to-stand movement given the effects of the disturbance $\mathbf{u}_{dist}$ on the biomechanical system. Comparing the work done by the joint actuators over the course of the movement for the perturbed and unperturbed cases (i.e. comparing the value of work in Table 5.15 to 5.8) gives a difference of 22 J. Thus, an additional effort, on the part of the joint actuators, of 22 J (or 6.5% of the work done in the unperturbed case) was required to correct for the disturbance $\mathbf{u}_{dist}$.

The disturbance is clearly seen at time $t = 2$ s in Figure 5.23b, which depicts the control actions delivered to the plant. The initial and final configurations of the biomechanical model, as well as the path traversed by the total body center of mass are illustrated in Figure 5.23a. Comparing the path traversed by the total body center of mass in Figure 5.23a with the one corresponding to the unperturbed case, given in Figure 5.11a, it can be seen that in the presence of the disturbance, $\mathbf{u}_{dist}$, a much more direct vertical rise takes place rather than a movement forward of the ankle as seen in Figure 5.11a. This would suggest that the forward momentum of the biomechanical model was hindered during seat off by the disturbance at time $t = 2$

Time of Disturbance t_1 (s)	**Time of Success** $t_{success}$ (s)	**Additional Time** $t_{success}$ - 8.34 (s)	**Work Done)** (J)
3	13.57	5.23	390

Table 5.16: Simulation Results for Impulse Response Test Case #3.

s. Despite this fact, the sit-to-stand controller was able to bring the model into the desired configuration without any progression of backward movement.

The sit-to-stand controller relied more heavily upon (i.e., weighted more heavily) the stability controller output during seat-off in the presence of the disturbance than without. This can be seen in Figure 5.23d where the weight assigned to the stability controller output is presented for both the disturbed and undisturbed cases. For comparison purposes, the stability controller weighting labeled "without disturbance" in Figure 5.23d is simply a reproduction of the results presented in Figure 5.14b of Section 5.6.1. The weight assigned to the goal controller in the presence of a disturbance is also provided in 5.23c.

5.8.3 Impulse Response: Test Case #3

In test case #3, the biomechanical model began in a seated configuration, given by $\boldsymbol{\theta}_i$, and progressed through the sit-to-stand movement. The disturbance, $\mathbf{u}_{dist}$, was applied to the biomechanical model as it entered the vertical ascension phase of sit-to-stand, at time $t_1 = 3$ s, where $\mathbf{u}_{dist}$ was redefined as

$$\mathbf{u}_{dist} = \begin{bmatrix} -400 & -300 & -200 \end{bmatrix}^T Nm \tag{5.9}$$

so as to cause a forward-going perturbation of the biomechanical system. With the model already committed to a forward leaning position, a strong forward-going perturbation is highly undesirable. The criteria for success were met at time $t =$ 13.57 s (i.e., $t_{success}$). Results of this test are summarized in Table 5.16.

Comparing the times required to reach the success criteria with disturbance versus

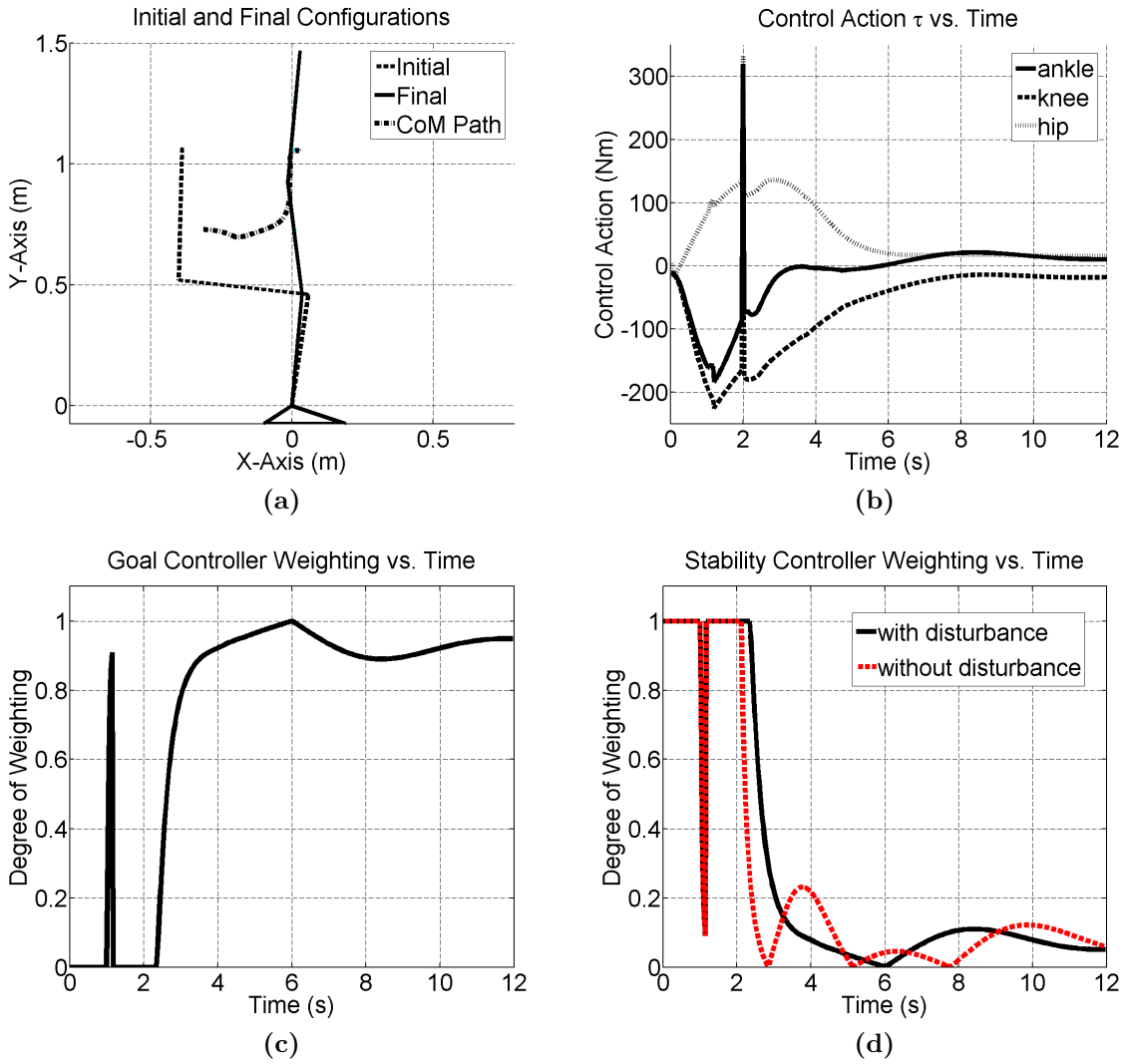

Figure 5.23: Simulation results for disturbance test case #2. (a) the initial and final configurations of the biomechanical model, (b) the control actions produced by the sit-to-stand controller plus disturbance $\mathbf{u}_{dist}$, (c) the weighting factor, μ_{stab}, applied to the goal controller output, and (d) the weighting factor, $(1-\mu_{stab})$, applied to the stability controller output.

without, given in Table 5.16 as the "Additional Time," an additional 5.23 s was required to complete the sit-to-stand movement given the effects of the disturbance $\mathbf{u}_{dist}$ on the biomechanical system. Comparing the work done by the joint actuators over the course of the movement, for the perturbed and unperturbed cases (i.e., comparing the value of work in Table 5.16 to 5.8), gives a difference of 54 J. Thus,

an additional effort, on the part of the joint actuators, of 54 J (or 16% of the work done in the unperturbed case) was required to correct for the disturbance $\mathbf{u}_{dist}$.

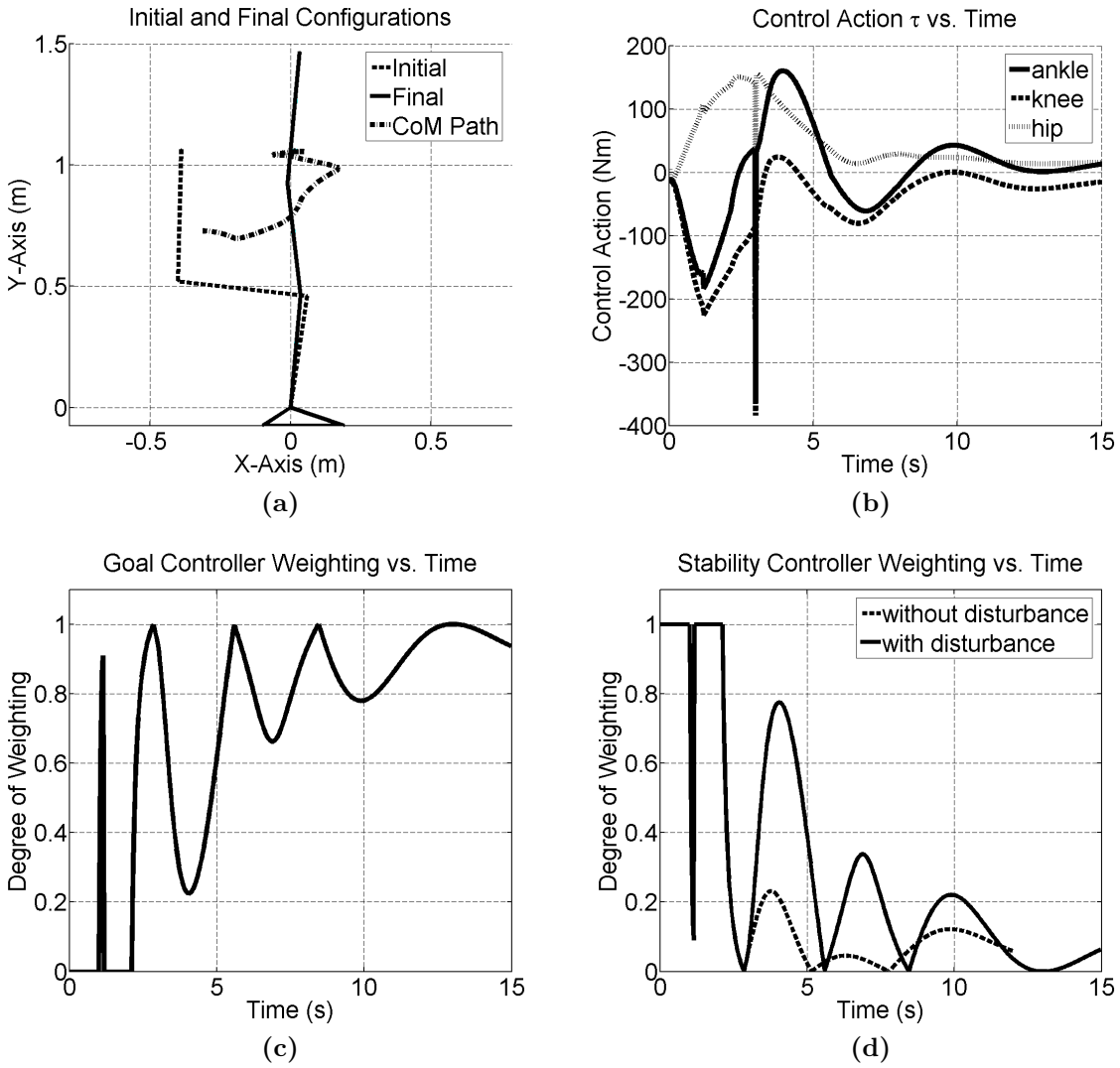

Figure 5.24: Simulation results for disturbance test case #3. (a) the initial and final configurations of the biomechanical model, (b) the control actions produced by the sit-to-stand controller plus disturbance $\mathbf{u}_{dist}$, (c) the weighting factor, μ_{stab}, applied to the goal controller output, and (d) the weighting factor, $(1-\mu_{stab})$, applied to the stability controller output.

The initial and final configurations of the biomechanical model are shown in Figure 5.24a, along with the path traversed by the total body center of mass. When compared to the path traversed by the center of mass in the unperturbed case (i.e., Figure 5.11a), a noticeable forward overshoot is observed as a result of the disturbance

at time $t = 3$ s. The total body center of mass is brought immediately backward, demonstrating a damped oscillatory response before coming to rest at is final location $\begin{bmatrix} x^f_{CoM} & y^f_{CoM} \end{bmatrix}$.

A damped oscillatory response is also seen in the control actions produced by the sit-to-stand controller as shown in Figure 5.24b, and in the weighting of the goal and stability controller output illustrated in Figures 5.24c and 5.24d respectively. The sit-to-stand controller brings the biomechanical model under control by weighting the stability controller output more heavily in the period following the disturbance, and again in instances where the total body center of mass shifted away from the base of support midpoint. Comparing the stability controller weighting in the perturbed case, depicted in Figure 5.24d to the unperturbed case, depicted in Figure 5.14b, it can be seen that the stability controller output was weighted much more heavily in the presence of the disturbance $\mathbf{u}_{dist}$.

5.8.4 Impulse Response Conclusions

In all three impulse response test cases the sit-to-stand control system was able to recover from the disturbances applied to it. The first test case demonstrated the controller's ability to recover from perturbation with the biomechanical model having achieved quiet standing. The errors developed in the biomechanical system, as a result of the perturbation, were suppressed returning the model to the quiet standing configuration in a time frame of 8.40 s - a not unreasonable recovery time given that the sit-to-stand controller required 9.71 s (and nearly 6.08 s) to recover from the near standing test case described in Section 5.6.3. A minor damped oscillatory response was observed in this test case.

Test case #2 provided a worst case scenario where the biomechanical model was disturbed during the most statically unstable period of the sit-to-stand movement (i.e., seat-off). The sit-to-stand controller was able to bring the biomechanical model to the desired standing configuration without any oscillatory behavior or backward

progression of the total body center of mass. As a result of the disturbance an additional 1.92 s was required to meet the criteria for success (as compared to the unperturbed case in Section 5.6.1.

In the third test case, an impulse disturbance was applied to the plant in a forward-going direction as the biomechanical model leaned forward preparing for vertical ascension. A damped oscillatory response was observed as the sit-to-stand controller brought the biomechanical system under control. An additional 5.23 s was required to achieve the criteria for success in this test case as compared to the unperturbed case described in Section 5.6.1.

Chapter 6

Conclusions and Future Work

6.1 Conclusions

In this work, a fuzzy-based control strategy for synthesizing the sit-to-stand movement was presented. A simple three-link biomechanical model (referred to as the "plant"), commonly used in sit-to-stand analysis, was used to simulate the movement. The aim of this work is to contribute to the machine intelligence being developed for advanced mobility support devices; and specifically, those which are able to assist the mobility impaired user with the sit-to-stand task. Three main fuzzy logic control systems were developed: 1) a stability controller which tended to move the biomechanical model into the "most stable" configuration, 2) a goal controller which guided the model toward the goal (i.e., standing) configuration, and 3) a fuzzy system which acted as a nonlinear interpolator combining the outputs of the first two controllers. The final composite control system design was referred to as the "sit-to-stand controller."

Chapter 2 introduced conventional control strategies which might be applied to a quasi robotic mechanism such as an advanced mobility support device. Model-based and fuzzy logic-based control concepts were also introduced.

Chapter 3 familiarized the reader with the biomechanical model (i.e., the plant) used to simulate the physical control process and reviewed, in detail, the sit-to-stand

task. A common technique for conducting sit-to-stand, known as the momentum-transfer strategy, was selected as the primary strategy to be employed by the automated sit-to-stand controller. Details of the forward simulation of the biomechanical model were also presented.

In Chapter 4, a fuzzy logic-based control strategy for synthesizing the sit-to-stand movement was presented. Just as some modern day robot manufacturers have done, a gravity model of the plant was included in the control law of the control system. This provided a model-based estimate of the joint torques required to counteract the effects due to gravity. The dynamic response of the control system was primarily determined by the functionality of three fuzzy-based control systems: the stability, goal, and nonlinear interpolator controllers, described earlier. The stability controller produced the majority of the forward lean component of the sit-to-stand movement, while the goal controller produced the majority of vertical rise. The third fuzzy system, (i.e., the nonlinear interpolator), combined the outputs of these controllers in a way which promoted biomechanical stability of the plant while also advancing it toward the end-goal configuration.

Chapter 5 presented the simulation results for each of the control systems developed in Chapter 4. The stability and goal controllers were implemented and tested independently before their output was incorporated into the sit-to-stand control system (by way of the nonlinear interpolator). In all three test cases used to investigate the response of the controllers, the stability controller was shown to always bring the biomechanical model into the "most stable" configuration, and the goal controller was shown to always bring the model into the goal configuration, as directly as possible. The simulation results of the sit-to-stand controller were compared against motion tracking data results collected for a single healthy male test subject (provided in Appendix C). The movement produced by the automated control system developed in this work and the one produced by the human test subject were found

to be quite similar (according to joint angle plots and the path traversed by the total body center of mass). Therefore, the goal of producing realistic sit-to-stand movement was achieved by the developed sit-to-stand controller solution. It is also believed, due to the similarity to the motion capture data, that a reasonably energy efficient movement has been realized.

The most influential mass of the biomechanical model, (i.e., the mass of the HAT), was varied by $\pm 25\%$ to investigate the effects of parameter variation on control system performance. The simulation results showed that the controller performance was virtually unaffected by this variation. Impulse testing of the control system showed that the sit-to-stand controller was able to recover from significant disturbances applied to the plant. In the worst case scenario, a perturbation during seat-off, no oscillatory behavior or counter-productive movement of the plant was observed. An acceptable level of damped oscillatory response was observed in two other test cases, while the controller brought the plant under control.

The proposed fuzzy logic-based control strategy is conceptually simple in its approach and intuitive in its operation. These aspects make it an attractive choice over conventional model-based trajectory generation methods which provide a solution to the problem for a particular instance (i.e., not the sit-to-stand task in general). Therefore, while a conventional control system can always be constructed which performs just as well, or possibly better than the fuzzy-based equivalent, it does so for a particular set of conditions (such as a particular individual). The incorporation of expert knowledge about the sit-to-stand task into the fuzzy control system allows us to solve the general problem which may be "tuned" to suit the needs of virtually any client. This approach to movement planning and control may prove to be the more cost effect, and ultimately, provide a clinically viable solution to synthesizing human movement using advanced mobility support devices.

6.2 Future Work

Future extensions of this work include using a five-link biomechanical model to simulate the sit-to-stand movement. While a three-link biomechanical model is commonly used to analyze and simulate sit-to-stand, a five-link model, where the legs are modelled as separate entities (and thereby no longer constrained to movements simply in the sagittal plane), would provide for a more detailed, and realistic simulation. The availability of a five-link biomechanical model would allow the control engineer to develop a control system which balanced the forces between the left and right legs over the course of the movement.

In addition to producing a slow controlled movement, future work includes developing support for typical speeds of movement, such as "slow", "normal", and "fast," which may be catered to specific individuals. The sit-to-stand control system developed in this work accommodates the selection of a single speed of movement. Therefore, the design of the stability and goal controllers (which dictate the dynamic response of the system) will be expanded upon to accommodate multiple speed of movement selections.

A third-party simulator, such as Mathworks SimMechanics^{TM} , should be used to independently validate the operation and performance of the sit-to-stand control system under a wider set of test scenarios.

Bibliography

[1] R. Aissaoui and J. Dansereau. Biomechanical analysis and modelling of sit to stand task: a literature review. In *Systems, Man, and Cybernetics, 1999. IEEE International Conference on*, volume 1, pages 141 –146, 1999.

[2] F. Bahrami., R. Riener, and G. Schmidt. Optimal trajectory generation for a paraplegic patient rising from a chair by means of fes. In *Proc. of the First Annual Conference of the International Functional Electrical Stimulation Society*, Cleveland, Ohio, USA, 1996.

[3] G. Bessonnet, P. Seguin, and P. Sardain. A parametric optimization approach to walking pattern synthesis. *The International Journal of Robotics Research*, 24(7):523–536, 2005.

[4] Lucie Cossette and Edith Duclos. A profile of disability in canada, 2001. Technical report, Statistics Canada, Ottawa, Ontario, 2002.

[5] J. J. Craig. *Introduction to Robotics: Mechanics and Control*. Addison-Wesley Longman Publishing Co., Inc., 1989.

[6] T. Hayashi, H. Kawamoto, and Y. Sankai. Control method of robot suit hal working as operator's muscle using biological and dynamical information. In *IEEE/RSJ International Conference on Intelligent Robots and Systems.*, pages 3063 – 3068, 2005.

[7] H. He and K. Kiguchi. A study on emg-based control of exoskeleton robots for human lower-limb motion assist. In *Information Technology Applications in Biomedicine, 2007. ITAB 2007. 6th International Special Topic Conference on*, pages 292 –295, 2007.

[8] S. F. Holford. The application of fuzzy logic to the adaptive control of a hydrographic survey craft. Master's thesis, University of Victoria, Victoria, British Columbia, Canada, 1994.

[9] K. Iqbal and A. Roy. Stabilizing pid controllers for a single-link biomechanical model with position, velocity, and force feedback. *Journal of Biomechanical Engineering*, 126:838–43, 2004.

[10] S. Kajita and K. Tani. Study of dynamic biped locomotion on rugged terrain-derivation and application of the linear inverted pendulum mode. In *Robotics and Automation, 1991. Proceedings., 1991 IEEE International Conference on*, volume 2, pages 1405 –1411, 1991.

[11] H. Kawamoto, Suwoong Lee, S. Kanbe, and Y. Sankai. Power assist method for hal-3 using emg-based feedback controller. In *Systems, Man and Cybernetics, 2003. IEEE International Conference on*, volume 2, pages 1648 – 1653, 2003.

[12] Hiroaki Kawamoto and Yoshiyuki Sankai. Power assist system hal-3 for gait disorder person. In *ICCHP '02: Proceedings of the 8th International Conference on Computers Helping People with Special Needs*, pages 196–203, London, UK, 2002. Springer-Verlag.

[13] H. Kazerooni, J.-L. Racine, Lihua Huang, and R. Steger. On the control of the berkeley lower extremity exoskeleton (bleex). In *Robotics and Automation, 2005. ICRA 2005. Proceedings of the 2005 IEEE International Conference on*, pages 4353 – 4360, 2005.

[14] K. Kiguchi, T. Tanaka, and T. Fukuda. Neuro-fuzzy control of a robotic exoskeleton with emg signals. *Fuzzy Systems, IEEE Transactions on*, 12(4):481 – 490, Aug. 2004.

[15] A. Kralj, R. J. Jaeger, and M. Munih. Analysis of standing up and sitting down in humans: definitions and normative data presentation. *Journal of Biomechanics*, 23(11):1123–1138, 1990.

[16] A.M. Mughal and K. Iqbal. A fuzzy biomechanical model for optimal control of sit-to-stand movement. In *Engineering of Intelligent Systems, 2006 IEEE International Conference on*, pages 1–6, 2006.

[17] T. Nakamura, K. Saito, and K. Kosuge. Control of wearable walking support system based on human-model and grf. In *Robotics and Automation, 2005. ICRA 2005. Proceedings of the 2005 IEEE International Conference on*, pages 4394 – 4399, 18-22 2005.

[18] J.H. Park and K.D. Kim. Biped robot walking using gravity-compensated inverted pendulum mode and computed torque control. In *Robotics and Automation, 1998. Proceedings. 1998 IEEE International Conference on*, volume 4, pages 3528–3533, 1998.

[19] Kevin M. Passino and Stephen Yurkovich. *Fuzzy Control*. Addison-Wesley Longman, Inc., 1998.

[20] J. Perry. *Gait analysis: normal and pathological function*. SLACK Inc., 1992.

[21] A. Prochazka. Comparison of natural and artificial control of movement. *Rehabilitation Engineering, IEEE Transactions on*, 1(1):7–17, Mar 1993.

[22] Arthur Prochazka. The fuzzy logic of visuomotor control. *Canadian Journal of Physiology and Pharmacology*, 74(4):456–462, 1996.

[23] R. Riener., F. Bahrami, and A. Schmidt. Trajectory generation by parametric optimization to predict the kinematics and kinetics of a subject rising from a chair. In *Proc. of the Ninth Conf. Biomechanics and Neural Control*, Deer Creek Restor and Conference Center, Mt. Sterling, Ohio, 1996.

[24] P. O. Riley, M. L. Schenkman, R. W. Mann, and W. A. Hodge. Mechanics of a constrained chair-rise. *Journal of Biomechanics*, 24(1):77–85, 1991.

[25] J. Rosen, M. Brand, M.B. Fuchs, and M. Arcan. A myosignal-based powered exoskeleton system. *Systems, Man and Cybernetics, Part A: Systems and Humans, IEEE Transactions on*, 31(3):210–222, May 2001.

[26] Timothy. J. Ross. *Fuzzy logic with engineering applications*. McGaw-Hill Inc., New York, 1995.

[27] A.B. Schultz, N.B. Alexander, and J. A. Ashtonmiller. Biomechanical analyses of rising from a chair. *Journal of Biomechanics*, 25(12):1383–1391, Dec 1992.

[28] T. Takagi and M. Sugeno. Fuzzy identification of systems and its applications to modeling and control. *IEEE Trans. on Systems, Man, and Cybernetics*, 15(1):116–132, January 1985.

[29] Argo Medical Technologies. Rewalk. http://www.argomedtec.com.

[30] Christopher L. Vaughan. Theories of bipedal walking: an odyssey. *Journal of Biomechanics*, 36(4):513 – 523, 2003.

[31] L. X. Wang. Fuzzy systems are universal approximators. In *Fuzzy Systems, 1992., IEEE International Conference on*, pages 1163 –1170, 1992.

[32] L. X. Wang. *Adaptive fuzzy systems and control - design and stability analysis*. Prentice Hall, 1994.

[33] James Watkins. *An Introduction to Biomechanics of Sport and Exercise*. Elsevier, 2007.

[34] M. W. Whittle. *Gait analysis: an introduction*. Butterworth-Heinemann Ltd., 3rd edition, 2003.

[35] D. A. Winter. *Biomechanics and Motor Control of Human Movement*. Wiley, 3rd ed. edition, 2005.

[36] D. A. Winter, H. G. Sidwall, and D. A. Hobson. Measurement and reduction of noise in kinematics of human movement. *J. Biomech.*, 7:157–159, 1974.

[37] H. Ying. General takagi-sugeno fuzzy systems are universal approximators. In *Fuzzy Systems Proceedings, 1998. IEEE World Congress on Computational Intelligence., The 1998 IEEE International Conference on*, volume 1, pages 819–823, 1998.

[38] L.A. Zadeh. Fuzzy sets. *Information and Control*, 8(3):338 – 353, 1965.

[39] A.B. Zoss, H. Kazerooni, and A. Chu. Biomechanical design of the berkeley lower extremity exoskeleton (bleex). *Mechatronics, IEEE/ASME Transactions on*, 11(2):128 –138, april 2006.

Appendix A

Anthropometric Data for the Biomechanical Model

Details of the anthropometric parameters for the three-link rigid body biomechanical model used throughout this work, depicted in Figure A.1, are given here. Anthropometric parameters of the model, including segment length, location of center of mass, segment mass, moment of inertia, etc., were determined using methods adopted from Winter [35]. A summary of the anthropometric data provided by Winter is included in Table A.1. The biomechanical model consisted of shank, thigh, and HAT, rigid body members, existing in the sagittal plane. Subscripted numbers 1, 2, and 3, represent the shank, thigh, and HAT respectively.

Each parameter given in Table A.1, is a proportion of either the total body mass, total body height, or segment length.

A.1 Total Body Height and Mass

A total body height (tbh) of 1.89 m and total body mass (tbm) of 86.4 kg were selected to match the test subject used to produce the motion capture data collected

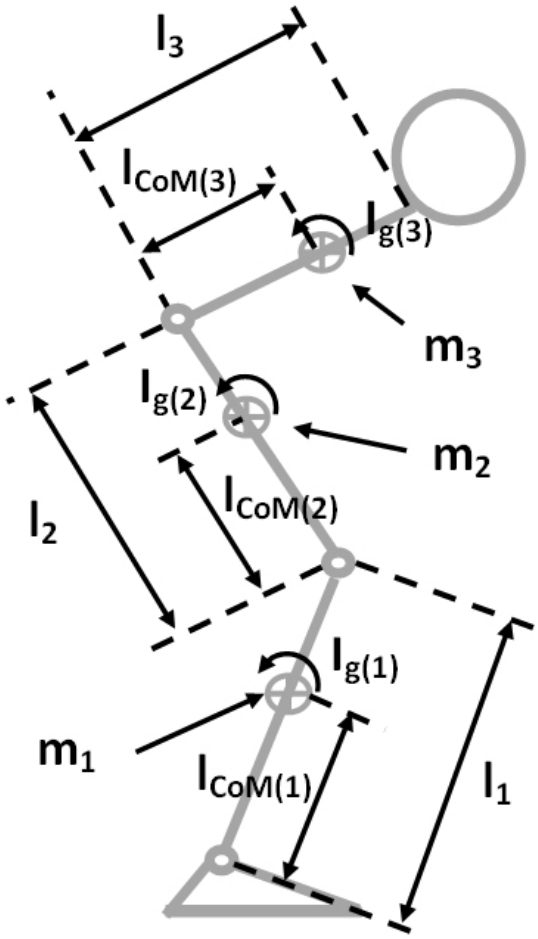

Figure A.1: Biomechanical model with anthropometric measures.

in support of this work (the details of which are included in Appendix C).

$$tbh = 1.89 \text{ m}$$

$$tbm = 86.4 \text{ kg}$$

A.2 Calculation of the Segment Mass

Using the segment mass ratios provided in Table A.1, the mass of each rigid body segment can be found, as given below. The mass of the shank and thigh segments must be doubled for the biomechanical model in this work, because the legs were

	Shank	Thigh	HAT
Segment Mass Ratio (Segment Mass/ Total Body Mass)	0.0465	0.100	0.678
Segment Length Ratio (Segment Length/ Total Body Height)	0.246	0.245	0.288
Center of Mass Ratio (Center of Mass/ Segment Length)	0.567	0.567	0.626
Radius of Gyration Ratio (Radius of Gyration/ Segment Length)	0.302	0.323	0.496

Table A.1: Anthropometric Data for the Biomechanical Model.

modelled as a single entity (due to bilateral symmetry about the sagittal plane).

$$m_1 = 2 \cdot 0.0465 \cdot tbm$$

$$m_2 = 2 \cdot 0.100 \cdot tbm$$

$$m_3 = 0.678 \cdot tbm$$

A.3 Calculation of Segment Length and Location of Center of Mass

The length of each body segment is found as

$$l_1 = 0.246 \cdot tbh$$

$$l_2 = 0.245 \cdot tbh$$

$$l_3 = 0.288 \cdot tbh$$

The location of the center of mass of each segment is found as

$$l_{CoM(1)} = 0.567 \cdot l_1$$

$$l_{CoM(2)} = 0.567 \cdot l_2$$

$$l_{CoM(3)} = 0.626 \cdot l_3$$

A.4 Calculation of Radius of Gyration and Moment of Inertia

The radius of gyration for each rigid body segment is calculated as

$$k_1 = 0.302 \cdot l_1$$

$$k_2 = 0.323 \cdot l_2$$

$$k_3 = 0.496 \cdot l_3$$

The moment of inertia for each rigid body segment about its center of mass is calculated as

$$I_{g(1)} = m_1 \cdot (l_1 \cdot k_1)^2$$

$$I_{g(2)} = m_2 \cdot (l_2 \cdot k_2)^2$$

$$I_{g(3)} = m_3 \cdot (l_3 \cdot k_3)^2$$

Appendix B

Derivation of the Dynamic Equations

The Lagrangian dynamic formulation (as discussed in [5]) was used to derive the dynamic equations (or equations of motion) of the three-link biomechanical model used in this work. The dynamics of the model are described by a set of nonlinear differential equations, usually written compactly in the (linear) form

$$\boldsymbol{\tau} = \mathbf{M}(\boldsymbol{\theta}) \cdot \ddot{\boldsymbol{\theta}} + \mathbf{V}(\boldsymbol{\theta}, \dot{\boldsymbol{\theta}}) + \mathbf{G}(\boldsymbol{\theta}) \tag{B.1}$$

where $\boldsymbol{\tau}$ is the set of joint torques (or moments of force) applied to each joint, $\mathbf{M}(\boldsymbol{\theta})$ is the 3 x 3 inertia matrix, $\ddot{\boldsymbol{\theta}}$ is a 3 x 1 vector of joint angular accelerations, $\mathbf{V}(\boldsymbol{\theta}, \dot{\boldsymbol{\theta}})$ is a 3 x 1 vector which includes the centrifugal and Coriolis terms, and $\mathbf{G}(\boldsymbol{\theta})$ is a 3 x 1 vector of gravity terms. Since the model's dynamics are nonlinear in nature, matrix $\mathbf{M}$, and vectors $\mathbf{V}$, and $\mathbf{G}$, contain nonlinear elements.

For the model used in this work, Equation B.1 is expanded, such that

$$\begin{bmatrix} \tau_1 \\ \tau_2 \\ \tau_3 \end{bmatrix} = \begin{bmatrix} M_{1,1} & M_{1,2} & M_{1,3} \\ M_{2,1} & M_{2,2} & M_{2,3} \\ M_{3,1} & M_{3,2} & M_{3,3} \end{bmatrix} \cdot \begin{bmatrix} \ddot{\theta}_1 \\ \ddot{\theta}_2 \\ \ddot{\theta}_3 \end{bmatrix} + \begin{bmatrix} V_1 \\ V_2 \\ V_3 \end{bmatrix} + \begin{bmatrix} G_1 \\ G_2 \\ G_3 \end{bmatrix} \tag{B.2}$$

where the arguments of the terms in Equation B.1 have been dropped for brevity.

The Lagrangian, denoted as $\mathbf{L}$, calculated as the difference between the kinetic and potential energies of a rigid body system, such that

$$\mathbf{L}(\boldsymbol{\theta}, \dot{\boldsymbol{\theta}}) = T(\boldsymbol{\theta}, \dot{\boldsymbol{\theta}}) - U(\boldsymbol{\theta}) \tag{B.3}$$

where $T(\boldsymbol{\theta}, \dot{\boldsymbol{\theta}})$ is the kenetic energy of the system, and $U(\boldsymbol{\theta})$ its potential energy.

The equations of motion for the biomechanical system are given by

$$\boldsymbol{\tau} = \frac{d}{dt}\left(\frac{\partial T}{\partial \dot{\boldsymbol{\theta}}}\right) - \frac{\partial T}{\partial \boldsymbol{\theta}} + \frac{\partial U}{\partial \boldsymbol{\theta}} \tag{B.4}$$

where $\boldsymbol{\tau}$ is the 3 x 1 vector of actuator torques, T is the total kinetic energy of the system given by Equation B.7, U is the total potential energy of the system given by Equation B.8, $\boldsymbol{\theta}$ is the set of joint angles $\begin{bmatrix} \theta_1 & \theta_2 & \theta_3 \end{bmatrix}^T$ and $\dot{\boldsymbol{\theta}}$ is the set of joint angular velocities $\begin{bmatrix} \dot{\theta}_1 & \dot{\theta}_2 & \dot{\theta}_3 \end{bmatrix}^T$.

The kenetic energy of the system is simply the sum of the kenetic energies of each limb segment, T_i, where, for the i^{th} rigid body segment

$$T_i = \frac{1}{2} \cdot m_i \cdot v_{G(i)}^2 + \frac{1}{2} \cdot I_{G(i)} \cdot \dot{\theta}_i^2 \tag{B.5}$$

and m_i is the mass of the i^{th} rigid body segment, $v_{G(i)}$ is the segments's translational velocity (with respect to its center of gravity), $I_{G(i)}$ is the moment of inertia of the body (about its center of gravity), and $\dot{\theta}_i$ is the angular velocity of the body (also about the center of gravity).

The potential energy of the i^{th} rigid body segment, denoted as U_i, is given by

$$U_i = m_i \cdot g \cdot y_{CoM(i)} \tag{B.6}$$

where m_i is the mass of the i^{th} rigid body segment, g is the acceleration due to gravity

$(9.81m/s^2)$, and $y_{CoM(i)}$ is the y-component of the body's center of mass location. The kinetic energies of each rigid body are summed to form T, the total kinetic energy of the system, as

$$T = T_1 + T_2 + T_3 \tag{B.7}$$

where T_1, T_2, and T_3, represent the kinetic energies of the shank, thigh, and HAT respectively. Similarly, the potential energies of each rigid body segment are summed to form the total potential energy of the system U, as

$$U = U_1 + U_2 + U_3 \tag{B.8}$$

Substituting the anthropometric data given in Appendix A for the biomechanical model into Equations B.7 and B.8 gives

$$T_1 = \frac{1}{2} \cdot (m_1 \cdot l_{CoM(1)}^2 + I_{G(1)}) \cdot \dot{\theta}_1^2 \tag{B.9a}$$

$$\begin{aligned} T_2 = {} & \frac{1}{2} \cdot m_2(l_1^2 \cdot \dot{\theta}_1^2 + l_{CoM(2)}^2 \cdot \dot{\theta}_{12}^2 + 2 \cdot l_1 \cdot l_{CoM(2)} \cdot \dot{\theta}_1 \cdot \dot{\theta}_{12} \cdot c_2) \\ & + \frac{1}{2} \cdot I_{G(2)} \cdot \dot{\theta}_{12}^2 \end{aligned} \tag{B.9b}$$

$$\begin{aligned} T_3 = {} & \frac{1}{2} \cdot m_3(l_1^2 \cdot \dot{\theta}_1^2 + l_2^2 \cdot \dot{\theta}_{12}^2 + l_{CoM(3)}^2 \cdot \dot{\theta}_{123}^2 \\ & + 2 \cdot l_1 \cdot l_2 \cdot \dot{\theta}_1 \cdot \dot{\theta}_{12} \cdot c_2 + 2 \cdot l_1 \cdot l_{CoM(3)} \cdot \dot{\theta}_1 \cdot \dot{\theta}_{123} \cdot c_{23} \\ & + 2 \cdot l_2 \cdot l_{CoM(3)} \cdot \dot{\theta}_{12} \cdot \dot{\theta}_{123} \cdot c_3) \\ & + \frac{1}{2} \cdot I_{G(3)} \cdot \dot{\theta}_{123}^2 \end{aligned} \tag{B.9c}$$

where l_i is the length of the i^{th} rigid body segment, m_i is its mass, $l_{CoM(i)}$ is the location of its center of mass, $I_{G(i)}$ its moment of inertia (about the center of mass),

and c_2 and c_3 represent the cosine of joint angles θ_2 and θ_3 respectively, and

$$U_1 = m_1 \cdot g \cdot l_{CoM(1)} \cdot c_1 \tag{B.10a}$$

$$U_2 = m_2 \cdot g \cdot (l_1 \cdot c_1 + l_{CoM(2)} \cdot c_{12}) \tag{B.10b}$$

$$U_3 = m_3 \cdot g \cdot (l_1 \cdot c_1 + l_2 \cdot c_{12} + l_{CoM(3)} \cdot c_{123}) \tag{B.10c}$$

where g is the acceleration due to gravity (i.e., 9.81 m/s^2), and c_12 and c_123 represent the cosine of the limb segment angles θ_12 and θ_123 respectively.

Substituting Equations B.9 and B.10 into Equation B.4, and gathering like terms, gives the inertia (or mass) matrix elements:

$$\begin{aligned} M_{1,1} &= I_{G(1)} + m_1 \cdot l_{CoM(1)}^2 + I_{G(2)} + m_2 \cdot ({l_1}^2 + {l_{CoM(2)}}^2 + 2 \cdot l_1 \cdot l_{CoM(2)} \cdot c_2) \\ &\quad + I_{G(3)} + m_3 \cdot ({l_1}^2 + {l_2}^2 + 2 \cdot l_1 \cdot l_2 \cdot c_2 + {l_{CoM(3)}}^2 + 2 \cdot l_1 \cdot l_{CoM(3)} \cdot c_{23} \\ &\quad + 2 \cdot l_2 \cdot l_{CoM(3)} \cdot c_3) \end{aligned}$$

$$\begin{aligned} M_{1,2} &= I_{G(2)} + m_2 \cdot ({l_{CoM(2)}}^2 + l_1 \cdot l_{CoM(2)} \cdot c_2) + I_{G(3)} \\ &\quad + m_3 \cdot ({l_2}^2 + {l_{CoM(3)}}^2 + l_1 \cdot l_2 \cdot c_2 + l_1 \cdot l_{CoM(3)} \cdot c_{23} \\ &\quad + 2 \cdot l_2 \cdot l_{CoM(3)} \cdot c_3 \end{aligned}$$

$$M_{1,3} = I_{G(3)} + m_3 \cdot ({l_{CoM(3)}}^2 + l_1 \cdot l_{CoM(3)} \cdot c_{23} + l_2 \cdot l_{CoM(3)} \cdot c_3)$$

$$M_{2,1} = M_{1,2} \text{ (due to matrix symmetry)}$$

$$M_{2,2} = I_{G(2)} + m_2 \cdot {l_{CoM(2)}}^2 + I_{G(3)} + m_3 \cdot ({l_2}^2 + {l_{CoM(3)}}^2 + 2 \cdot l_2 \cdot l_{CoM(3)} \cdot c_3)$$

$$M_{2,3} = I_{G(3)} + m_3 \cdot ({l_{CoM(3)}}^2 + l_2 \cdot l_{CoM(3)} \cdot c_3)$$

$$M_{3,1} = M_{1,3} \text{ (due to matrix symmetry)}$$

$$M_{3,2} = M_{2,3} \text{ (due to matrix symmetry)}$$

$$M_{3,3} = I_{G(3)} + m_3 \cdot {l_{CoM(3)}}^2$$

the Coriolis and centrifugal terms:

$$\begin{aligned} V_1 = & -\left[(m_2 \cdot l_1 \cdot l_{CoM(2)} + m_3 \cdot l_1 \cdot l_2) \cdot s_2 + (m_3 \cdot l_1 \cdot l_{CoM(3)}) \cdot s_3\right] \cdot (2 \cdot \dot{\theta}_1 \cdot \dot{\theta}_2 \\ & + {\dot{\theta}_2}^2) - \left[(m_3 \cdot l_1 \cdot l_{CoM(3)}) \cdot s_{23} + m_3 \cdot l_2 \cdot l_{CoM(3)} \cdot s_3)\right] \cdot (2 \cdot \dot{\theta}_1 \cdot \dot{\theta}_3 \\ & + 2 \cdot \dot{\theta}_2 \cdot \dot{\theta}_3 + {\dot{\theta}_3}^2) \end{aligned}$$

$$\begin{aligned} V_2 = & \left[(m_2 \cdot l_1 \cdot l_{CoM(2)} + m_3 \cdot l_1 \cdot l_2) \cdot s_2 + m_3 \cdot l_1 \cdot l_{CoM(3)}) \cdot s_{23}\right] \cdot {\dot{\theta}_1}^2 \\ & - m_3 \cdot l_2 \cdot l_{CoM(3)} \cdot s_3 \cdot (2 \cdot \dot{\theta}_1 \cdot \dot{\theta}_3 + 2 \cdot \dot{\theta}_2 \cdot \dot{\theta}_3 + {\dot{\theta}_3}^2) \end{aligned}$$

$$V_3 = -m_3 \cdot l_1 \cdot l_{CoM(3)} \cdot s_{23} \cdot {\dot{\theta}_1}^2 - m_3 \cdot l_2 \cdot l_{CoM(3)} \cdot s_3 \cdot (\dot{\theta}_1 + \dot{\theta}_2)^2$$

and the gravity terms:

$$
\begin{aligned}
G_1 &= -m_1 \cdot g \cdot l_{CoM(1)} \cdot s_1 - m_2 \cdot g \cdot (l_1 \cdot s_1 + l_{CoM(2)} \cdot s_{12}) - m_3 \cdot g(l_1 \cdot s_1 \\
&\quad + l_2 \cdot s_{12} + l_{CoM(3)} \cdot s_{123}) \\
G_2 &= -m_2 \cdot g \cdot l_{CoM(2)} \cdot s_{12} - m_3 \cdot g \cdot (l_2 \cdot s_{12} + l_{CoM(3)} \cdot s_{123}) \\
G_3 &= -m_3 \cdot g \cdot l_{CoM(3)} \cdot s_{123}
\end{aligned}
$$

Appendix C

Motion Capture of the Sit-to-Stand Task

C.1 Data Collection

A Vicon^{TM} motion capture system was used to track a single healthy male subject while performing the sit-to-stand movement. The locations of the optical markers pertinent to this movement are listed in Table C.1. The left side of the body was predominantly used to extract the motion capture information of interest. Although either side of the body could have been used given the bilateral symmetry of the sit-to-stand movement.The Vicon^{TM} system uses a four letter code to uniquely identify each marker location. The sampling frequency was 120 Hz (typical of a Vicon^{TM} optical tracking system).

It should be noted that the defintions for the locations of the hip and shoul-

Marker Location	Code	Additional Anatomical Information
left heel	LHEE	
left toe	LTOE	
left ankle	LANK	
let knee	LKNE	
left hip	LHIP	located at the left greater trochanter
left shoulder	LSHO	located at the left glenohumeral joint

Table C.1: Optical Marker Locations Used to Capture the Sit-to-Stand Movement.

der marker locations are consistent with Winter's definitions used to produce the anthropometric data provided in Table A.1.

Figure C.1 illustrates the marker locations and how they relate to the biomechanical model employed in this work. The joint angles corresponding to the ankle, knee, and hip joints are given by θ_1, θ_2, and θ_3 respectively.

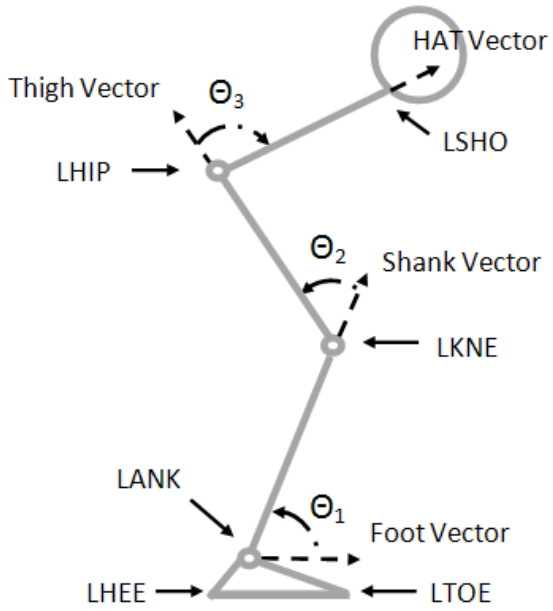

Figure C.1: Optical marker locations and their relation to a three-link biomechanical model used for the analysis of sit-to-stand.

The rigid body vectors, labeled as the "foot vector," "shank vector," "thigh vector," and "HAT vector," in Figure C.1, were computed as the **foot**, **shank**, **thigh**, and **HAT** rigid body vectors given in Equation C.1.

$$\mathbf{foot}(k\Delta t) = LTOE(k\Delta t) - LHEE(k\Delta t) \tag{C.1a}$$

$$\mathbf{shank}(k\Delta t) = LKNE(k\Delta t) - LANK(k\Delta t) \tag{C.1b}$$

$$\mathbf{thigh}(k\Delta t) = LHIP(k\Delta t) - LKNE(k\Delta t) \tag{C.1c}$$

$$\mathbf{HAT}(k\Delta t) = LSHO(k\Delta t) - LHIP(k\Delta t) \tag{C.1d}$$

where $LTOE$, $LHEE$, $LANK$, $LKNE$, $LHIP$, and $LSHO$ are the 2-Dimensional $[X, Y]$ locations of the markers listed in Table C.1, k is an integer, and Δt is the sampling period.

C.2 Marker Data Digital Filtering

Optical marker data, corresponding to the locations identified in Table C.1, were collected over the entire sit-to-stand movement. The data was filtered using a 10^{th} order Butterworth Filter with a corner frequency of 2 Hz. This filter order and corner frequency were selected based upon human movement analyses conducted by Winter [35,36]. It was discovered in human walking trials that frequencies below 6 Hz contained 99.7% of the signal power associated with leg and foot markers. Movement of the foot was responsible for the highest frequency components in that frequency band. In sit-to-stand, where the foot remains stationary, the vast majority of signal power resides in frequencies below 2 Hz. Therefore, using a corner frquency of 2 Hz resulted in removing noise components in the data set without adversely affecting the signals of interest.

C.3 Calculation of Joint Angle

The joint angles, θ_1, θ_2, and θ_3 were calculated as given in Equation C.2.

$$\theta_1 = acos\left(\frac{\mathbf{foot} \cdot \mathbf{shank}}{\|\mathbf{foot}\| \, \|\mathbf{shank}\|}\right) \tag{C.2a}$$

$$\theta_2 = acos\left(\frac{\mathbf{shank} \cdot \mathbf{thigh}}{\|\mathbf{shank}\| \, \|\mathbf{thigh}\|}\right) \tag{C.2b}$$

$$\theta_3 = acos\left(\frac{\mathbf{thigh} \cdot \mathbf{HAT}}{\|\mathbf{thigh}\| \, \|\mathbf{HAT}\|}\right) \tag{C.2c}$$

Figure C.2 illustrates the joint angles calculated over the course of a sit-to-stand movement (using Equation C.2) as conducted by a single healthy male subject.

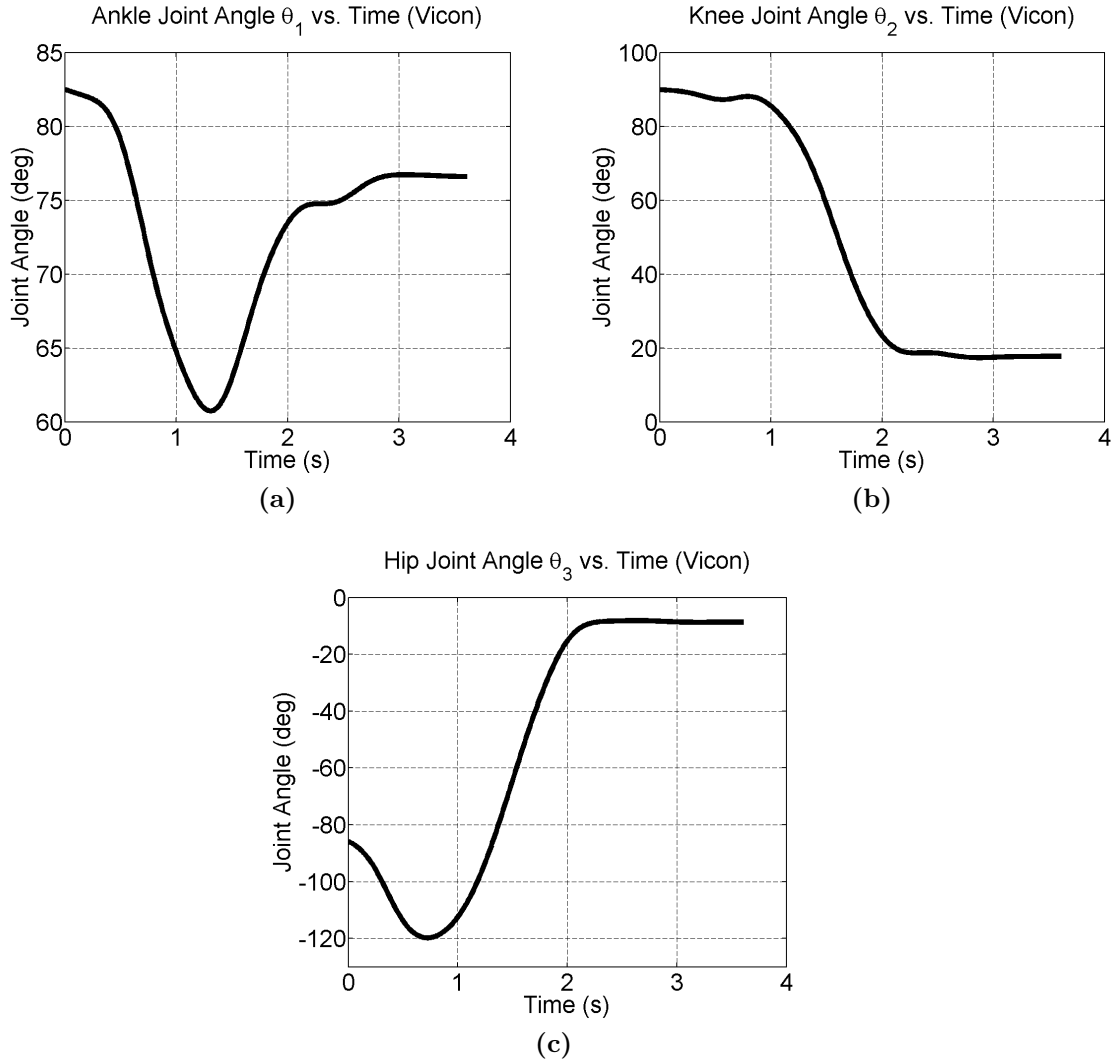

Figure C.2: Joint angles calculated using motion capture data for a single healthy male subject. (a) ankle, (b) knee, and (c) hip.

C.3.1 Calculation of Center of Mass for a Rigid Body Segment

The location of the center of mass for the shank $\begin{bmatrix} x_{CoM(1)} & y_{CoM(1)} \end{bmatrix}^T$, thigh $\begin{bmatrix} x_{CoM(2)} & y_{CoM(2)} \end{bmatrix}^T$, and HAT $\begin{bmatrix} x_{CoM(3)} & y_{CoM(3)} \end{bmatrix}^T$ were computed as

$$\begin{bmatrix} x_{CoM(1)} \\ y_{CoM(1)} \end{bmatrix} = {}^0_1R \cdot \begin{bmatrix} l_{CoM(1)} \\ 0 \end{bmatrix} \tag{C.3a}$$

$$\begin{bmatrix} x_{CoM(2)} \\ y_{CoM(2)} \end{bmatrix} = {}^0_2R \cdot \begin{bmatrix} l_{CoM(2)} \\ 0 \end{bmatrix} + LKNE(k\Delta t) \tag{C.3b}$$

$$\begin{bmatrix} x_{CoM(3)} \\ y_{CoM(3)} \end{bmatrix} = {}^0_3R \cdot \begin{bmatrix} l_{CoM(3)} \\ 0 \end{bmatrix} + LHIP(k\Delta t) \tag{C.3c}$$

where ${}^0_iR$ is a 2 x 2 rotation matrix which represents the rotation of the i^{th} rigid body segment with respect to the foot rigid body vector (given by **foot**) as given in Equation C.4, and $l_{CoM(i)}$ is the distance to the center of mass (from the base) of the

i^{th} rigid body segment, given in Appendix A.

$$
{}^{0}_{1}R = \begin{bmatrix} cos(\theta_1) & -sin(\theta_1) \\ sin(\theta_1) & cos(\theta_1) \end{bmatrix}
$$

$$
{}^{0}_{2}R = \begin{bmatrix} cos(\theta_1 + \theta_2) & -sin(\theta_1 + \theta_2) \\ sin(\theta_1 + \theta_2) & cos(\theta_1 + \theta_2) \end{bmatrix}
$$

$$
{}^{0}_{3}R = \begin{bmatrix} cos(\theta_1 + \theta_2 + \theta_3) & -sin(\theta_1 + \theta_2 + \theta_3) \\ sin(\theta_1 + \theta_2 + \theta_3) & cos(\theta_1 + \theta_2 + \theta_3) \end{bmatrix} \tag{C.4a}
$$

where θ_1, θ_2, and θ_3 are the ankle, knee, and hip joint angles respectively.

C.4 Calculation of Total Body Center of Mass

Applying the anthropometric data supplied in Table A.1 to the rigid body segments defined by **foot**, **shank**, **thigh**, and **HAT**, it is possible to estimate the location of the total body center of mass of the biomechanical model, denoted as $\begin{bmatrix} x_{CoM} & y_{CoM} \end{bmatrix}$, using using Equation C.5.

$$
x_{CoM} = \frac{m_1 \cdot x_{CoM(1)} + m_2 \cdot x_{CoM(2)} + m_3 \cdot x_{CoM(3)}}{m_1 + m_2 + m_3} \tag{C.5a}
$$

$$
y_{CoM} = \frac{m_1 \cdot y_{CoM_(1)} + m_2 \cdot y_{CoM_(2)} + m_3 \cdot y_{CoM_(3)}}{m_1 + m_2 + m_3} \tag{C.5b}
$$

where the locations of the centers of mass of the rigid body segments, denoted $\begin{bmatrix} x_{CoM(i)} & y_{CoM(i)} \end{bmatrix}$ for $i = 1, 2, 3$ are given in Equation C.3, and the segment masses m_1, m_2, and m_3, are given in Appendix A.

Figure C.3 illustrates the initial and final configurations of the test subject (as

given by the motion catpure data) at the onset and final position of the sit-to-stand movement. The path traversed by the estimated location of the total body center of mass, given by Equation C.5, is also included in the figure.

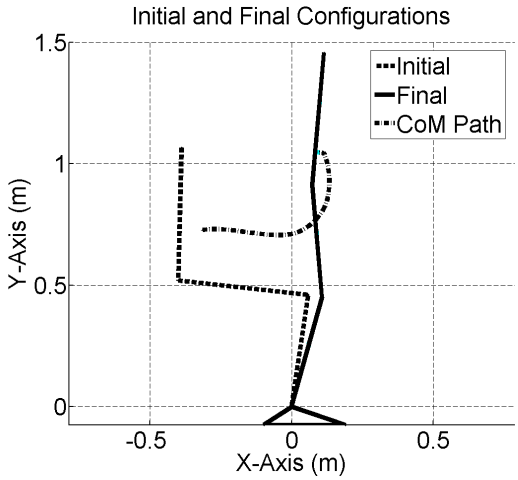

Figure C.3: Initial and final configurations of the sit-to-stand movement, and the path traversed by the estimated location of the total body center of mass using motion capture data for a single healthy male subject.

University of Victoria

Partial Copyright License

Title of Thesis: Synthesizing the sit-to-stand movement using fuzzy logic-based control and a simple biomechanical model.

Author: _____

Robert K. Prinz

Aug 18, 2010